4-13-2017

Biochemical and Functional Studies of S-nitrosoglutathione Reductase and Neutral Sphingomyelinase II

Bei Sun
University of Windsor

Biochemical and Functional Studies of *S*-nitrosoglutathione Reductase and Neutral Sphingomyelinase II

By

Bei Lei Sun

A Dissertation
Submitted to the Faculty of Graduate Studies
through the Department of Chemistry and Biochemistry
in Partial Fulfillment of the Requirements for
the Degree of Doctor of Philosophy
at the University of Windsor

Windsor, Ontario, Canada
2017

Biochemical and Functional Studies of *S*-nitrosoglutathione Reductase and Neutral Sphingomyelinase II

by

Bei Lei Sun

APPROVED BY:

_____

B. Gaston, External Examiner
Case Western Reserve University

_____

L. Porter
Department of Biological Sciences

_____

S. Ananvoranich
Department of Chemistry and Biochemistry

_____

P. Vacratsis
Department of Chemistry and Biochemistry

_____

B. Mutus, Advisor
Department of Chemistry and Biochemistry

January 12, 2017

DECLARATION OF CO-AUTHORSHIP / PREVIOUS PUBLICATION

I. Co-Authorship Declaration

I hereby declare that this dissertation incorporates material that is result of joint research, as follows:

All chapters of this dissertation incorporate research conducted under the supervision of Dr. Bulent Mutus at the University of Windsor. Experiments were designed jointly by the author and B. Mutus. Execution of experiments and subsequent data analyses were done by the author.

Chapter 2 includes research done in collaboration with Dr. Lisa Palmer, Dr. Shagufta Rehman, Kathleen Brown-Steinke and Dr. Ammasi Periasamy from the University of Virginia; as well as Itunuoluwa Adekoya from the University of Windsor. Fluorogenic substrate was designed by B. Mutus. Synthesis and purification of substrate were performed jointly by the author and B. Mutus. Kinetic studies and data analyses were done by the author. Murine lung endothelial cell isolation and cellular imaging studies were conducted at the University of Virginia by L. Palmer, S. Rehman, K. Brown-Steinke and A. Periasamy. I. Adekoya worked on the initial phase of this project as a fourth year thesis student at the University of Windsor.

Chapter 3 includes research done in collaboration with Sahar Nikoo and Dr. James Gauld from the University of Windsor. Experimental design for computational simulation and modeling of GSNOR was performed jointly by the author, B. Mutus, S. Nikoo and J. Gauld. Computational modeling and simulation were done by S. Nikoo under the supervision of J. Gauld. Cloning, mutagenesis, protein purification and kinetic

studies were done by the author. Results were interpreted jointly by the author and B. Mutus.

I am aware of the University of Windsor Senate Policy on Authorship and I certify that I have properly acknowledged the contribution of other researchers to my dissertation, and have obtained written permission from each of the co-authors to include the above material in my dissertation.

I certify that, with the above qualification, this dissertation, and the research to which it refers, is the product of my own work.

II. Declaration of Previous Publication

This dissertation includes one original paper that has been submitted for publication in Free Radical Biology & Medicine (Elsevier), as follows:

Dissertation Chapter	Publication Title	Publication Status
Chapter 2	*O*-aminobenzoyl-*S*-nitrosoglutathione is a fluorogenic, cell permeable, pseudo-substrate for *S*-nitrosoglutathione reductase	Under Revision

I certify that I have obtained a written permission from the copyright owner(s) to include the above submitted material in my dissertation. I certify that the above material describes work completed during my registration as graduate student at the University of Windsor.

I declare that, to the best of my knowledge, my dissertation does not infringe upon anyone's copyright nor violate any proprietary rights and that any ideas, techniques, quotations, or any other material from the work of other people included in my

dissertation, published or otherwise, are fully acknowledged in accordance with the standard referencing practices. Furthermore, to the extent that I have included copyrighted material that surpasses the bounds of fair dealing within the meaning of the Canada Copyright Act, I certify that I have obtained a written permission from the copyright owner(s) to include such material in my dissertation.

I declare that this is a true copy of my dissertation, including any final revisions, as approved by my dissertation committee and the Graduate Studies office, and that this dissertation has not been submitted for a higher degree to any other University or Institution.

ABSTRACT

S-nitrosation is the covalent attachment of nitric oxide (NO) moiety to cysteine thiol side chain. This reversible modification represents an important mechanism of post-translational regulation for a large number of proteins. In the cellular environment, *S*-nitrosoglutathione (GSNO) can transfer its NO group to reactive cysteine residues within proteins via transnitrosation reactions. Similarly, *S*-nitrosated protein can transfer its NO moiety to reduced glutathione (GSH). Due to the existence of this equilibrium, the GSNO metabolizing enzyme GSNO reductase (GSNOR) indirectly drives protein de-nitrosation. To date, aberrant GSNOR activity has been implicated in a large spectrum of human diseases. In this dissertation, we report the synthesis and characterization of *O*-aminobenzoyl-*S*-nitrosoglutathione (OAbz-GSNO), a novel fluorogenic substrate for GSNOR. OAbz-GSNO reduction mediated by GSNOR results in significant increases in fluorescence; and this increase in fluorescence is attenuated by GSNOR inhibitor treatment. In addition, OAbz-GSNO is cell membrane permeable and can be used to monitor endogenous GSNOR activity in cultured cells. Overall, our work demonstrates that OAbz-GSNO is a useful tool for assessing GSNOR activity, both *in vitro* and in cells. Site-directed mutagenesis and kinetic studies conducted using recombinant GSNOR suggest acetylation of Lys101 negatively affects enzyme activity; while computational simulations uncovered a putative allosteric GSNO binding site. We have experimental evidence supporting our model that GSNO binding to this allosteric site enhances GSNOR activity. Both lysine acetylation and allosteric substrate binding represent potential mechanisms involved in the post-translation regulation of GSNOR activity.

Neutral sphingomyelinase II (NSMase II) is a mediator of cellular stress response. It catalyzes the hydrolysis of plasma membrane sphingomyelin to generate bioactive ceramide and phosphocholine. This project looks into whether chronic cortisol exposure (as a stressor) affects NSMase II expression/activity. Experimental results demonstrate exposure to cortisol leads to increased cell size, but NSMase II expression and activity are unaffected. However, NSMase II over-expressing cells appear to have less cholesterol in the plasma membrane. Since cholesterol is important for the formation of lipid rafts, these finding suggest that in addition to ceramide generation, modulation of plasma membrane cholesterol content may represent an alternative mechanism by which NSMase II exerts its biological effects.

ACKNOWLEDGEMENTS

First and foremost, I would like to extend my heart felt gratitude to my supervisor, Dr. Bulent Mutus, for the guidance and support he has given me throughout my graduate studies. Thank you for teaching me the skills that I need as a scientific researcher and for giving me the opportunity to grow as an individual.

My appreciation is further extended to members of my PhD committee, Drs. Benjamin Gaston, Lisa Porter, Sirinart Ananvoranich, and Panayiotis Vacratsis, for their advice, thoughtful suggestions and the critical evaluation of my dissertation; with a special thank you to Sirinart for teaching me molecular cloning techniques.

I would like to thank our collaborators: Dr. Lisa Palmer and her group for performing live cell imaging studies; Dr. James Gauld and Sahar for the computational insights. I would also like to acknowledge and thank Drs. Matthew Revington, Janeen Auld, and Artur Jarosz for running our samples using NMR and mass spectrometry.

To my fellow lab members, it was a pleasure to have worked with each of you. To the faculty, staff and graduate student community in the department of Chemistry and Biochemistry, your knowledge, skills, and empathy created a co-operative and supportive learning environment; and truly made this department unique. To our graduate secretary, Mrs. Marlene Bezaire, thank you for looking out for me during my graduate years.

I would like to thank members of my Bible study group, for their encouragement during difficult times; and Qiudi Geng, for her unwavering friendship.

Finally, I am forever grateful to my family, and to my boyfriend Artur, for their unconditional love and support.

TABLE OF CONTENTS

LIST OF TABLES

LIST OF FIGURES

LIST OF APPENDICES

LIST OF ABBREVIATIONS

ADH	Alcohol dehydrogenase
APL	Anionic phospholipid
ATRA	All-trans retinoic acid
CcO	Cytochrome c oxidase
CF	Cystic fibrosis
CFTR	Cystic fibrosis transmembrane conductance regulator
cGMP	Cyclic guanosine monophosphate
COSY	Correlation spectroscopy
DMEM	Dulbecco's modified eagle medium
DMSO	Dimethyl sulfoxide
DTT	Dithiothreitol
eNOS	Endothelial nitric oxide synthase
ER	Endoplasmic reticulum
FAD	Flavin adenine dinucleotide
FAN	Factor associated with neutral sphingomyelinase
FDH	Formadehyde dehydrogenase
FMN	Flavin mononucleotide
GSH	Glutathione, reduced
GSNO	*S*-nitrosoglutathione
GSNOR	*S*-nitrosoglutathione reductase
GTP	Guanosine triphosphate
HAEC	Human airway epithelial cell
HBSS	Hanks balanced saline solution
HMBC	Heteronuclear multiple bond correlation
HMGSH	Hydroxymethylglutathione
HMQC	Heteronuclear multiple quantum correlation
HSP 60	Heat shock protein 60
iNOS	Inducible nitric oxide synthase
IPTG	Isopropyl β-D-1-thiogalactopyranoside

LDL	Low density lipoprotein
MAPK	Mitogen activated protein kinase
MS	Mass spectrometry
NAD^+	β-nicotinamide adenine dinucleotide, oxidized
NADH	β-nicotinamide adenine dinucleotide, reduced
NADPH	Nicotinamide adenine dinucleotide phosphate, reduced
nNOS	Neuronal nitric oxide synthase
NO	Nitric oxide
NOS	Nitric oxide synthase
NSD	Neutral sphingomyelinase activation domain
NSMase	Neutral sphingomyelinase
OAbz-GSNO	*O*-aminobenzoyl-*S*-nitrosoglutathione
PBS	Phosphate buffered saline
PCR	Polymerase chain reaction
PECAM-1	Platelet/endothelial cell adhesion molecule 1
PKC	Protein kinase C
PMSF	Phenylmethylsulfonyl fluoride
RACK 1	Receptor for activated C-kinase 1
sGC	Soluble guanylate cyclase
SM	Sphingomyelin
SNO	*S*-nitrosothiol
SOD	Superoxide dismutase
Sp	Specificity protein
TNF	Tumour necrosis factor

CHAPTER 1

General Introduction

1.1 Nitric Oxide

Nitric oxide (NO) is a diatomic free radical gasotransmitter. In the 1980s, multiple research groups independently identified NO as the endothelium derived relaxing factor responsible for eliciting vascular smooth muscle relaxation [1-4]. Since then, the field of NO biochemistry has expanded significantly and NO is now a well-established signaling molecule known to affect a vast number of physiological processes. For instance, NO is involved in the control of vascular tone [5-7] and blood pressure [8, 9]; promotes angiogenesis [10]; and mediates neurotransmission [11, 12], immune response [13, 14], as well as wound healing [15].

1.1.1 NO Synthases

Endogenous NO is enzymatically synthesized in mammalian tissues by 3 isoforms of nitric oxide synthase (NOS; EC 1.14.13.39). The isoforms have been named neuronal NOS (nNOS, NOS 1), inducible NOS (iNOS, NOS 2) and endothelial NOS (eNOS, NOS 3) based on their tissue of constitutive expression or basal level of activity. All NOS isoforms function as homodimers and catalyze the oxidation of L-arginine to L-citrulline and NO [16]. Molecular oxygen and reduced nicotinamide adenine dinucleotide phosphate (NADPH) are co-substrates for this reaction. The overall reaction utilizes 2 mol of O_2 and 1.5 mol of NADPH for every mol of NO produced [17, 18]. In addition to substrates, NOS catalyzed NO production requires a number of cofactors/coenzymes, including flavin adenine dinucleotide (FAD), flavin mononucleotide (FMN), tetrahydrobiopterin (BH4) and calmodulin [18].

nNOS is constitutively expressed in the neurons of the central and peripheral nervous system, as well as epithelial cells of various organs [19, 20]. Its activity is

regulated by intracellular Ca^{2+} levels through calmodulin binding. nNOS derived NO mediates synaptic plasticity, which affects complex physiological functions such as neurogenesis, learning and memory formation [21, 22]. nNOS is also involved in the central regulation of blood pressure [23, 24]. iNOS expression is usually induced by agents such as bacterial lipopolysaccharide and cytokines. Once expressed, iNOS produces large amounts of NO and its activity is not affected by Ca^{2+}. In macrophages, NO produced by iNOS contributes to host immune defense by exerting cytotoxic effects on pathogens [14, 19]. eNOS is mainly expressed in endothelial cells and its activity is regulated by a number of factors, including intracellular Ca^{2+} concentration and fluid shear stress [25]. NO produced by endothelial cells results in vasorelaxation; and protects blood vessels from thrombosis by inhibiting platelet aggregation and adhesion [26, 27].

1.1.2 Mechanisms of NO Signaling

Multiple mechanisms have been identified for NO-mediated signaling **(Figure 1.1.2-1)**. Canonical signaling involves NO activating soluble guanylate cyclase (sGC) by binding to its heme iron [28]. Once activated, sGC converts guanosine triphosphate (GTP) to cyclic guanosine monophosphate (cGMP). Subsequent down-stream effects are mediated by cGMP-dependent protein kinases [29]. Within the mitochondria, NO competes with O_2 for binding to cytochrome *c* oxidase (CcO), the terminal enzyme of the electron transport chain [30]. NO binding inhibits CcO. This inhibition is reversible and can initiate biochemical events such as reactive oxygen species generation and AMP-kinase activation [31]. NO can also signal through covalent post-translational modifications of target proteins. These modifications include *S*-nitrosation, *S*-glutathionylation and

tyrosine nitration [29]. The modification most relevant to this dissertation is *S*-nitrosation, which is discussed in detail in the next section.

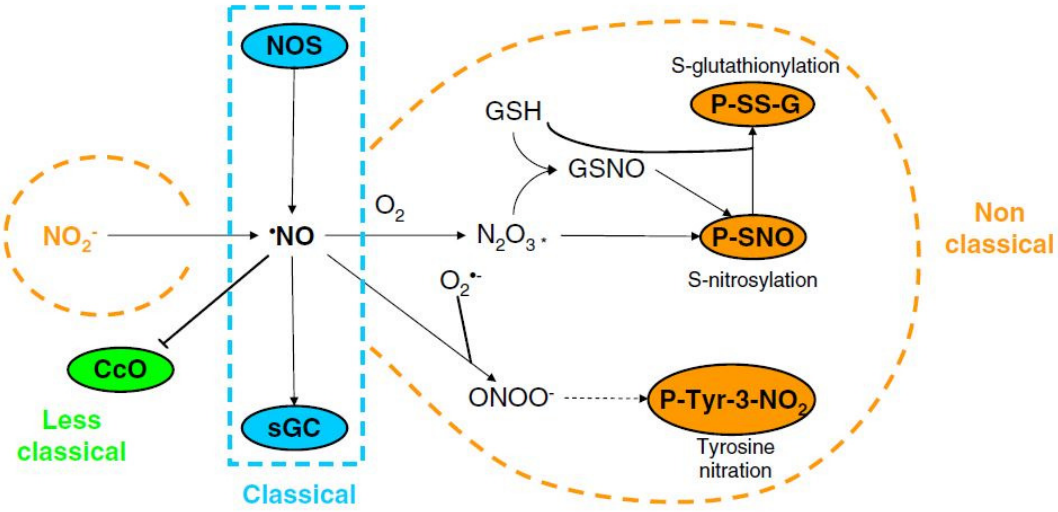

Figure 1.1.2-1 Overview of nitric oxide signaling mechanisms

Classical signaling involves nitric oxide (NO) production by nitric oxide synthase (NOS) and the activation of soluble guanylate cyclase (sGC). Less classical signaling is based on NO mediated inhibition of cytochrome *c* oxidase (CcO) in the mitochondria. Non-classical pathways include the formation of post-translational modifications. Image from: Martinez-Ruiz *et al*. (2011). "Nitric oxide signaling: classical, less classical, and non classical mechanisms." Free Radical Biology and Medicine **51**(1): 17-29. With permission.

1.2 Protein *S*-nitrosation

S-nitrosation refers to the covalent attachment of NO derived nitroso group to a cysteine thiol, which results in the formation of *S*-nitrosothiol (SNO). This modification is also commonly known as *S*-nitrosylation. Chemically, the term 'nitrosation' describes the addition of nitrosonium cation (NO^+) to a nucleophilic group such as thiolate; whereas 'nitrosylation' refers to direct addition of NO to a reactant [32]. However, when the mechanism of SNO formation is unknown or ambiguous, questions arise as to which term should be used. Some researchers have adopted '*S*-nitrosylation' as a general biological term to describe the formation of SNO species regardless of mechanism (analogous to phosphorylation or acetylation) [33], while others feel this analogy is unwarranted since 'nitrosylation' carries mechanistic implications and NO alone cannot react with thiols or thiolates under physiological conditions [32]. In this dissertation, the term '*S*-nitrosation' will be used to describe this thiol modification and to highlight the involvement of NO^+.

Cysteine residues within proteins can be modified by *S*-nitrosation. This post-translational modification is reversible and constitutes an important mechanism by which NO exerts its biological effects **(Figure 1.1.2-1)** [29]. Over the years, there is increasing research evidence suggesting that *S*-nitrosation participates in both normal physiology and in the pathogenesis for a large spectrum of human diseases [34]. Aberrant protein *S*-nitrosation typically involves hypo- or hyper-*S*-nitrosation of specific targets. This could result from changes in the expression, localization, and/or activity of enzymes such as NOS, which generates NO from L-arginine, and *S*-nitrosoglutathione reductase (GSNOR), which promotes protein de-nitrosation by metabolizing the transnitrosating agent *S*-nitrosoglutathione (GSNO).

Evidence to date indicates that unlike other post-translational modifications, *S*-nitrosation of proteins is not directly catalyzed by enzymes. Instead, signaling specificity is largely dictated by the chemical reactivity between the nitrosating agent and target cysteine thiol [35]. Particular protein microenvironments lead to increased reactivity for certain cysteine residues, thus favouring their modification. Several attempts have been made to describe a putative "nitrosation motif" [36-38]. However, since *S*-nitrosation could occur via multiple mechanisms [39, 40], which are still not fully understood, the existence of a single consensus motif seems unlikely.

As previously mentioned, NO alone does not react with thiols or thiolates under physiological conditions. For *S*-nitrosation to occur, NO needs to be first oxidized to higher oxides of nitrogen such as nitrogen dioxide (NO_2) or dinitrogen trioxide (N_2O_3). Of the potential *S*-nitrosating species, N_2O_3 could react with thiols directly according to **Equation 1.2-1**. However, questions have been raised regarding the slow kinetics of initial NO oxidation under physiological NO and O_2 concentrations [41-43].

(1.2-1) $RS^- + N_2O_3 \rightarrow RSNO + NO_2^-$

NOS activation effectively increases local NO concentrations, potentially favoring the generation of *S*-nitrosating species. In this context, co-localization or direct interaction with active NOS can positively influence *S*-nitrosation [44, 45]. Accelerated NO oxidation by O_2 has also been reported in hydrophobic compartments such as biological membranes [46], further implicating the importance of subcellular compartmentalization in controlling the occurrence and specificity of *S*-nitrosation.

An alternative mechanism proposed for SNO formation involves NO reacting with a reduced thiol to form a radical intermediate. Then, in the presence of an electron

acceptor (such as O_2) SNO and superoxide are formed [47]. In 1996, Schmidt and colleagues attempted to measure NOS-produced NO radical directly (rather than nitrate or nitrite) and reported that NOS did not yield detectable NO unless superoxide dismutase (SOD) was also present. Based on experimental findings, this group concluded NOS activity produces NO^- as an NO precursor, which is acted upon by SOD to generate NO. In addition, when both SOD and GSH are present, the formation of GSNO was detected [48]. These observations provided strong evidence for enzyme mediated SNO formation.

Proteins can become *S*-nitrosated via transnitrosation. These reactions are fully reversible and often involve low molecular weight SNO such as GSNO **(Equation 1.2-2)**.

(1.2-2) $RS^- + GSNO \leftrightarrow RSNO + GS^-$

Interestingly, ferric cytochrome *c* can promote GSNO formation; the proposed mechanism involves initial weak binding between GSH and cytochrome *c*, followed by reaction with NO to generate GSNO and ferrous cytochrome *c* [49]. This increase in GSNO levels in turn promotes *S*-nitrosation of proteins [50]. In addition to cytochrome *c*, dinitrosyl iron complexes have also been shown to enhance *S*-nitrosation of proteins through transnitrosation [51, 52].

More recently, de-nitrosation pathways have emerged as another important regulatory mechanism for signaling through *S*-nitrosation [53]. Due to the reversible nature of transnitrosation, increases in cellular glutathione (GSH), as well as decreased levels of GSNO, both contribute to protein de-nitrosation. A number of enzyme systems (including GSNOR [54], superoxide dismutase [55], glutathione peroxidase [56], thioredoxin [57], and carbonyl reductase 1 [58]) have been proposed to be involved in

GSNO metabolism in humans. Of these enzymes, only GSNOR and carbonyl reductase 1 are capable of irreversibly removing the NO equivalents stored in GSNO, while kinetic comparisons suggest GSNOR is the most efficient GSNO-metabolizing enzyme [59].

1.3 *S*-nitrosoglutathione Reductase

1.3.1 From Class III Alcohol Dehydrogenase to S-nitrosoglutathione Reductase

Mammalian alcohol dehydrogenase (ADH) belongs to the protein superfamily of medium chain dehydrogenases / reductases [60] and consists of at least six known classes based on primary structure and function [61]. ADH is the major enzyme system responsible for ethanol metabolism **(Reaction 1.3.1-1)** and can also catalyze the oxidation of other primary and secondary alcohols using nicotinamide adenine dinucleotide (NAD^+) as the co-factor.

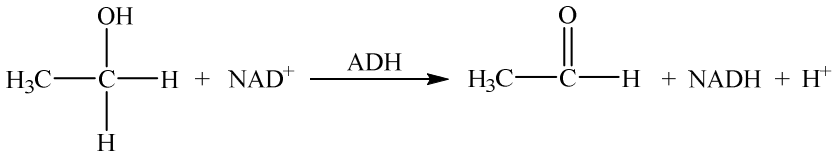

Reaction 1.3.1-1 ADH catalyzed ethanol oxidation, forming acetaldehyde as the product.

Class III alcohol dehydrogenase (ADH III) was first isolated and purified to homogeneity from the human liver in the 1980s [62, 63]. Early studies revealed that even though ADH III resembles previously discovered ADH isozymes in terms of molecular weight, metal ion binding, and optimal pH for catalytic activity, it differs remarkably from other known ADH members by exhibiting very poor activity towards ethanol, with an apparent K_m of more than 2 M [62, 63]. Instead, ADH III prefers long chain primary alcohols and aldehydes as substrates [63, 64]. In 1989, Koivusalo *et al.* reported evidence that ADH III is actually homologous to the ubiquitous cytosolic enzyme formaldehyde

dehydrogenase which catalyzes the oxidation of *S*-hydroxymethylglutathione (HMGSH) to *S*-formylglutathione **(Reaction 1.3.1-2)** [65, 66]. The adduct HMGSH is formed spontaneously between formaldehyde and glutathione. By metabolizing HMGSH, ADH-III was noted as an important component in formaldehyde detoxification [67].

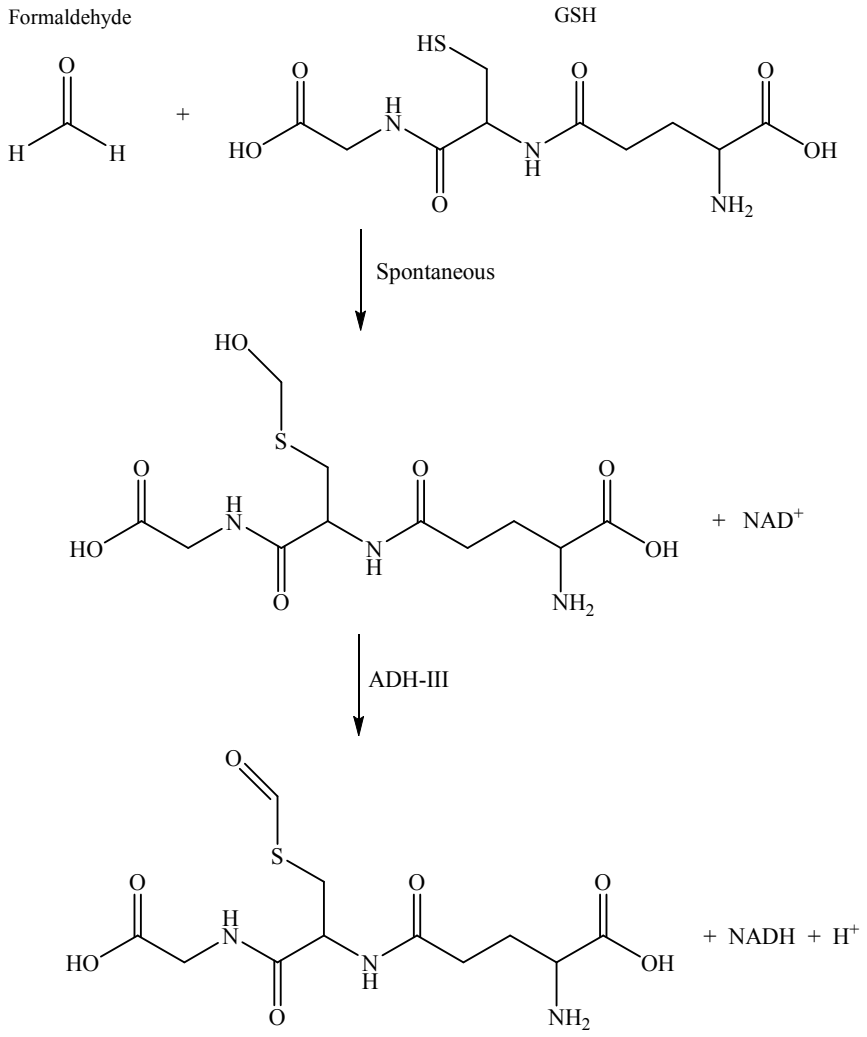

Reaction 1.3.1-2 Formaldehyde is a highly toxic metabolite. In the presence of GSH, it forms the adduct HMGSH, which in turn is converted to *S*-formylglutathione by ADH III using NAD^+ as the cofactor.

Later in 1998, Jensen and colleagues discovered that in addition to activity towards HMGSH, ADH III can efficiently catalyze the NADH-dependent reduction of GSNO [54]. As a result, this enzyme is sometimes referred to as GSNO reductase (GSNOR). Since GSNO is considered to be an endogenous mediator of NO signaling, this enzyme with GSNO reductase activity rapidly caught the attention of researchers in the NO signaling field.

Many different nomenclatures (including ADH III, chi-chi alcohol dehydrogenase, glutathione-dependent formaldehyde dehydrogenase, and GSNO reductase) have been used in literature to describe this enzyme. In all subsequent sections of this dissertation, the name GSNOR will be consistently used to refer to this enzyme.

1.3.2 Regulation of GSNOR Gene Expression

In humans, there are 7 identified ADH genes located in a cluster on chromosome 4q. GSNOR is encoded by the gene ADH5, which consists of 9 exons. The 5' untranslated region of ADH5 is GC rich and lacks a TATA or CAAT box; both of which are characteristics of housekeeping genes with ubiquitous expression [68]. Several research groups have looked into the regulation of ADH5 expression. A study by Kwon *et al.* revealed two specificity protein 1 (Sp1) binding sites critical for transcription initiation, while competitive binding by Sp3 or Sp4 represses ADH5 expression [69]. Interestingly, high levels of GSNO can decrease/inhibit Sp3 binding on the cystic fibrosis transmembrane conductance regulatory gene (CFTR) [70]. If GSNO also negatively affects Sp3 binding on ADH5, this could represent a regulatory feedback loop for GSNOR such that when GSNO concentration is high, Sp3 binding is inhibited to favour

Sp1 binding and ADH5 transcription; which in turn leads to increased GSNOR expression and increased GSNO metabolism until homeostasis is restored.

In addition to Sp binding sites, ADH5 also contains an up-stream open reading frame with two possible AUG start codons. These up-stream open reading frames are an unusual feature in mammalian mRNAs and have been postulated to play a regulatory role as mutations at one or both of these up-stream AUG codons led to an increase in ADH5 gene expression [71].

1.3.3 GSNOR Protein Structure

Crystal structure of human GSNOR shows that it is a homodimer with 40 kDa subunits **(Figure 1.3.3-1)**. Each subunit contains a catalytic domain and a coenzyme binding domain. The catalytic domain is completely solvent exposed and displays a semi-open conformation. This conformation provides the structural basis for GSNOR's ability to accommodate larger substrates such as HMGSH and GSNO [72]. Mutagenesis studies suggest that the positively charged Arg115 is critical for HMGSH binding. When this residue is changed to Asp, catalytic efficiency for HMGSH oxidation decreases significantly [73]. In addition to Arg115, HMGSH also interacts with the highly conserved Thr47, Asp56 and Glu58 [74]. Whether the same residues facilitate the binding of GSNO is currently unknown.

Similar to all other members of the ADH family, GSNOR is a zinc containing enzyme. Each subunit contains one catalytic zinc, as well as one structural zinc **(Figure 1.3.3-1)**. The catalytic zinc is located within the active site and acts as a Lewis acid during catalysis; while the structural zinc is critical for the maintenance of proper protein structure.

A number of studies have looked at the coordination environment of the active site zinc [74-77]. In the apoenzyme, the active site zinc is coordinated by Cys45, His67, Cys174 and a water molecule. Upon coenzyme binding, the active site zinc is displaced towards Glu68. This displacement decreases interaction with the solvent water molecule and has been postulated to facilitate ligand exchange at the active site [76].

The structural zinc is coordinated by four closely spaced cysteine residues (Cys97, Cys100, Cys103 and Cys111). This coordination pattern is highly conserved for all classes of ADH [78]. Even though the structural zinc does not directly participate in catalysis, it is still a critical feature and mutating any one of these four cysteine residues results in inactive and unstable enzyme [79]. Although the sensitivity of these cysteine residues towards oxidation has not yet being evaluated, it is feasible that the peptide microenvironment contributes to the maintenance of proper oxidation state.

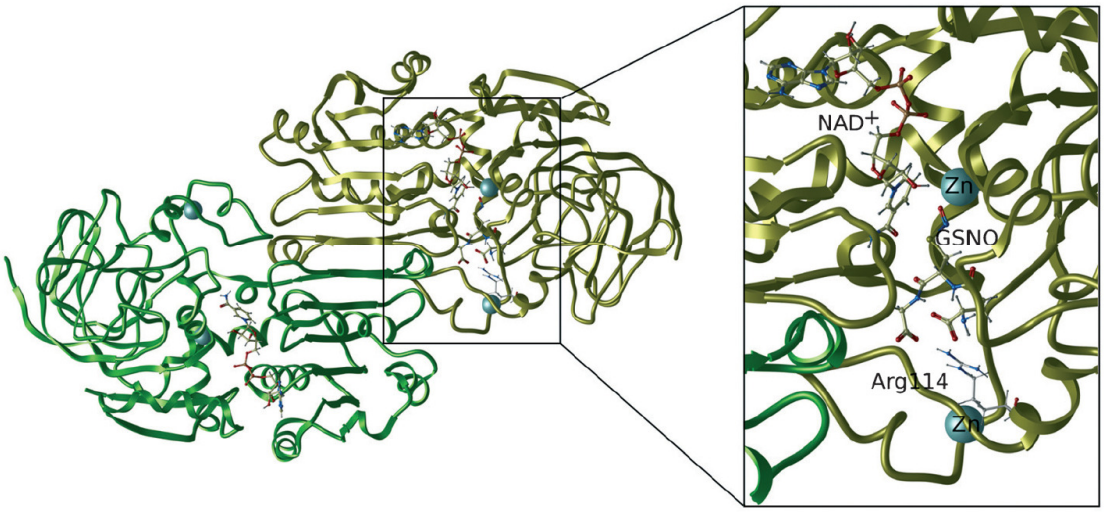

Figure 1.3.3-1 GSNOR protein structure

Left: dimeric structure of GSNOR with the monomers shown in green and yellow. *Right:* close up view of the active site. Image from: Staab *et al*. (2008). "Medium- and short-chain dehydrogenase/reductase gene and protein families: Dual functions of alcohol dehydrogenase 3: implications with focus on formaldehyde dehydrogenase and *S*-nitrosoglutathione reductase activities." Cellular and Molecular Life Sciences **65**(24): 3950-3960. With permission.

1.3.4 Functions of GSNOR

GSNOR is highly conserved in both prokaryotic and eukaryotic organisms [80-83], and is ubiquitously expressed in all human tissues studied [84, 85]. This universal pattern of expression suggests that GSNOR likely performs important cellular functions. Over the years, numerous studies have presented evidence that GSNOR participates in a number of pathways, ranging from first-pass ethanol metabolism in the gastric lumen following ethanol consumption [86], to ω-hydroxy fatty acid oxidation [54, 65], formaldehyde detoxification [67, 87-89], and GSNO metabolism [54, 90-93]. Two of the better characterized activities of GSNOR are glutathione-dependent formaldehyde oxidation **(Reaction 1.3.1-2)**, and NADH-dependent GSNO reduction **(Figure 1.3.4-1)**.

The glutathione-dependent formaldehyde dehydrogenase (FDH) activity is an important mechanism for the elimination of formaldehyde, which is a classified carcinogen due to its high reactivity towards DNA and proteins [94-96]. Sources of cellular formaldehyde include both endogenous metabolism and environmental exposure [97-100]. Under physiological conditions, formaldehyde readily reacts with glutathione (GSH) to form HMGSH [87], which is in turn converted to *S*-formylglutathione by GSNOR, using NAD^+ as the cofactor. Finally, *S*-formylglutathione is broken down to glutathione and the less reactive formate by *S*-formylglutathione hydrolase [101, 102]. Immunocytochemical studies demonstrate that GSNOR is localized to the cytoplasm as well as over condensed chromatin in the nucleus [103]. The nuclear localization of GSNOR supports its role in protecting DNA from formaldehyde toxicity.

In addition to GSNOR, there are enzymes (ALDH1A1 and ALDH2 in humans) from the aldehyde dehydrogenase superfamily that can metabolize free formaldehyde

directly [104-106]. However, their K_m values for formaldehyde are much greater than the one GSNOR shows with HMGSH, suggesting that GSNOR is the more efficient enzyme for formaldehyde detoxification [65, 91, 106].

The functional aspect of GSNOR most relevant to this dissertation is its GSNO reductase activity. In 1998, Jensen and co-workers reported that GSNO is a substrate for GSNOR and this reduction reaction uses one mol of NADH per mol of GSNO metabolized [54]. Product analyses performed by the same research group suggest the major stable product is glutathione sulfinamide. However, when an excess of GSH was included in the reaction mix *in vitro*, the formation of GSSG and hydroxylamine appeared to be favoured **(Figure 1.3.4-1)** [54]. A few years later, Liu *et al.* reported the purification of GSNOR from *Escherichia coli, Saccharomyces cerevisiae* and mouse macrophages and demonstrated that GSNOR is highly specific towards GSNO with no activity observed towards *S*-nitrosocysteine and *S*-nitrosohomocysteine [107].

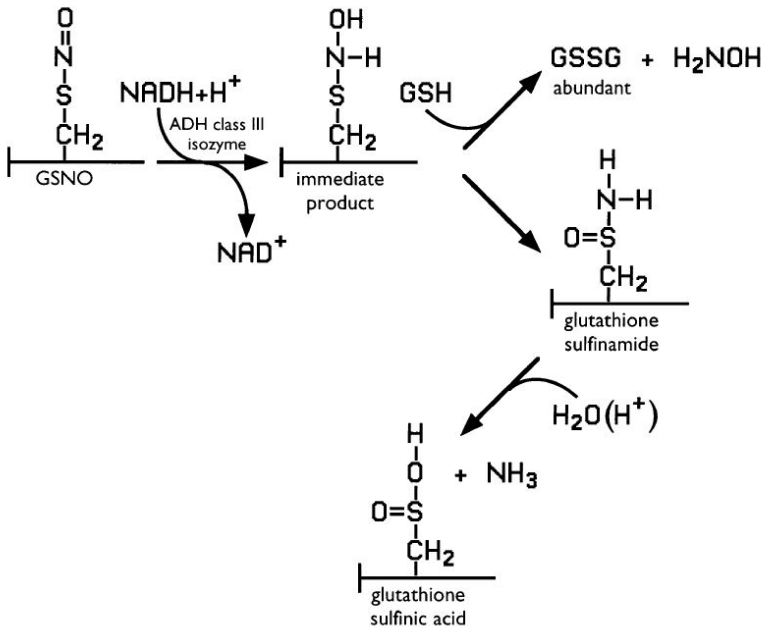

Figure 1.3.4-1 Proposed reaction scheme for GSNOR catalyzed GSNO degradation

Image from: Jensen *et al.* (1998). "*S*-nitrosoglutathione is a substrate for rat alcohol dehydrogenase class III isoenzyme." Biochemical Journal **331 (Pt 2)**: 659-668. With permission.

Under physiological redox conditions, the ratio of free NADH / NAD^+ is usually low [108]. This is considered unfavorable for reductive pathways which require NADH and implies that the reductase activity of GSNOR might depend on cofactor availability. Various factors could trigger an increase in cellular NADH levels, such as ADH mediated ethanol metabolism [109] and the inhibition of NADH dehydrogenase [91]. However, whether these events directly contribute to the activation of GSNOR reductase activity remain unclear. A more recent study by Staab *et al*. suggests that NADH produced by GSNOR catalyzed oxidation reactions remain bound to the enzyme and could promote GSNO reduction via direct cofactor recycling [110]. In addition, steady state kinetics of human GSNOR show that the k_{cat} / K_m for GSNO reduction is approximately twice the k_{cat} / K_m for HMGSH oxidation, and the reduction reaction is essentially irreversible as neither glutathione sulfinamide nor GSSG works as substrate or inhibitor for GSNOR [111]. With these factors considered, it becomes feasible to drive the reaction in the reductive direction despite unfavourable NADH / NAD^+ ratios, lending further support that GSNOR is a physiologically relevant enzyme for GSNO metabolism.

Furthermore, GSNOR deficient mice (GSNOR $^{-/-}$) has been shown to exhibit substantial increases in protein *S*-nitrosation [112]. Since it is generally accepted that in the cellular environment, GSNO is in equilibrium with a subset of *S*-nitrosated proteins via reversible transnitrosation **(Figure 1.3.4-2)**, the observation that GSNOR deficient mice experience increased levels of *S*-nitrosation places GSNOR in a crucial role in maintaining SNO homeostasis via its GSNO reductase activity.

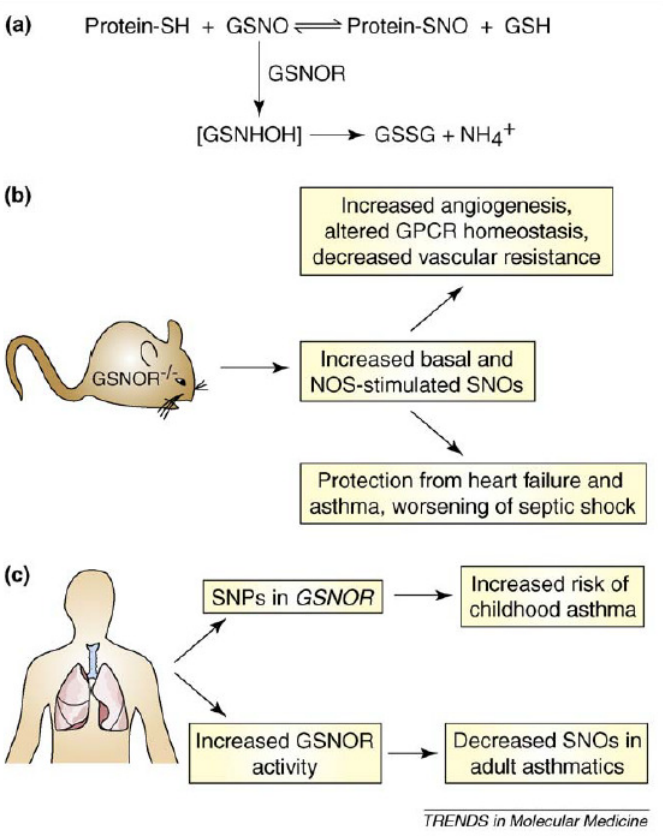

Figure 1.3.4-2 Regulation of SNO homeostasis by GSNOR

(a) GSNO is in equilibrium with a subset of *S*-nitrosated proteins. By metabolizing GSNO, GSNOR removes NO equivalents from the bioactive NO pool; and indirectly promotes protein de-nitrosation. **(b)** GSNOR knockout mice exhibit increased SNO levels with physiological consequences. **(c)** GSNOR expression and activity are associated with human asthma. Image from: Foster *et al.* (2009). "Protein *S*-nitrosylation in health and disease: a current perspective." Trends in Molecular Medicine **15**(9): 391-404. With permission.

1.3.5 GSNOR's Involvement in Physiology

In 2004, Liu *et al.* generated GSNOR deficient mice (GSNOR $^{-/-}$) using homologous recombination. These animals exhibit increased level of whole cell *S*-nitrosation, increased level of SNO in their red blood cells, and are more susceptible to endotoxic or bacterial challenge [112]; suggesting immunity could be affected by SNO and GSNOR activity. A number of subsequent studies using this animal model offered additional insights into GSNOR's involvement in physiology. Lima *et al.* observed an increase in myocardial capillary density and cardio-protective characteristics in GSNOR deficient animals. These findings are further supported by another study which demonstrated that GSNOR $^{-/-}$ mice have preserved cardiac function after myocardial infarction [113].

In pulmonary physiology, GSNO has been identified as a long-lived and potent relaxant of human airways [114]. This endogenous bronchodilator appears to be depleted in the airway linings of individuals with asthma, which is a chronic disease characterized by airway inflammation and hyper-responsiveness [115]. Interestingly, following an allergen challenge, GSNOR null mice have substantially higher levels of SNO in the lungs than their wild-type counterparts and are protected from airway hyper-responsivity [116]. These observations led researchers to propose a novel therapeutic approach of targeted GSNOR inhibition to restore SNO levels and alleviate asthma symptoms. In 2013, Ferrini *et al.* reported intranasal administration of the GSNOR inhibitor SPL334 reduces airway hyper-reactivity, inflammation, and mucus production in a mouse model of allergic asthma [117]. A year later, Blonder *et al.* published findings showing treatment with the GSNOR inhibitor N6022 restores GSNO levels and leads to

bronchodilation, as well as reduced inflammation [118]. N6022 is currently undergoing clinical evaluation for the treatment of inflammatory lung disease.

GSNOR and its ability to modulate SNO levels also play a role in cystic fibrosis (CF). Development of CF is attributed to mutations in the CFTR gene. The common ΔF508 mutation causes protein misfolding, in which case the protein fails to mature and is degraded in the endoplasmic reticulum (ER) [119]. A number of studies have demonstrated that GSNO can increase CFTR maturation and partially restore the function of ΔF508 CFTR by directing it to the plasma membrane [120-122]. Most recently, Zaman *et al.* reported an inverse relationship between GSNOR activity and the expression and maturation of CFTR [123], with the implication that pharmacological inhibition of GSNOR could potentially benefit patients with CF.

Since increasing GSNO levels appear to have beneficial consequences in a number of cardiovascular and pulmonary conditions, the synthesis and characterization of small molecule GSNOR inhibitors have gained attention. [124-127]. However, this promising therapeutic approach is complicated by findings which suggest GSNOR activity is important for protecting cells from nitrosative stress. For example, the DNA repair protein *O*(6)-alkylguanine-DNA alkyltransferase confers protection against alkylation induced mutagenesis in the liver; but GSNOR deficiency results in *S*-nitrosation and proteosomal degradation of this key repair protein under inflammatory conditions [128-130]. In this context, GSNOR deficient mice are more susceptible to both spontaneous and carcinogen-induced hepatocellular carcinoma. Similarly, decreased GSNOR activity is associated with human lung cancer via Ras *S*-nitrosation and

activation [131]. These oncogenic potentials should be taken into consideration when evaluating therapies involving pharmacological GSNOR inhibition.

1.4 Neutral Sphingomyelinase II

1.4.1 A Brief History of Discovery

Sphingomyelinase (EC.3.1.4.12) is a family of enzymes which catalyzes the hydrolysis of the sphingolipid sphingomyelin (SM) to form bioactive ceramide and phosphocholine. Ceramide, along with its downstream metabolites, are important second messenger molecules capable of modulating a variety of cellular events, such as cell cycle arrest, differentiation, inflammation and apoptosis [132-134].

The family of sphingomyelinase enzymes can be further divided into three groups based on their distinct catalytic pH optimum. Acid sphingomyelinase is responsible for the catabolism of SM within lysosomes and deficiency of this enzyme leads to the human Niemann-Pick disease [135, 136]. More recently, acid sphingomyelinase has been reported to contribute to stress induced ceramide generation and subsequent pro-apoptotic signaling pathways [137-142]. On the other hand, alkaline sphingomyelinase is found in the intestinal tract, bile and liver; and participates in sphingomyelin digestion [143, 144]. Findings by Zhang *et al.* also suggest the potential involvement of alkaline sphingomyelinase in regulating mucosal growth, as well as alkaline phosphatase function [145].

Neutral magnesium-dependent sphingomyelinase activity was first reported by Scheider and Kennedy in 1967 [136]. Since then, several mammalian forms have been identified and studied. Neutral sphingomyelinase I was cloned based on remote sequence similarity to known bacterial sphingomyelinases in 1998 [146]. A year later, results from

overexpression and radiolabeling experiments suggest that this integral membrane protein does not hydrolyze sphingomyelin in cultured cells; and instead functions as a lyso-platelet activating factor (lysoPAF) phospholipase C [147]. However, studies involving neutral sphingomyelinase I knockout mouse do not support the proposed lysophospholipase C activity [148]. To date, the physiological roles of mammalian neutral sphingomyelinase I remain elusive.

In 2000, Hofmann and colleagues reported the identification of mammalian neutral sphingomyelinase II (NSMase II) based on remote similarity to bacterial sphingomyelinases using a bioinformatics-based gene discovery approach coupled with phylogenetic analysis [149]. This membrane protein consists of 655 amino acid residues and has an overall predicted molecular weight of 71 kDa. Biochemical studies of NSMase II suggest that it is magnesium-dependent and can be activated by unsaturated fatty acids as well as anionic phospholipids, such as phosphatidylserine [149, 150]. Unlike neutral sphingomyelinase I, NSMase II exhibits genuine sphingomyelinase activity both *in vitro* and *in vivo* with overexpression of this enzyme resulting in accelerated SM catabolism and an increase in ceramide levels [150]. As a result, NSMase II is viewed by many researchers as a prime candidate involved in ceramide generation and signaling.

More recently, neutral sphingomyelinase III was identified using peptide sequence from purified bovine sphingomyelinases [151]. A study by Cororan *et al.* suggests this 97 kDa protein may be linked to tumorigenesis and cellular stress response [152]. Independent confirmation of its activity and functional roles are yet to be reported.

1.4.2 NSMase II Protein Structure

Crystal structures of mammalian neutral sphingomyelinases have not yet been reported. Therefore, the currently accepted domain structures are based on a combination of amino acid sequence analysis, comparison to known bacterial neutral sphingomyelinase structures and various biochemical studies. Among the different neutral sphingomyelinase enzymes reported, structural homology is relatively low **(Figure 1.4.2-1).**

The proposed domain structure of NSMase II consists of two hydrophobic segments near the N-terminus, followed by a 200 residue collagen-like triple helices and a catalytic domain near the C-terminus **(Figure 1.4.2-1)** [149]. Although the two hydrophobic segments were initially proposed to be transmembrane domains, subsequent analysis of NSMase II membrane topology suggested that these segments do not actually span the entire membrane [153]. Two discrete anionic phospholipid (APL) binding domains were identified near the N-terminus which allow NSMase II to interact specifically with certain APLs including phosphatidylserine and phosphatidic acid [154]. The two APL binding domains partially overlap with the hydrophobic segments and additional mutagenesis studies reveal that Arg33, Arg45 and Arg48 are essential for interaction with APL in the first domain while Arg92 and Arg93 are critical for the second domain [154]. NSMase II can also be palmitoylated in two cysteine clusters via thioester bonds. This modification appears to be important for protein stability, as well as protein localization with palmitoylation deficient mutants showing rapid degradation and reduced membrane association [155].

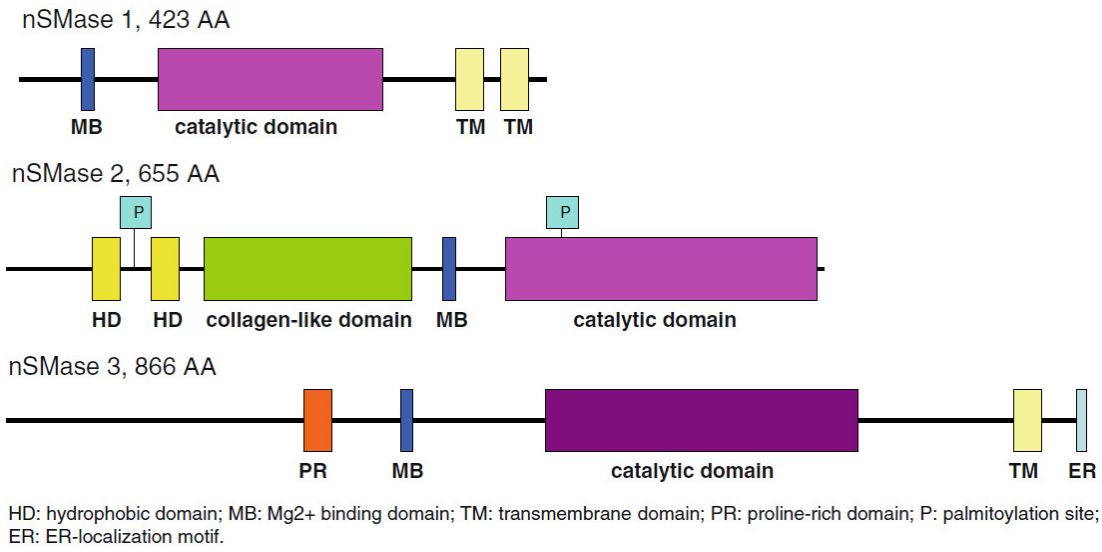

HD: hydrophobic domain; MB: Mg2+ binding domain; TM: transmembrane domain; PR: proline-rich domain; P: palmitoylation site; ER: ER-localization motif.

Figure 1.4.2-1 Proposed domain structures of human neutral sphingomyelinases

Neutral sphingomyelinase I (accession number O60906), neutral sphingomyelinase II (accession number Q9NY59) and neutral sphingomyelinase III (accession number NP060421). Image from Wu *et al.* (2010). "Mammalian Neutral Sphingomyelinases: Regulation and Roles in Cell Signaling Responses." Neuromolecular Medicine **12**(4): 320-330. With permission.

1.4.3 Subcellular Localization of NSMase II

The subcellular localization of NSMase II has been reported mainly in two organelles. Hofmann *et al.* observed localization predominantly at the Golgi in several cell lines derived from the brain [149]. In contrast, Marchesini *et al.* reported localization at the plasma membrane in confluence arrested MCF7 cells [156]. This apparent discrepancy in localization could be explained by results from subsequent studies which demonstrate NSMase II is transported between the plasma membrane and intracellular sites [157]. Using A549 epithelial cells, Clarke *et al.* observed acute translocation of NSMase II to the plasma membrane in response to tumor necrosis factor α [158]. In the same year, Levy *et al.* reported preferential trafficking of NSMase II to the plasma membrane under conditions of oxidative stress. Conversely, exposure to the antioxidant glutathione leads to nuclear localization of NSMase II, where both ceramide generation and apoptosis appear to be attenuated [159]. Together, these findings suggest subcellular localization of NSMase II affect its function and intracellular trafficking is one of the mechanisms regulating its catalytic activity.

1.4.4 Physiological Roles of NSMase II

Since its discovery, NSMase II has been shown to participate in a large number of physiological processes. This section will highlight some of the major biological functions attributed to NSMase II.

Role of NSMase II in Oxidative Stress

NSMase II is an important mediator of cellular stress response, mainly through the production of ceramide. In human airway epithelial cells (HAEC), exposure to oxidative stressors (H_2O_2 and cigarette smoke) selectively induces the activation of NSMase II;

with the resultant increase in cellular ceramide leading to HAEC apoptosis and lung injury. This apoptotic response to oxidative stress is lost upon siRNA silencing of NSMase II [159, 160]. In addition, NSMase II expression level is significantly higher in lung tissues obtained from smokers with pulmonary emphysema as compared to normal control subjects [161], suggesting an *in vivo* role of NSMase II in oxidative stress induced ceramide generation and lung injury. Interestingly, another study presented evidence that NSMase II and ceramide are critical for lung development. Poirier *et al.* studied lung phenotype from fro/fro mice, which express catalytically inactive NSMase II due to gene mutation, and noticed these animals exhibit symptoms similar to emphysema [162]. This raises the possibility that perhaps basal levels of NSMase II activity are required for normal lung development. More research is needed to fully understand this enzyme's biological function in pulmonary physiology.

In addition to pulmonary physiology, Clement *et al.* [163] demonstrated that certain types of neuronal cells can adapt to chronic oxidative stress by down-regulating NSMase activity. These cells exhibit increased intracellular cholesterol levels and are resistant to apoptosis. Extracellular treatment of the stress resistant cells with NSMase reverses the stress-resistant phenotype; while treating oxidative stress sensitive neuronal cells with NSMase inhibitors made the cells more resistant to oxidative stress.

Effect of NSMase II Activity on NOS

ER stress inhibits NSMase II activity in bovine aortic endothelial cells [164]. When cells were treated with the ER stressor palmitate or tunicamycin, reduced NSMase II activity leads to less ceramide generation, which attenuates ceramide dependent eNOS activation and results in decreases in NO production [165]. Similarly, siRNA mediated knock-down

of NSMase II also results in decreased NO generation [164]. This reduced bioavailability of NO promotes the dominance of vasoconstriction over vasodilation. As a result, decreased NSMase II activity is proposed to be a contributing factor in the induction of endothelial dysfunction.

In C6 rat glioma cells, inhibition of NSMase II activity prevents lipopolysaccharide induced iNOS expression, whereas inhibition of acid sphingomyelinase activity or ceramide *de novo* synthesis have no effect; suggesting ceramide generated by NSMase II is critical in the regulation of iNOS expression [166]. In agreement with this line of evidence, treatment with GW4869, a specific NSMase inhibitor, decreases iNOS expression in cultured human retinal pigment epithelial cells. This reduces nitrosative stress experienced by these cells and protects them from ER stress-induced apoptosis [167]. Overall, it appears that NSMase II catalyzed ceramide generation enhances NOS expression and activity.

Role of NSMase II in Inflammation

Long-term as well as acute stimulation with the pro-inflammatory cytokine tumour necrosis factor alpha (TNF-α) activates NSMase II in cultured cells, leading to rapid sphingomyelin hydrolysis and ceramide generation [165, 168, 169]. Clark *et al.* observed that exposure to TNF-α results in the translocation of NSMase II to the plasma membrane in a time- and dose-dependent manner; and this translocation and activation are dependent on p38 MAPK [158] and protein kinase C-delta [170]. In 2012, Barth and colleagues reported that TNF-α activates NSMase II in both neurons and non-neuron cells, causing ceramide accumulation, ROS formation and apoptosis [171]. Mechanistically, residues 309 to 319 of TNF-α receptor (p55) form the neutral

sphingomyelinase activation domain (NSD) [172]. However, this domain does not directly interact with NSMase II. Instead, NSD binds factor-associated with neutral sphingomyelinase (FAN) [173, 174], which interacts with receptor for activated C-kinase 1 (RACK1) [175], which in turn interacts with the polycomb group protein EED [176]. EED has been identified as a direct interaction partner for NSMase II [176] and physically couples NSMase II to the [RACK1-FAN-TNF receptor] complex allowing the transduction of signals initiated by TNF-α. Two other inflammatory cytokines, interleukin-1 beta [177, 178] and interferon gamma [179], can also increase NSMase II activity. Due to its involvement in these signaling pathways, NSMase II has been suggested as a potential drug target for inflammatory diseases [180].

Role of NSMase II in Cancer

The functional role of NSMase II in cancer initiation and progression has been under examination with some conflicting results reported. Nucleotide sequencing in a panel of human cancers discovered mutations in the gene encoding NSMase II in a subset of human leukemia. These mutations appear to result in defects in NSMase II stability and localization [181]. Another study looked at the genome-wide methylation status in hepatocellular carcinoma and identified NSMase II as a tumour suppressor, with overexpression leading to 50% reduction in proliferation [182]. However, NSMase II has also been reported to promote angiogenesis [183] and metastasis in breast cancer by regulating exosomal microRNA secretion [184]. Additional research in this area is needed before we can determine whether these conflicting findings are due to tissue-specific functions of NSMase II or some other unknown factors.

A number of anti-cancer drugs have been shown to act through NSMase II. Ito *et al.* observed that treatment with the chemotherapeutic drug daunorubicin increases NSMase II mRNA and protein levels in MCF7 cells. This up-regulation of NSMase II facilitates daunorubicin-induced cell death via ceramide generation [185]. In oligodendrocytes, NSMase II over-expression leads to increased ceramide generation and enhances apoptosis induced by staurosporine or C(2) ceramide [186]. In addition, protopanaxadiol, from the root extract of Panax ginseng, exerts cytotoxic effects against 5 different cancer cell lines through NSMase II activation and disruption of membrane lipid rafts [187].

1.4.5 Regulation of NSMase II

NSMase II is a redox sensitive enzyme and the antioxidant GSH inhibits its upregulation [159, 188]. In MCF7 cells, pre-treatment with GSH prevents diamide (thiol depleting agent) induced NSMase activation [189]. Similarly, treatment with GSH also protects HAEC from oxidative stress induced ceramide generation and apoptosis [159, 160]. It is interesting to note that human NSMase II has 23 cysteine residues. Whether these residues participate in the redox regulation of NSMase II activity, via modifications such as *S*-nitrosation, remain under investigation.

All-trans retinoic acid (ATRA) causes G_0/G_1 growth arrest in many cell types. Using MCF7 cells as a model system, Clarke *et al.* demonstrated that ATRA induced growth arrest is mediated by increased NSMase II activity and cellular ceramide levels [190]. This increase in NSMase II activity was later found to be mostly due to enhanced transcription. Ito *et al.* [191] uncovered 3 Sp1 sites within the 5' promoter region of NSMase II and presented evidence that ATRA treatment activates PKCδ which

phosphorylates Sp1. The phosphorylated Sp1 transcription factor then binds to the NSMase II promoter, resulting in increased level of transcription.

More recently, Filosto and colleagues reported that NSMase II is a phosphoprotein with phosphorylation occurring exclusively at serine residues [192]. This phosphorylation event was proposed to occur downstream of p38 MAPK and PKC [192]. In human airway epithelial cells, exposure to oxidative stress enhances NSMase II phosphorylation, which results in increased activity [192, 193]. The phosphatase calcineurin has also been reported to bind directly to NSMase II; and when the binding site was mutated away, NSMase II would exhibit constitutively elevated phosphorylation and activity [192]. Subsequent publication by the same research group identified five serine residues which are phosphorylated. Three of these residues (Ser289, Ser292 and Ser299) are positioned near the catalytic domain, while the other two (Ser173 and Ser208) are adjacent to the calcineurin binding site [193]. Overall, phosphorylation of these five serine residues appears to play a critical role in NSMase II activation under oxidative stress. In addition, NSMase II protein stability could also be regulated post-translationally by phosphorylation; with phosphorylation of Ser208 leading to increased stability [193].

In summary, NSMase II mediated sphingomyelin hydrolysis and ceramide generation has emerged as an important component in a number of signaling pathways. And as such, aberrant activation or inhibition of NSMase II could potentially contribute to the development of pathological conditions.

CHAPTER 2

O-aminobenzoyl-*S*-nitrosoglutathione is a Novel Fluorogenic Substrate for *S*-nitrosoglutathione Reductase

2.1 Introduction

Class III alcohol dehydrogenase (ADH III) was first isolated and purified from the human liver in 1984 by Wagner *et al.* [63]. Early studies have shown that this enzyme exhibits very poor activity towards ethanol, and instead, prefers long chain primary alcohols and aldehydes as substrates [63, 64]. A few years later, Koivusalo *et al.* provided strong evidence that ADH III is identical to formaldehyde dehydrogenase which catalyzes the NAD^+-dependent oxidation of hydroxymethylglutathione (HMGSH) [65]. In 1998, Jensen and colleagues discovered that in addition to formaldehyde dehydrogenase activity, ADH III can specifically and efficiently reduce *S*-nitrosoglutathione (GSNO) using NADH as the cofactor [54]. As a result of this enzymatic activity, ADH III was renamed GSNO reductase (GSNOR) by researchers in the *S*-nitrosothiol (SNO) signaling field.

SNO is the collective term used to describe molecules containing an NO group covalently attached to the sulfur atom of a thiol. GSNO, the substrate for GSNOR, is an endogenous SNO derived from glutathione, which is the most abundant cellular thiol. GSNO contributes to nitric oxide signaling via transnitrosation (the transfer of its NO group to reactive cysteine residues on target proteins). Once *S*-nitrosated, proteins often exhibit altered properties and/or functions. Over the years, there is increasing evidence which suggest that dysregulation of *S*-nitrosation correlates with a broad range of human pathologies [34, 194-196]. Since GSNO exists in equilibrium with *S*-nitrosated proteins, many of the biological functions of GSNOR are based on its ability to metabolize GSNO and drive protein denitrosation. This implies aberrant expression and/or activity of GSNOR could disturb cellular SNO homeostasis and contribute to pathogenesis.

Research has demonstrated various roles for GSNOR related to cardiovascular and respiratory health and disease. For example, GSNOR deficient mice are protected from experimentally induced asthma [116] and show cardio-protection with myocardial infarction [197]. GSNOR is linked to asthmatic responsiveness in humans with single nucleotide polymorphisms influencing responsiveness to bronchodilators [198, 199]. GSNOR also plays roles in vasculogenesis [200], bronchopulmonary dysplasia [201, 202], lung cancer [131] and cystic fibrosis [123]. The involvement of GSNOR in these significant heart- and lung-related pathologies has made it a promising therapeutic target for modulating intracellular SNO levels [118, 203, 204].

The conventional method for measuring GSNOR activity involves monitoring the decrease in absorbance at 340 nm. This decrease in absorbance is due to both NADH and GSNO consumption [54]. While this assay is easy to use, its application is limited to purified enzyme *in vitro*. Currently, there are no direct and specific spectroscopic probes to monitor GSNOR activity in cultured cell. Such probes would permit studies related to the localization and regulation of the enzyme within organelles as well as the direct assessment of the effectiveness of GSNOR-specific therapeutics.

In this chapter, we introduce *O*-aminobenzoyl-*S*-nitrosoglutathione (OAbz-GSNO) as a fluorogenic substrate for GSNOR. The characterization of OAbz-GSNO includes *in vitro* catalytic properties, cell permeability and usefulness in measuring GSNOR activity in live, primary murine lung endothelial cells.

2.2 Materials

DNase I (DN25), glutathione, reduced (G4251), imidazole (I0125), isatoic anhydride (I12808), isopropyl β-D-1-thiogalactopyranoside (I6758), lysozyme (L7651), β-nicotinamide adenine dinucleotide, reduced (N8129), phenylmethylsulfonyl fluoride (7626), QAE sephadex (Q25120), sodium nitrite (S2252), sodium phosphate dibasic (S7907), sodium phosphate monobasic (S8282) and Triton X-100 (T9284) were purchased from Sigma-Aldrich. Glycerol (G3700) and sodium chloride (S2830) were purchased from ACP Chemicals. Kanamycin (BP906) and Tris-HCl (BP153) were purchased from Fisher Scientific. Dithiothreitol (100597) was purchased from MP Biomedicals. The inhibitor N6022 was obtained from MedChem Express, Princeton, NJ.

2.3 Methods

2.3.1 S-nitrosoglutathione (GSNO) synthesis

Reduced glutathione (5 mmol) was dissolved in 8 mL of cold water and 2.5 mL of 2 M HCl. Equal amount of sodium nitrite (5 mmol) was added and the reaction mixture was stirred at 4°C in the dark for 40 minutes. After 40 minutes, GSNO was precipitated using 10 mL of cold acetone. Finally, the pink product was washed with cold water (5 X 1 mL) and cold acetone (3 X 10 mL) before it was lyophilized for storage at -20°C.

2.3.2 O-aminobenzoyl GSNO synthesis

GSNO (0.15 mmol) was dissolved in 3.0 mL of 0.5 M phosphate buffer (pH 8.5). To this, excess isatoic anhydride (0.9 mmol), which has been previously recrystallized from isopropanol, was added and the mixture was stirred at 4°C for 24 hours. After the insoluble salts were removed by centrifugation, the clear supernatant was applied onto a BioRad econo-column containing 2 mL of packed QAE-Sephadex pre-equilibrated with

distilled water. Unreacted isatoic anhydride was removed with 10 mL of wash buffer (0.1 M phosphate, pH 7.4). OAbz-GSNO, visualized as the red-orange band adhering to the top of the column, was then eluted with wash buffer containing 1 M NaCl. 5 µl from each of the red-orange fractions corresponding to the product was added to a fluorescence cuvette containing 1.0 mL of phosphate buffered saline (PBS). The emission at 415 nm was monitored (excitation at 312 nm) before and after the addition of 10 mM dithiothreitol (DTT). Fractions which showed maximal fluorescence enhancement in the presence of DTT were pooled and aliquoted for subsequent studies. OAbz-GSNO is stable for at least 1 year when stored at -80°C, in the absence of repeated freeze-thaw cycles.

2.3.3 NMR characterization

Pooled OAbz-GSNO was lyophilized and then re-dissolved in minimum volume D_2O. Spectra were collected on a Bruker 500 MHz Avance III spectrometer using a BBFO probe. Peak assignments were based on a ^{1}H-^{1}H COSY45 spectrum. ^{1}H-^{13}C HMQC and HMBC experiments were also performed to help determine ^{1}H-^{13}C correlations.

2.3.4 ADH5 sub-cloning

Human ADH5, which encodes full length GSNOR, was purchased from Origene (SC119755) and sub-cloned into the bacterial expression vector pET28b using Cold Fusion Cloning Kit (MJS BioLynx Inc. SYMC010A1). Cloning strategy involves direct ligation of PCR amplified gene of interest to the linearized destination vector.

Primers used for PCR were designed according to manufacturer's guidelines and contain bases complimentary to the gene of interest as well as bases complementary to the linearized destination vector. The following primers were used for ADH5 sub-cloning:

Forward 5'– GTGCCGCGCGGCAGCCATATGGCGAACGAGGTTATCAAG –3'

Reverse 5'– GTGGTGGTGGTGGTGCTCGAGAATCTTTACAACAGTTCGAATG –3'

Prior to the ligation reaction, destination vector pET28b was linearized by digestion with restriction enzymes NdeI and XhoI; and both PCR amplified ADH5 and linearized pET28b were gel purified. Ligation was performed according to manufacturer's protocol and the ligated plasmid DNA was transformed directly into chemically competent DH5 *E.coli*. Colonies were screened using diagnostic restriction enzyme digest and later by partial sequencing (Robart's Research Institute, London Regional Genomics Center, London, Ontario, Canada). The final recombinant GSNOR contains two 6X-histidine tags, one at each terminus.

2.3.5 GSNOR expression and purification

pET28b_ADH5 was transformed into BL21(DE3) *E.coli*. This plasmid encodes full length human GSNOR with terminal 6X-histidine tags to facilitate purification. A single colony from the transformation plate was inoculated into 25 mL of 2X YT medium containing 50 µg/mL kanamycin and the culture was grown overnight at 37°C with shaking. This overnight starter culture was then used to inoculate 1L of 2X YT medium containing 50 µg/mL kanamycin and the culture was again grown at 37°C until optical density reached approximately 0.6. At this point, GSNOR expression was induced by the addition of IPTG to a final concentration of 0.4 mM. The induced culture was grown for an additional 24 hours at room temperature with shaking before cells were harvested by

centrifugation (4000 *g*, 30 minutes, 4°C). Following centrifugation, the supernatant was discarded and the bacterial cell pellet was resuspended in lysis buffer (50 mM Tris-HCl pH 8, 150 mM NaCl, 15 mM imidazole, 1 mM DTT, 1 mM PMSF, 0.5% Triton X-100, 50 µg/mL DNase I and 100 µg/mL lysozyme). The crude lysate was incubated on ice for 30 minutes and further lysed by pulse sonication (20 seconds on, 20 seconds off, 30 cycles). Another round of centrifugation (11300 *g*, 30 minutes, 4°C) was performed to clarify the lysate and the clarified supernatant was applied to nickel affinity column (Sigma P6611) pre-equilibrated with lysis buffer. Affinity purification was performed strictly following manufacturer's protocol published by Sigma Aldrich with some modifications in buffer composition. The wash buffer contains 50 mM Tris-HCl pH 8, 150 mM NaCl and 50 mM imidazole while the elution buffer contains 50 mM Tris-HCl pH 8, 150 mM NaCl and 300 mM imidazole. Finally, the eluted protein was buffer exchanged into storage solution (58 mM Na_2HPO_4, 17 mM NaH_2PO_4, 68 mM NaCl, 15% glycerol) using Amicon centrifugal filter (Millipore UFC903008). When stored at -80°C, purified GSNOR is stable and can retain its activity for at least 6 months.

2.3.6 GSNOR enzyme assay using GSNO as the substrate

NADH stock solution (20 mM) was prepared with MilliQ water. GSNO stock solutions (10 mM and 1 mM) were prepared fresh daily using PBS. Total reaction volume was kept at 500 µL using PBS as the reaction buffer. Each reaction contained 80 µM NADH and indicated concentration of GSNO. Reaction was initiated by the addition of purified GSNOR (1 µg) and the rate of NADH consumption was quantified by measuring the rate of absorbance decrease at 340 nm. Each reaction was monitored for 120 seconds using Agilent 8453 UV/Vis spectrophotometer at 25°C.

2.3.7 GSNOR enzyme assay using OAbz-GSNO as the substrate

OAbz-GSNO concentration was determined by measuring its absorbance at 320 nm ($\varepsilon \approx 2800\ M^{-1}\ cm^{-1}$). Necessary dilutions were made using PBS. NADH stock solution (20 mM) was prepared using MilliQ water. Total reaction volume was kept at 500 µL using PBS as the reaction buffer. Each reaction contained 80 µM NADH and indicated concentration of OAbz-GSNO ranging from 0 to approximately 720 µM. Reaction was initiated by the addition of purified GSNOR (1 µg) and initial reaction rates were determined by monitoring fluorescence increase (excitation 312 nm; emission 415 nm) for 2 minutes using Cary Eclipse fluorescence spectrophotometer.

2.3.8 GSNOR inhibition studies

Stock solutions (50 mM) of the GSNOR-specific inhibitors N6022 and C3 were prepared using DMSO. Similar to the assay mentioned in Section 2.3.7, total reaction volume was 500 µL and each reaction contained 40 µM NADH, 1 µg GSNOR and various amounts of inhibitor. The range of inhibitor concentration studied was 0 to 1000 nM for N6022 and 0 to 50 µM for C3. Reaction was initiated by adding 110 µM OAbz-GSNO and changes in fluorescence were monitored for 2 minutes.

2.3.9 Isolation and culture of murine lung endothelial cells

C57BL/6 mice (4 – 6 weeks) were anesthetized by CO_2 inhalation. After the animal's skin was cleaned with 70% ethanol, lung tissues were removed and placed in a 50 mL conical tube containing DMEM and shipped to Cell Biologics (Chicago, Il) for isolation of primary lung endothelial cells. Tissue slices were prepared, washed and suspended in Hanks balanced saline solution (HBSS). After excess HBSS was removed, tissue slices were minced and transferred to a sterile tube. Minced tissues were digested and the

released cells were harvested by centrifugation. Cells collected were incubated with primary antibody against platelet/endothelial cell adhesion molecule 1 (PECAM-1), followed by the addition of magnetic beads pre-coated with secondary antibody. Finally, cells released from the magnetic beads were washed and cultured on gelatin coated culture dishes. These primary lung endothelial cells were characterized by their typical cobblestone morphology, PECAM-1/CD31 and VE-cadherin expression as well as Dil-Ac LDL uptake. Isolated endothelial cells were grown in complete mouse endothelial cell medium (Cell Biologics) supplemented with attachment factor (Cell Biologics). Cells between passage 3 and 7 were used for all subsequent studies.

2.3.10 Live cell imaging

Primary pulmonary endothelial cells from C57BL/6 mice were grown on glass coverslips, washed 2 times with Dulbecco's phosphate buffered saline (DPBS with Ca^{2+} and Mg^{2+}) and loaded with 1.85 mM OAbz-GSNO for 10 mins at 37°C in the cell culture incubator. Unloaded cells were used as negative controls. For studies involving GSNOR inhibitors, cells were first treated with either 25 μM C3 or 25 μM N6022 for 1 hour at 37°C and then loaded with OAbz-GSNO. Their respective paired controls (+ inhibitor / - OAbz-GSNO) were included for comparison. Following OAbz-GSNO loading, cells were washed 4 times with DPBS before imaging. When cells were ready to be imaged, the coverslip with cells was placed in a stainless steel chamber and mounted on Zeiss 780 confocal microscope stage. Cells were imaged in DPBS with 40X NA1.1 water objective. During the course of imaging, cells were maintained at 37°C using stage temperature control and under humidified gas flow. The compound OAbz-GSNO was excited using

2p 740 nm at 3% and emission was collected from 411-482 nm range with 800v PMT at 5 second intervals over 5 minutes using Time Series.

2.4 Results and Discussion

2.4.1. OAbz-GSNO synthesis

OAbz-GSNO synthesis consists of two steps. In the first step, reduced glutathione is reacted with acidified nitrite to form GSNO **(Figure 2.4.1-1 A)**. This well-characterized reaction is fast with high yields. Product can be precipitated using acetone and stored as solid powder. When stored at -20°C, GSNO is stable for at least 6 month. In the second step, OAbz-GSNO is formed by the nucleophilic attack of the α-amino group of glutathione on the anhydride carbonyl of isatoic anhydride **(Figure 2.4.1-1 B)**. The final product OAbz-GSNO can either be lyophilized or stored directly as a solution in -80°C.

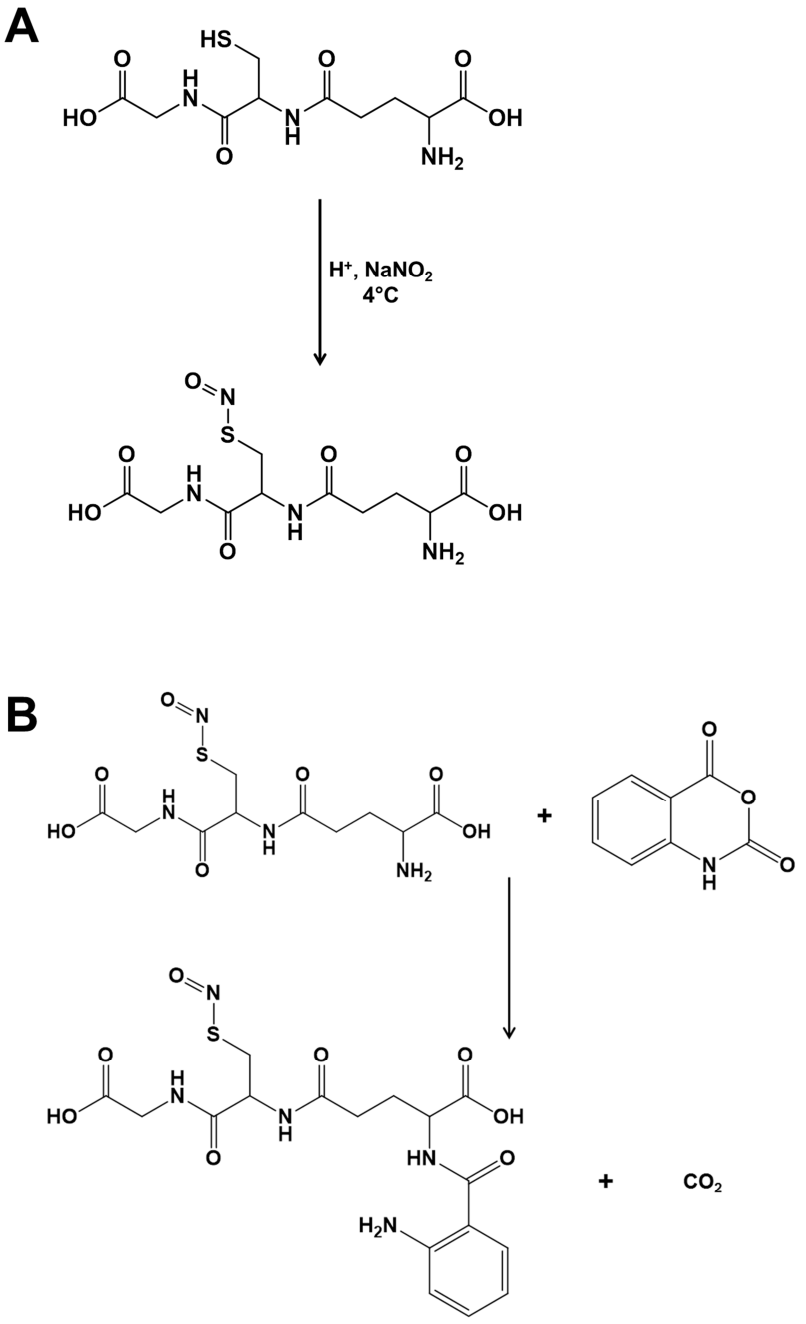

Figure 2.4.1-1 OAbz-GSNO synthesis is a two-step process

(A) Synthesis of GSNO using GSH and acidified sodium nitrite. **(B)** GSNO reacts with isatoic anhydride to produce OAbz-GSNO.

2.4.2 NMR characterization

NMR spectra were used to confirm the success of OAbz-GSNO synthesis. By comparison to the starting material GSNO, attachment of the *O*-aminobenzoyl group resulted in significant chemical shift for the glutamate α proton (3.74 ppm to 4.22 ppm) as well as the appearance of aromatic proton signals **(Figures 2.4.2-1 and 2.4.2-2, Table 2.4.2)**. These observations are in agreement with predicted chemical shift changes, and provide strong evidence for the successful synthesis of OAbz-GSNO.

In addition to OAbz-GSNO, NMR also identified a minor chemical species in which the nitroso-group is absent (i.e. OAbz-GSH, peaks denoted by *). Formation of OAbz-GSH is most likely due to small amounts of GSH present in the starting material rather than NO loss post-synthesis as peaks corresponding to GSH were detected in the starting material.

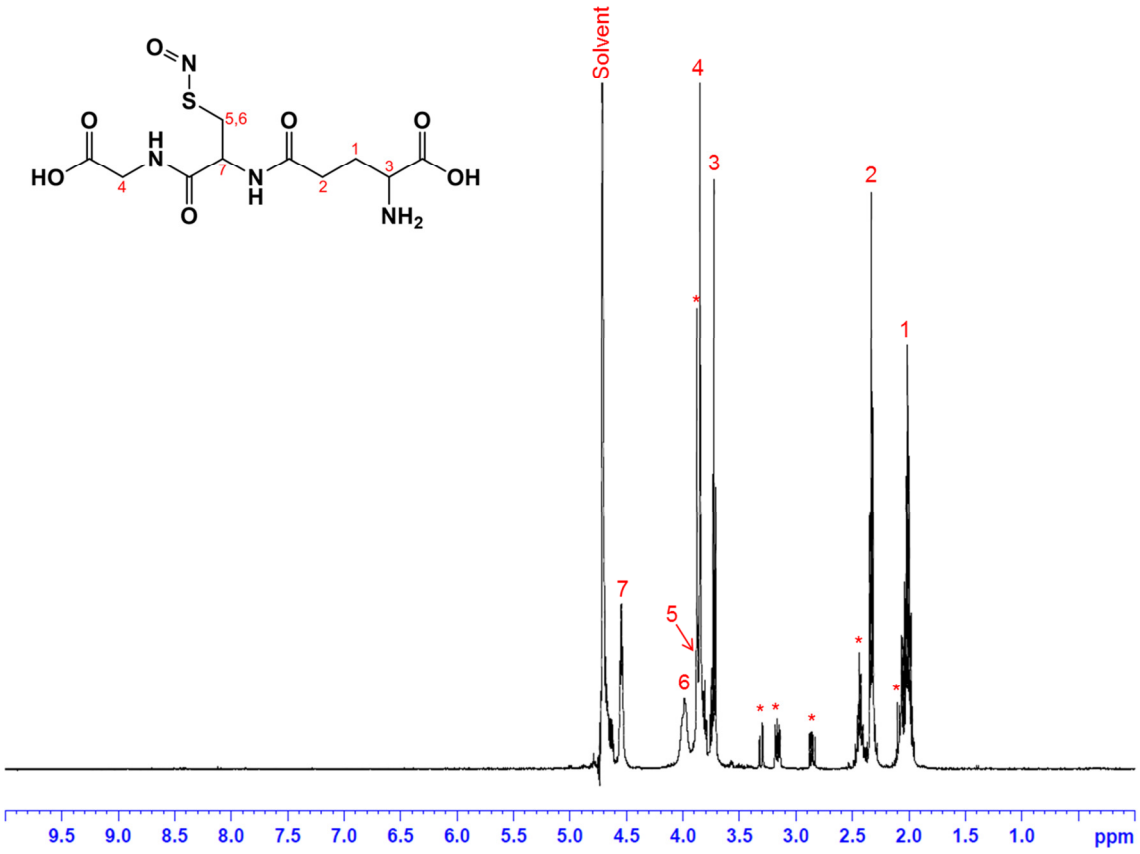

Figure 2.4.2-1 ^{1}H NMR of GSNO

Lyophilized GSNO was dissolved in minimum volume D_2O. Spectrum was collected on a Bruker 500 MHz Avance III spectrometer using a BBFO probe.

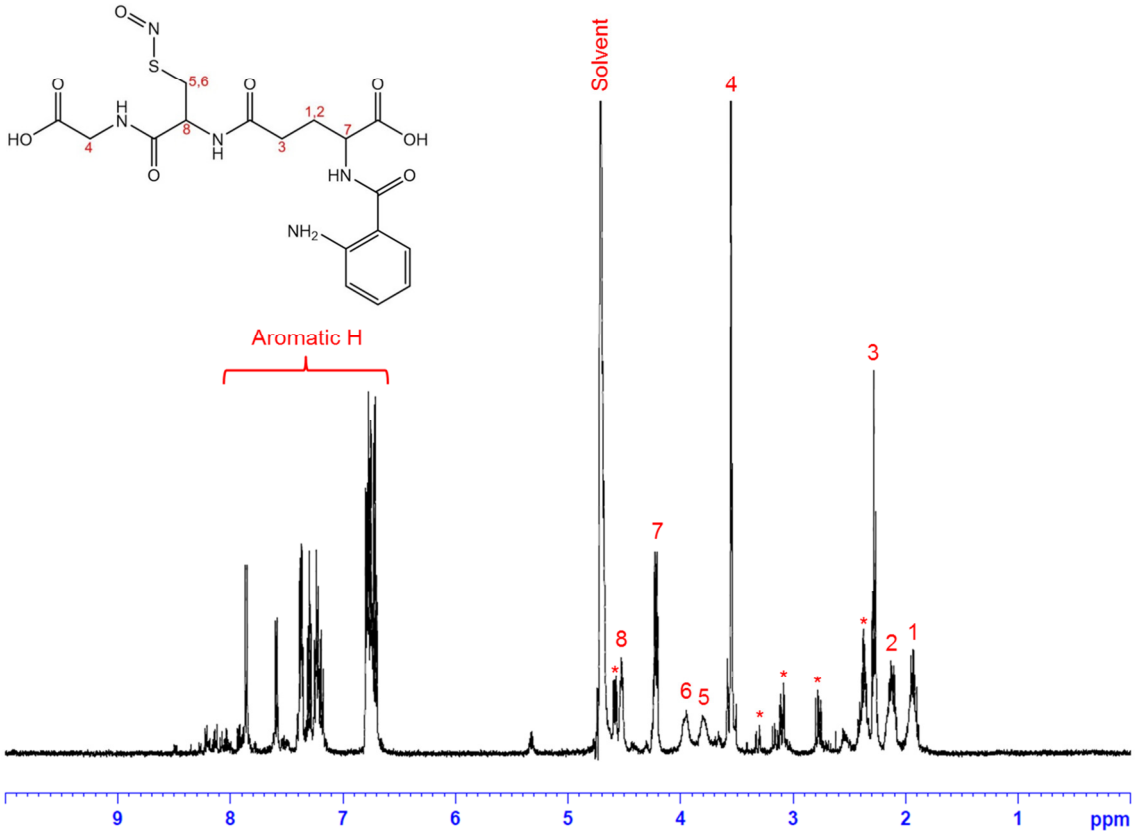

Figure 2.4.2-2 ^{1}H NMR of OAbz-GSNO

Lyophilized OAbz-GSNO was dissolved in minimum volume D_2O. Spectrum was collected on a Bruker 500 MHz Avance III spectrometer using a BBFO probe.

Table 2.4.2 ^{1}H NMR chemical shifts of GSNO and OAbz-GSNO

GSNO (500 MHz, D_2O, δ)	2.04 (m, 2H, Glu Hβ) 2.33 (t, 2H, Glu Hγ) **3.74 (t, 1H, Glu Hα)** 3.84 (s, 1H, Gly Hα) 3.87 (b, 1H, Cys Hβ) 4.00 (b, 1H, Cys Hβ) 4.54 (t, 1H, Cys Hα)
OAbz-GSNO (500 MHz, D_2O, δ)	1.94 (m, 1H, Glu Hβ) 2.12 (m, 1H, Glu Hβ) 2.28 (t, 2H, Glu Hγ) 3.55 (s, 2H, Gly Hα) 3.80 (b, 1H, Cys Hβ) 3.96 (b, 1H, Cys Hβ) **4.22 (q, 1H, Glu Hα)** 4.52 (t, 1H, Cys Hα) **6.75-7.90 (aromatic H)**
Abbreviations: δ, chemical shift in parts per million (ppm) downfield from the standard Multiplicities: s, singlet; t, triplet; q, quartet; m, multiplet; b, broadened	

2.4.3 Fluorescence properties of OAbz-GSNO

Based on previous studies with fluorescently tagged *S*-nitrosothiols [205-207], the –SNO group can quench a fluorophore if two conditions are met:

1) The fluorophore excitation spectrum overlaps the –SNO absorbance spectrum.

2) The overall structure of the molecule permits the fluorophore and the –SNO moiety to be in close physical proximity.

The fluorophore *O*-aminobenzoyl fulfills both conditions. First, the excitation spectrum of *O*-aminobenzoyl exhibits λ_{max} at around 312 nm. This overlaps the –SNO absorbance spectrum with its λ_{max} at around 335 nm. Second, since GSNO is a small molecule, its physical structure allows *O*-aminobenzoyl and –SNO to come into close proximity, resulting in fluorescence quenching. Chemical changes to the –SNO functionality, such as loss of NO via denitrosation or reduction of –SNO to –SNHOH by GSNOR, would lead to a loss in spectra overlap **(Figure 2.4.3-1)**. This in turn results in enhanced fluorescence that could be detected.

Consistent with this concept, OAbz-GSNO is only weakly fluorescent upon synthesis. Denitrosation mediated by the addition of strong reducing agent DTT increases OAbz-GSNO fluorescence by approximately 14 fold **(Figures 2.4.3-2)**. This increase in fluorescence is the direct consequence of NO loss, which removes the quenching effect.

In addition to OAbz-GSNO, Eosin-GSNO and dansyl-GSNO were also synthesized and screened for their applicability. Both Eosin-GSNO and dansyl-GSNO exhibit insufficient fluorescence quenching and are determined to be poor substrates for GSNOR.

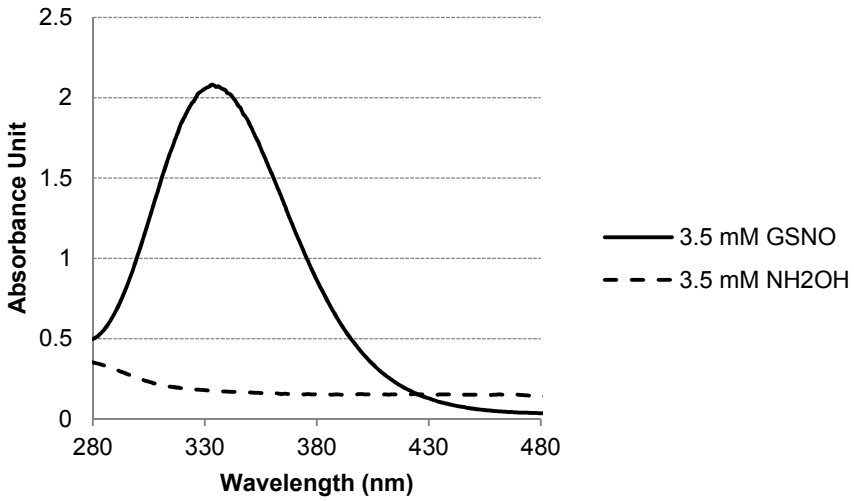

Figure 2.4.3-1 Spectral difference between GSNO and NH_2OH

GSNO exhibits maximum absorbance at 335 nm. This overlaps with the *O*-aminobenzoyl excitation spectrum. Hydroxylamine (NH_2OH), on the other hand, does not absorb in this wavelength range.

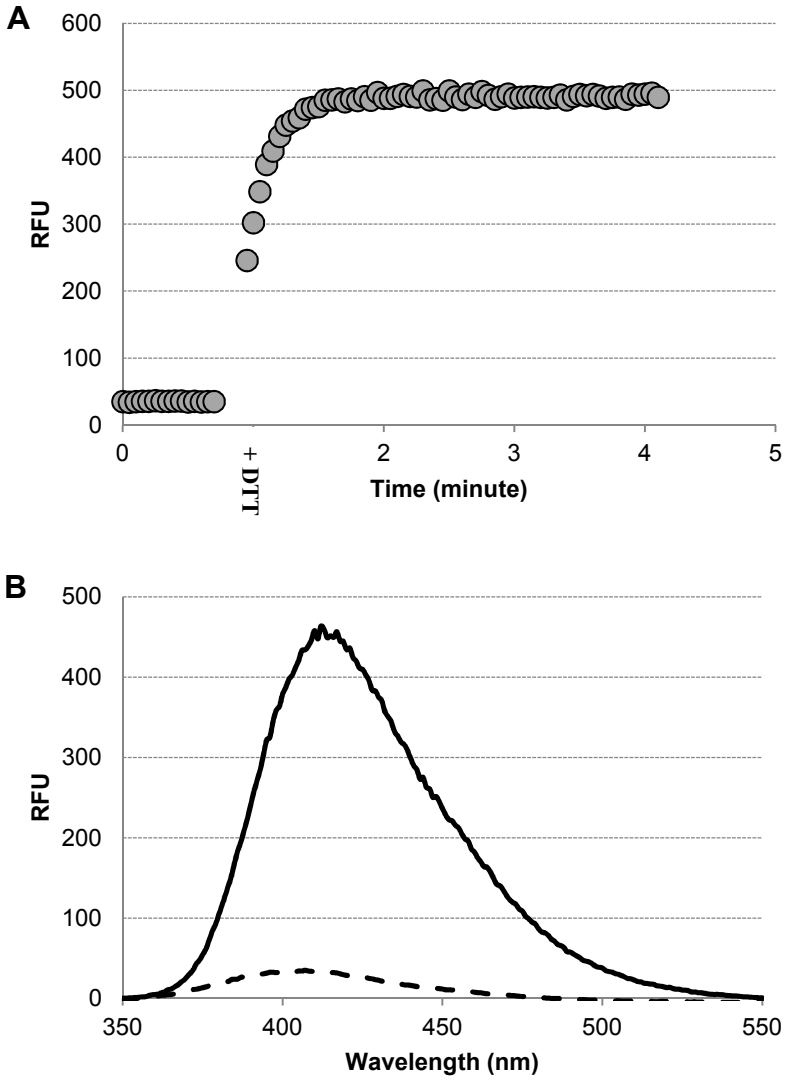

Figure 2.4.3-2 DTT mediated OAbz-GSNO denitrosation results in significant fluorescence enhancement

(A) Addition of DTT to the final concentration of 10 mM increases OAbz-GSNO fluorescence (excitation 312 nm, emission 415 nm) by approximately 14 fold. **(B)** Fluorescence emission spectra of 75 μM OAbz-GSNO before (dash line) and after (solid line) the addition of 10 mM DTT. Excitation wavelength is set to 312 nm.

2.4.4 OAbz-GSNO is a fluorogenic substrate for GSNOR

To assess whether OAbz-GSNO works as a fluorogenic substrate for GSNOR *in vitro*, full length human ADH5 (NCBI reference sequence NM_000671.3), which encodes GSNOR, was cloned into an *E. coli* expression vector for recombinant protein production. Cloning success was verified by diagnostic restriction digest and partial DNA sequencing.

The recombinant GSNOR protein carries two poly-histidine tags, one at each terminus, to facilitate Nickel affinity purification. Purified GSNOR exhibits monomeric mass of approximately 40 kDa **(Appendix C)**. Conventional NADH consumption assay was used to determine whether the purified GSNOR is active *in vitro*. As shown in **Figure 2.4.4-1**, in the absence of substrate, absorbance at 340 nm was relatively constant. When substrate (50 μM GSNO) was included in the reaction mixture, GSNOR catalyzed GSNO reduction led to a rapid decrease in absorbance as both GSNO and the cofactor NADH were being consumed.

Next, a series of experiments were performed using OAbz-GSNO as the substrate. Results show that GSNOR mediated reduction of OAbz-GSNO is capable of removing the quenching effect and causes OAbz-GSNO fluorescence to increase in a time dependent manner **(Figure 2.4.4-2)**. Specifically, OAbz-GSNO is stable in the absence of GSNOR for up to 45 minutes, as evidenced by no fluorescence increase. Upon the addition of GSNOR, fluorescence begins to increase over time. After 45 minutes, approximately 10 fold increase in fluorescence was observed. When compared to the chemical reduction of OAbz-GSNO by DTT, the full 14 fold increase in fluorescence was

not observed in this enzymatic reaction since not all of the OAbz-GSNO was converted to product within 45 minutes.

The kinetic parameters of GSNOR using OAbz-GSNO as the substrate were also assessed. Time dependent changes in fluorescence were monitored as a function of OAbz-GSNO concentration in the presence of catalytic amounts of purified GSNOR. The initial rates of fluorescence change per unit time were hyperbolic with an apparent K_m of 320 μM **(Figure 2.4.4-3)**. V_{max} was estimated to be 19.1 fluorescent units per minute, which equals approximately 1.65 nmol –SNO reduced per minute based on the calibration curve **(Figure 2.4.4-4)**. Both K_m and V_{max} were calculated using the Excel analysis tool *Solver*. The observed K_m value of 320 μM for OAbz-GSNO is much larger than the previously reported K_m value of 28 μM for GSNO [54, 111]. This is likely due to the bulk of the *O*-aminobenzoyl group not being well accommodated by the GSNOR active site.

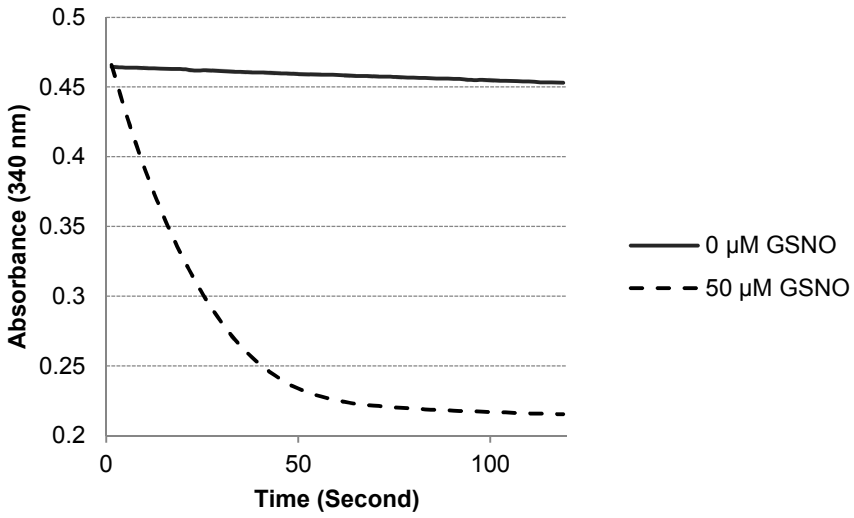

Figure 2.4.4-1 Purified recombinant GSNOR is active

Absorbance at 340 nm was monitored as a function of time. Each reaction contains 1 μg GSNOR, 80 μM NADH, and GSNO at indicated concentrations. PBS was used as the reaction buffer.

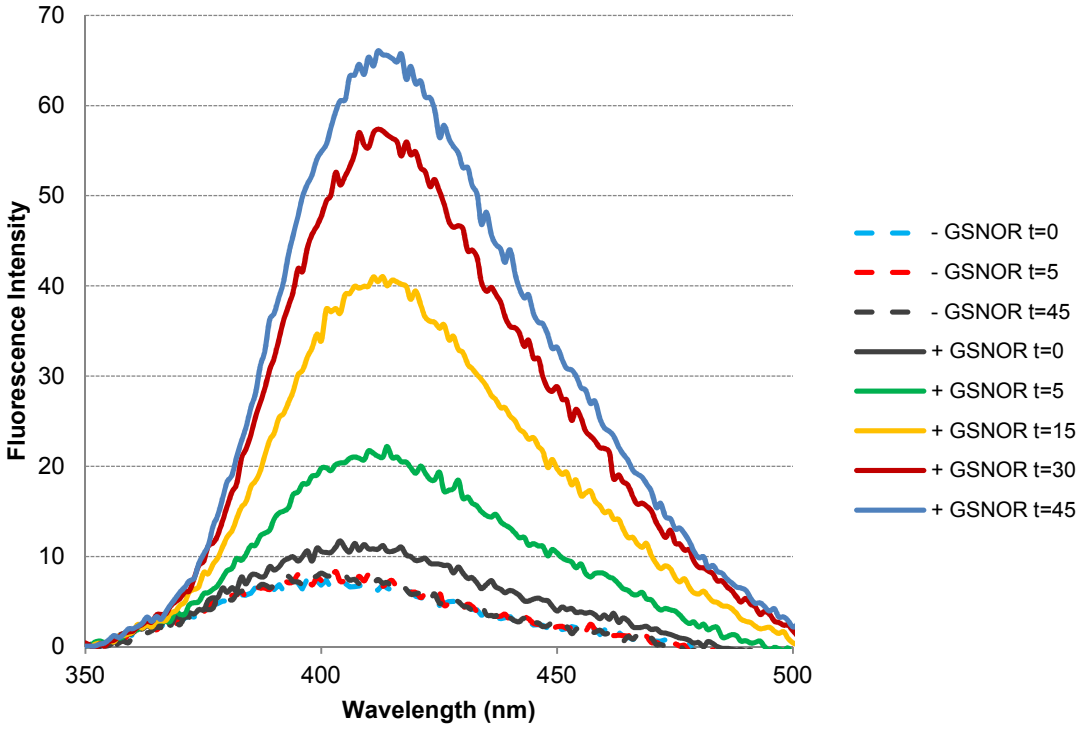

Figure 2.4.4-2 GSNOR mediated reduction of OAbz-GSNO leads to increased fluorescence

Comparison of OAbz-GSNO (10 µM) fluorescence emission spectra in the presence of NADH (10 µM) without GSNOR at t= 0, 5 and 45 minutes; as well as in the presence of GSNOR (6 µg) and NADH (10 µM) at t= 0, 5, 15, 30 and 45 minutes. PBS was used as the reaction buffer. Excitation wavelength was set to 312 nm.

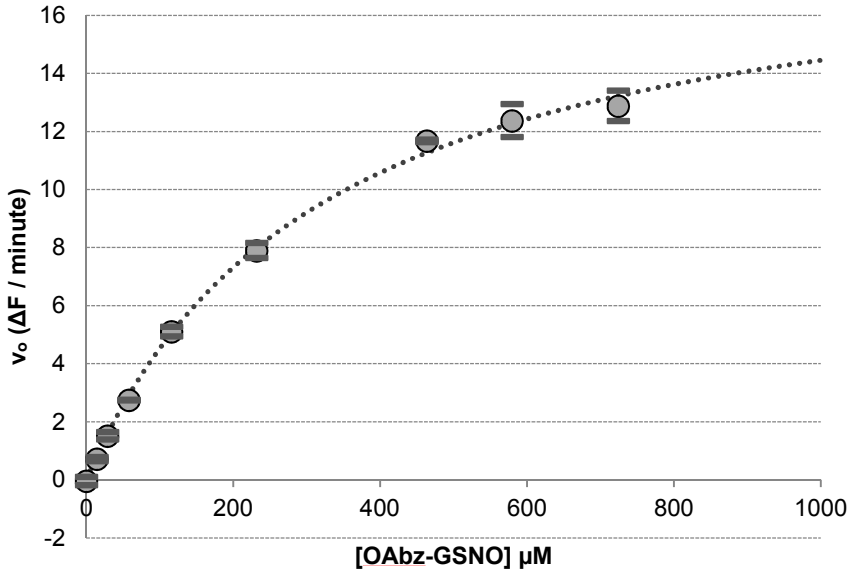

Figure 2.4.4-3 Kinetic characterization of OAbz-GSNO

Initial rates of OAbz-GSNO fluorescence increase (excitation at 312 nm, emission at 415 nm) were determined as a function of OAbz-GSNO concentration in the presence of GSNOR (1 µg) and NADH (80 µM). Error bars represent standard deviation (n=5).

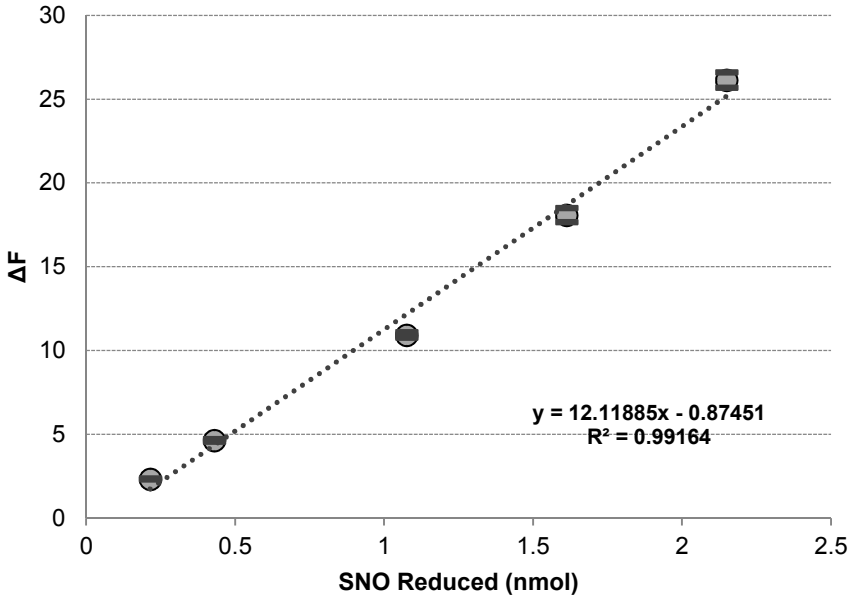

Figure 2.4.4-4 OAbz-GSNO calibration curve

Known amounts of OAbz-GSNO were fully reduced using DTT. Quantitative changes in fluorescence (excitation at 312 nm, emission at 415 nm) were recorded. Error bars represent standard deviation (n=5).

2.4.5 In vitro GSNOR inhibition studies

To further confirm that the observed fluorescence increase was specifically due to GSNOR mediated –SNO reduction, GSNOR inhibitors N6022 and C3 were used **(Figure 2.4.5-1)**. Both inhibitors were able to prevent OAbz-GSNO fluorescence increase *in vitro*. This demonstrates substrate fluorescence is responsive to GSNOR activity.

Based on this set of experiments, the IC_{50} of N6022 was estimated to be 21.1 nM ± 3.1 nM **(Figure 2.4.5-2 A)**; while the estimated IC_{50} of C3 was 1.9 μM ± 0.2 μM **(Figure 2.4.5-2 B)**. The IC_{50} value obtained for C3 was very close to the previously reported value of 1.1 μM [124]. On the other hand, the estimated IC_{50} of 21.1 nM for N6022 was slightly larger than the reported value of 8 nM [126]. This lower affinity observed for N6022 with OAbz-GSNO is likely related to the fact that N6022, as an uncompetitive inhibitor, binds to the enzyme-substrate complex. The higher IC_{50} observed suggests that the bulkiness of the *O*-aminobenzoyl moiety might decrease interactions between active site bound substrate and N6022. Conversely, noncompetitive inhibitors (such as C3) bind to a site peripheral to the active site. In this case, the binding of C3 was not affected, as evidenced by the close to reported IC_{50} obtained using OAbz-GSNO as the substrate.

N6022

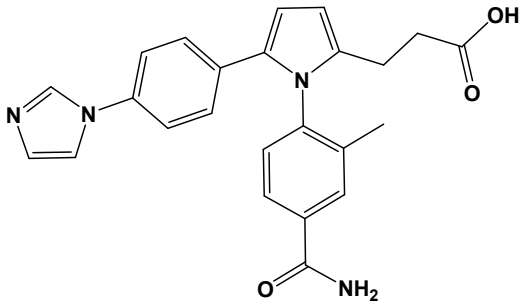

C3

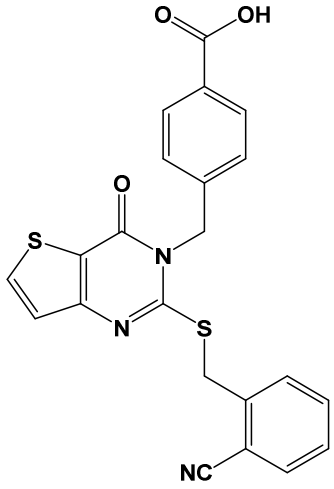

Figure 2.4.5-1 Structures of GSNOR-specific inhibitors

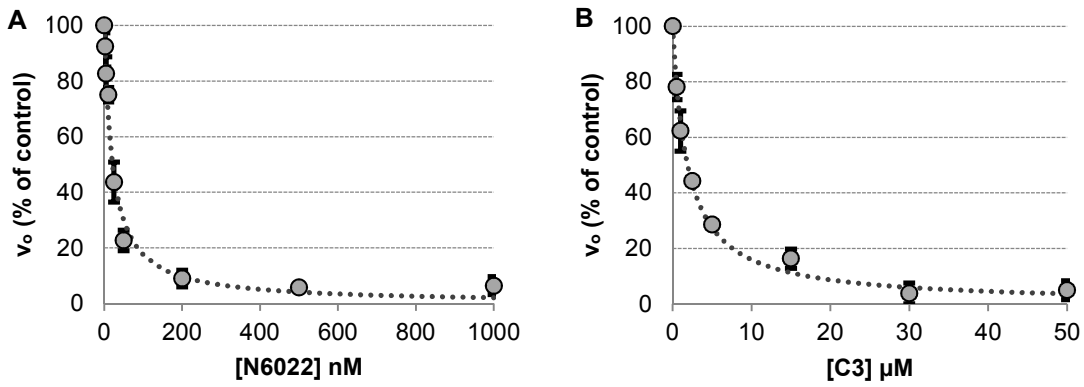

Figure 2.4.5-2 GSNOR-specific inhibitors N6022 and C3 inhibit GSNOR-mediated OAbz-GSNO reduction *in vitro*

(A) Initial rates of OAbz-GSNO fluorescence change were monitored at 415 nm (excitation at 312 nm). Each reaction contained 110 µM OAbz-GSNO, 1 µg GSNOR, 80 µM NADH and varying amounts of N6022. **(B)** Similarly, initial rates of OAbz-GSNO fluorescence change were monitored at 415 nm with varying amounts of C3 included in each reaction. Error bars represent standard deviation (n=3).

2.4.6 OAbz-GSNO is cell permeable

Confocal microscopy was used to assess membrane permeability of OAbz-GSNO. GSNO alone is largely hydrophilic and does not readily cross cell membranes. However, the addition of aromatic groups to make charged hydrophilic compounds membrane permeable is a well-established technique in pharmacology [208]. By exposing primary endothelial cells to OAbz-GSNO and monitoring fluorescence at 410 nm, strong fluorescence was observed in the perinuclear/Golgi region of these cells **(Figure 2.4.6-1 B)**, clearly demonstrating that OAbz-GSNO is cell membrane permeable. Furthermore, GSNOR is localized to the same subcellular region as visualized by immunofluorescence **(Figure 2.4.6-1 A)**. Since both enzyme and substrate are in the same subcellular compartment, this will likely facilitate GSNOR mediated reduction of OAbz-GSNO.

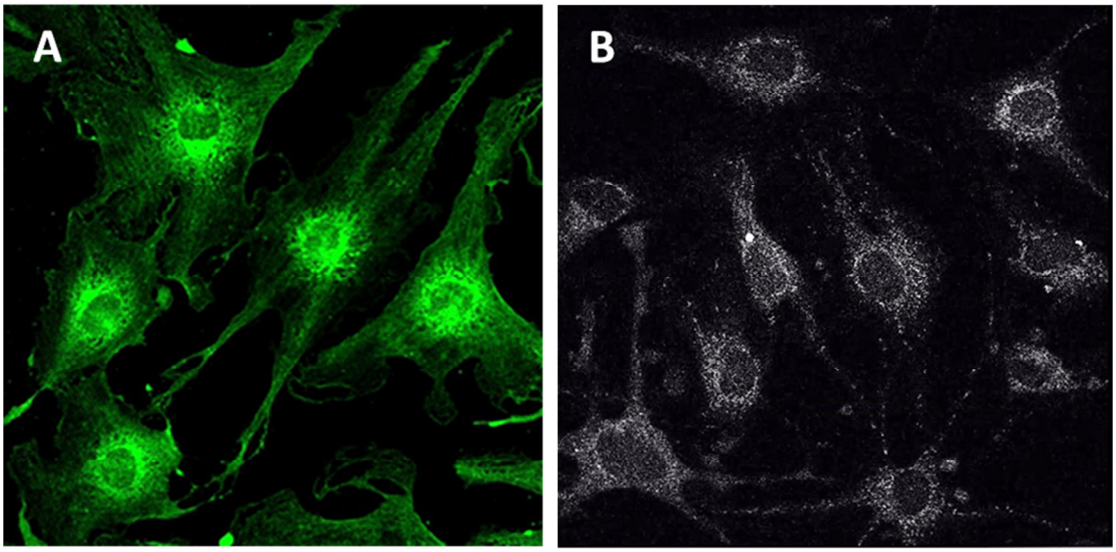

Figure 2.4.6-1 GSNOR and OAbz-GSNO exhibit similar subcellular localization patterns in primary murine lung endothelial cells

(A) Primary mouse lung endothelial cells were grown on coverslips, fixed with 3.7% formaldehyde and permeabilized with digitonin. GSNOR expression was visualized using anti-GSNOR primary antibodies and Alexa Fluor 488 secondary antibodies. **(B)** Primary mouse lung endothelial cells were grown on glass coverslips and loaded with 1.85 mM OAbz-GSNO for 10 minutes at 37°C. Fluorescence from live cells was visualized using Zeiss 780 confocal microscope. Imaging studies were performed by Dr. Lisa Palmer and colleagues at the University of Virginia.

2.4.7 Live-cell imaging studies

Similar to the *in vitro* experiments, live-cell imaging studies demonstrate that the fluorescence of OAbz-GSNO loaded cells increases over time, indicating that the –SNO functionality of OAbz-GSNO is being altered **(Figure 2.4.7-1)**. To determine if the observed fluorescence change is due to endogenous cellular GSNOR activity, cells were treated with GSNOR-specific inhibitors (N6022 or C3) prior to OAbz-GSNO loading. Upon GSNOR inhibition, the rate of fluorescence increase in OAbz-GSNO loaded cells is reduced to levels comparable to no treatment control cells **(Figure 2.4.7-1)**. This offers strong evidence that the observed increase in live cell fluorescence is reporting on endogenous GSNOR activity.

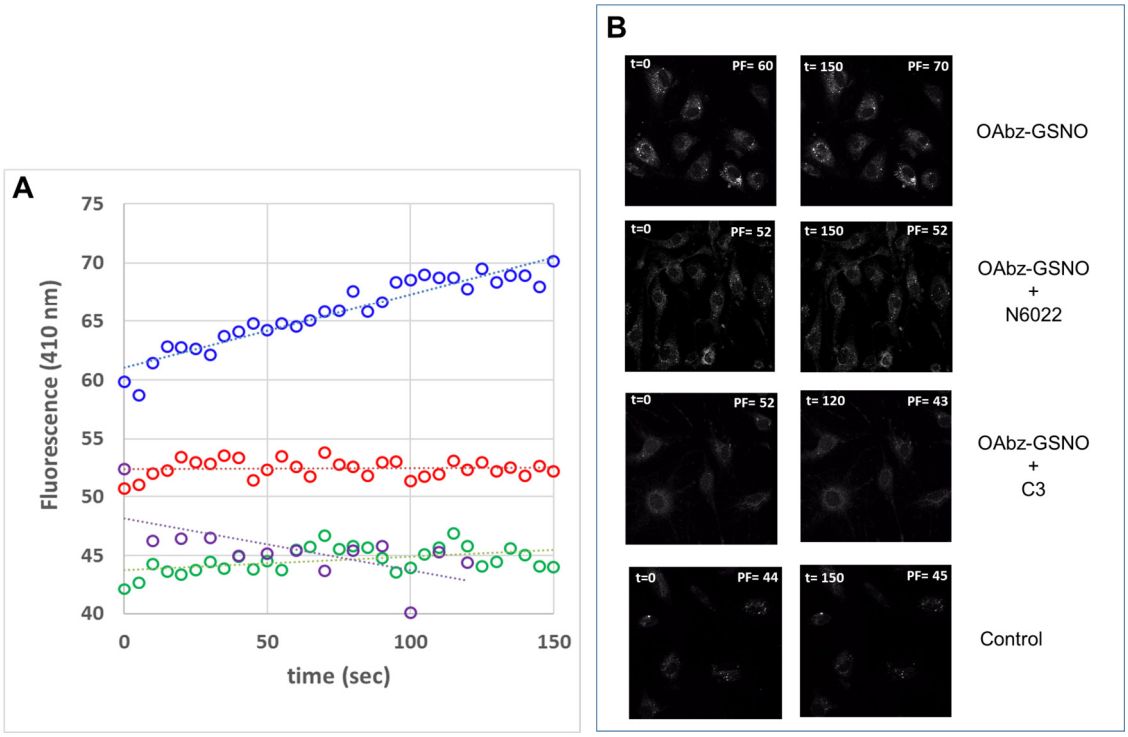

Figure 2.4.7-1 N6022 and C3 inhibit GSNOR-mediated fluorescence increase in cells loaded with OAbz-GSNO

(A) Average perinuclear fluorescence **(PF)**, in all cells in the field of view, was obtained from time-image stack, digitized with ImageJ and the Time Series Analyzer V3 plugin. **Blue circles** – cells were loaded with 1.85 mM OAbz-GSNO; **red circles** – cells were first treated with 25 µM N6022 for 1 hour, and then loaded with OAbz-GSNO; **purple circles** – cells were first treated with 25 µM C3 for 1 hour, and then loaded with OAbz-GSNO; **green circles** – no treatment control cells. **(B)** Images collected from stack at t=0 and t=150 second (t=120 second for C3) with **PF** values indicated. Imaging studies were performed by Dr. Lisa Palmer and colleagues at the University of Virginia.

2.5 Conclusion

In this chapter, we report the synthesis and characterization of OAbz-GSNO as a fluorogenic substrate for the enzyme GSNOR **(Figure 2.5)**. The fluorescence of OAbz-GSNO can be turned on by either chemical or enzyme-mediated reduction of its –SNO moiety *in vitro*. Furthermore, this substrate can be taken up by primary cells in culture and accumulates in the same subcellular compartment as GSNOR. Results from live-cell imaging studies demonstrate endogenous GSNOR activity results in detectable increases in OAbz-GSNO fluorescence; and this increase in fluorescence is abolished by GSNOR inhibitor treatment. To the best of our knowledge, OAbz-GSNO is the first compound which is capable of reporting on endogenous GSNOR activity in live cells.

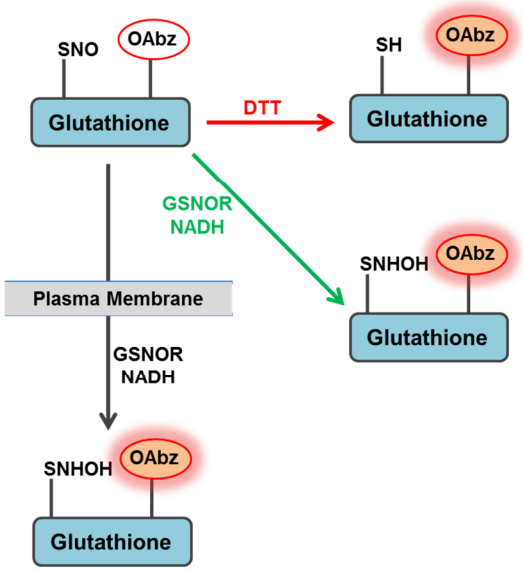

Figure 2.5 OAbz-GSNO is a fluorogenic substrate for GSNOR

OAbz-GSNO experiences fluorescence quenching and exhibits minimal fluorescence. Chemical or enzymatic reduction of its –SNO functional group leads to significant fluorescence increase. OAbz-GSNO is membrane permeable and can be used to assess endogenous GSNOR activity in live cells.

CHAPTER 3

Investigations into the Regulation of *S*-nitrosoglutathione Reductase Activity at the Post-Translational Level

3.1 Introduction

S-nitrosoglutathione reductase (GSNOR) is an evolutionarily conserved, multi-functional enzyme. It can effectively catalyze both the oxidation of hydroxymethylglutathione (HMGSH) [65], and the reduction of *S*-nitrosoglutathione (GSNO) [54, 107]. As a result of these enzymatic activities, functional studies of GSNOR have largely focused on its involvement in cellular formaldehyde detoxification; as well as *S*-nitrosothiol (SNO) homeostasis and nitric oxide (NO) signaling. Despite its universal pattern of expression [85] and demonstrated involvement in human physiology, not much is known regarding the regulation of its activity, especially at the post-translational level.

Structurally, GSNOR is a metalloenzyme with two coordinated zinc ions (Zn^{2+}) per subunit. Primary amino acid sequence analysis reveals a CxxC zinc finger motif as a part of the structural zinc binding site. In addition to metal binding, the CxxC motif, in which two cysteine residues are separated by two other residues, is a well characterized redox motif [209]. Proteins such as thioredoxins and protein disulfide isomerase (PDI) use this motif for the formation, reduction and isomerization of protein disulfide bonds [210-212]. It is widely accepted that the two residues in between the cysteines exert substantial influences on the redox potential of this motif. More recently, Kimura *et al.* studied the conserved lysine residue immediately following the CxxC motif in PDI and demonstrated that this lysine residue (CxxC**K**) significantly increases PDI isomerase activity [213]. Acetylation of this lysine was subsequently suggested as a possible post-translational modification involved in the regulation of PDI activity [214]. Interestingly, the zinc binding CxxC motif within GSNOR is also flanked by a highly conserved lysine

residue (CxxC**K$_{101}$**). Whether K101 contributes to the regulation of GSNOR activity is currently unknown.

This chapter focuses on *in vitro* kinetic evaluation of wild-type and mutant GSNOR to assess the role of K101 and to investigate potential post-translational regulations of GSNOR activity.

3.2 Materials

Acetic anhydride (320102), DNase I (DN25), glutathione, reduced (G4251), imidazole (I0125), isopropyl β-D-1-thiogalactopyranoside (I6758), lysozyme (L7651), β-nicotinamide adenine dinucleotide, reduced (N8129), phenylmethylsulfonyl fluoride (7626), sodium nitrite (S2252), sodium phosphate dibasic (S7907), sodium phosphate monobasic (S8282) and Triton X-100 (T9284) were purchased from Sigma-Aldrich. Glycerol (G3700) and sodium chloride (S2830) were purchased from ACP Chemicals. Kanamycin (BP906) and Tris-HCl (BP153) were purchased from Fisher Scientific. Dithiothreitol (100597) was purchased from MP Biomedicals.

3.3 Methods

3.3.1 Computational modeling and simulations

The Molecular Operating Environment (MOE, 2013.08; Chemical Computing Group Inc. Montréal, QC, Canada) software package was used to perform all docking and molecular dynamics (MD) simulations.

GSNOR crystal structure (PDB ID: 3QJ5) was used as the template for the investigation. Initial crystallographic data was prepared using MOE software by removing the waters and resolving the system up to 6 Å away from any residue. The structure was then allowed to relax using the AMBER12: EHT force field to remove any

strain from the preparation of the protein structure. Finally, in order to allow for thermal relaxation and multiple conformers generation, the minimized structure was used as starting point for a 3 ns MD simulation. An estimated average structure found in the production run was selected for additional analysis.

For docking experiments, the substrate GSNO was docked into its known active site using the induced fit formulism. Virtual screening was then employed to identify other potential GSNO binding sites. To evaluate the top poses, London dG scoring function was used with the AMBER12: EHT force field refinement keeping the top 10 scores.

3.3.2 GSNO synthesis

Reduced glutathione (5 mmol) was dissolved in 8 mL of cold water and 2.5 mL of 2 M HCl. To this solution, 5 mmol of sodium nitrite was added and the reaction was stirred at 4°C in the dark for 40 minutes. After 40 minutes, GSNO was precipitated using 10 mL of cold acetone. The precipitate was collected via filtration, washed with cold water (5 X 1 mL), cold acetone (3 X 10 mL), and lyophilized for storage at -20°C.

3.3.3 Site-directed mutagenesis

The residue Lys101 of human GSNOR was mutated to either alanine (K101A) or glutamine (K101Q) using Q5 Site-Directed Mutagenesis Kit (New England BioLabs E0554). PCR primers were designed to be end-to-end with the forward primer carrying the mutagenic sequence resulting in single amino acid substitution. The following primers were used:

K101A Forward 5’ – TGG AGA ATG CGC ATT TTG TCT AAA TCC – 3’

K101A Reverse 5’ – CAC TGT GGG ATG TAA AGT G – 3’

K101Q Forward 5’ – GGA GAA TGC CAA TTT TGT CTA AAT CCT – 3’

K101Q Reverse 5’ – ACA CTG TGG GAT GTA AAG TG – 3’

PCR reaction was set up according to manufacturer’s recommendations and thermal cycling conditions were optimized for each primer set. The resultant PCR product was treated with Kinase, Ligase, Dpn1 enzyme mix according to manufacturer’s protocol and used to transform chemically competent DH5 *E.coli* (New England BioLabs C2987). Individual colonies from the transformation plates were selected and each colony was inoculated into 3 mL of LB medium (with 50 µg/mL kanamycin) for overnight growth at 37°C. Plasmid DNA was then isolated from these cultures using a standard bacterial miniprep procedure (Qiagen). Isolated plasmid DNA was resuspended in TE buffer and sequenced at Robart’s Research Institute (London Regional Genomics Center, London, Ontario, Canada) using T7 sequencing primer. Successful mutants were selected for subsequent transformation and protein expression.

3.3.4 Protein expression and purification

Expression plasmids pET28b_GSNOR, pET28b_GSNOR_K101A and pET28b_GSNOR_K101Q were individually transformed into chemically competent BL21(DE3) *E.coli* (New England BioLabs C2527). Recombinant proteins contain terminal 6X-histidine tags to facilitate purification. A single colony from the transformation plate was inoculated into 25 mL of 2X YT medium containing 50 µg/mL kanamycin and the culture was grown overnight at 37°C. This overnight starter culture was then used to inoculate 500 mL of 2X YT medium containing 50 µg/mL kanamycin and the culture was grown at 37°C until optical density reached approximately 0.6. At

this point, protein expression was induced by the addition of IPTG to a final concentration of 0.4 mM. The induced culture was grown for an additional 24 hours at room temperature before cells were harvested by centrifugation (4000 *g*, 30 minutes, 4°C). Following centrifugation, supernatant was discarded and the bacterial cell pellet was resuspended in 15 mL of lysis buffer (50 mM Tris-HCl pH 8, 150 mM NaCl, 15 mM imidazole, 1 mM DTT, 1 mM PMSF, 0.5% Triton X-100, 50 µg/mL DNase I and 100 µg/mL lysozyme). The crude lysate was incubated on ice for 30 minutes and further lysed by pulse sonication (20 seconds on, 20 seconds off, 30 cycles). Another round of centrifugation (11300 *g*, 30 minutes, 4°C) was performed and the clarified supernatant was applied to nickel affinity column (Sigma P6611) pre-equilibrated with lysis buffer. Affinity purification was performed strictly following manufacturer's protocol published by Sigma Aldrich with some modifications in buffer composition. The wash buffer contained 50 mM Tris-HCl pH 8, 150 mM NaCl and 50 mM imidazole while the elution buffer contained 50 mM Tris-HCl pH 8, 150 mM NaCl and 300 mM imidazole. Finally, eluted protein was buffer exchanged into storage solution (58 mM Na_2HPO_4, 17 mM NaH_2PO_4, 68 mM NaCl, 15% glycerol) using Amicon centrifugal filter (Millipore UFC903008). When stored at -80°C, purified proteins are stable and can retain their activity for at least 6 months in the absence of repeated freeze-thaw cycles.

3.3.5 Kinetic assays

NADH stock solution (20 mM) was prepared with MilliQ water. GSNO stock solutions (10 mM and 1 mM) were prepared fresh daily using PBS. Total reaction volume was kept at 500 µL using PBS as the reaction buffer. The various GSNO and NADH concentrations used in the assays are noted in the Figure legends.

For the set of GSNO pre-treatment experiments, wild-type and mutant GSNOR were incubated with 0.5 mM GSNO in the dark for 30 minutes at room temperature. Following incubation, unreacted GSNO was removed using Zeba desalting columns (Fisher Scientific 89882). For chemical acetylation experiments, acetic anhydride (1 M) stock solution was prepared using methanol due to its reactivity. Wild-type and mutant GSNOR were then treated with 20 mM acetic anhydride for 1 hour at room temperature before enzyme activities were assayed. Each individual reaction was initiated by the addition of enzyme (2 μg) and decreases in absorbance at 340 nm were monitored for 90 seconds using Agilent 8453 UV/Vis spectrophotometer.

3.3.6 Immunoblotting

Wild-type and mutant GSNOR were treated with 20 mM acetic anhydride for 1 hour at room temperature. Enzymes mock-treated with equal volume of methanol or GSNOR storage buffer were used as controls. Following treatment, samples were resolved using 10% SDS-PAGE gels and transferred onto polyvinylidene difluoride (PVDF) membranes. Blocking was carried out for 1 hour at room temperature using 5% skim milk. Membranes were then incubated with primary antibodies against acetyl-lysine (1:1000; Abcam ab61384) or 6X histidine (1:1000; Signal Chem H99-61M) overnight at 4°C, washed 3 times with TBST, and incubated with HRP-conjugated secondary antibody (1:5000; Abcam ab97023) for 1 hour. Finally, the membranes were washed 3 times again and visualized using enhanced chemiluminescence reagents (Thermo Scientific 34095).

3.4 Results and Discussion

3.4.1 Computational modeling and simulations

GSNOR is a dimeric protein. Each subunit contains a CGEC motif **(Figure 3.4.1-1 A)**. This motif participates in the coordination of GSNOR structural zinc. We are interested in the highly conserved lysine residue adjacent to the CGEC motif (CGEC$\mathbf{K_{101}}$) and whether acetylation of K101 affects GSNOR function.

Computational modeling and molecular dynamic simulations were performed to predict changes due to K101 acetylation. Results show modification of K101 leads to significant alterations in protein structure within the structural zinc binding site **(Figure 3.4.4-1 B)**. This is associated with changes in the distance between GSNOR structural zinc and each of the four Cys residues (C97, C100, C103 and C111) involved in its coordination **(Table 3.4.1-1)**. Cysteine thiol pKa values were also predicted based on average protein structures. Interestingly, the predicted thiol pKa for C97 increases from 6.33 to 12.21 following K101 acetylation; while the pKa for C111 increases from 6.26 to 8.23 **(Table 3.4.1-2)**. Higher pKa values do not favour thiolate ($-S^-$) formation, which could negatively affect cysteine's ability to coordinate zinc. The predicted increase in thiol pKa for C97 and C111 is also correlated with increased distance to the zinc they coordinate. This could be due to weakened interaction between the two.

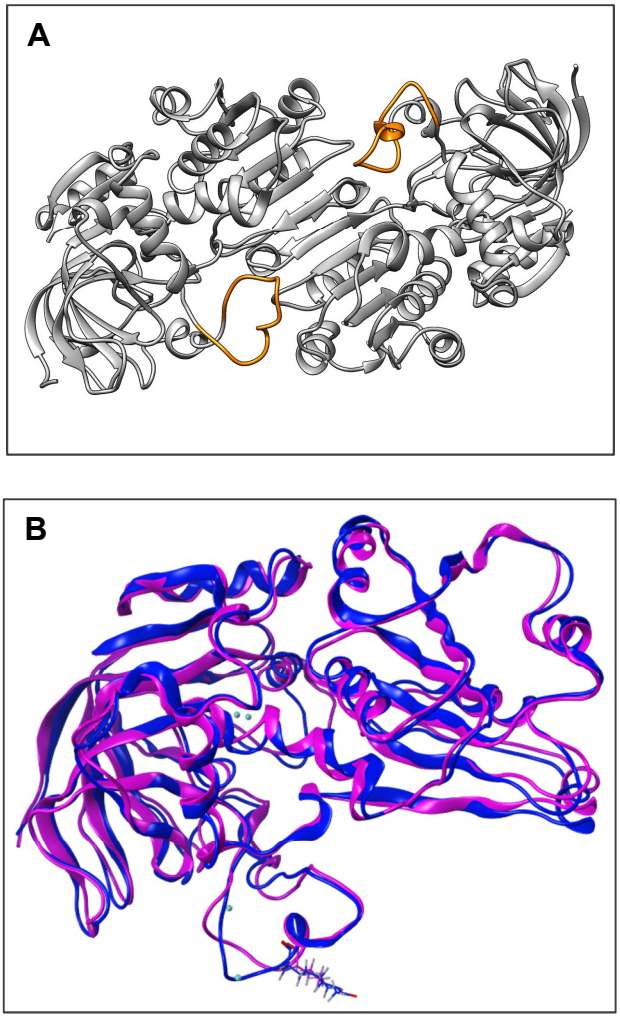

Figure 3.4.1-1 Acetylation of Lys101 effects GSNOR protein structure around the structural zinc binding site

(A) GSNOR is a dimeric protein. Each subunit contains a CxxC motif as part of the structural zinc binding site (shown in orange). **(B)** Average protein structures of unmodified wild-type GSNOR (magenta) and K101_acetylated wild-type GSNOR (blue) from MD simulations were overlaid for comparison.

Table 3.4.1-1 Distance (Å) between GSNOR structural Zn and Cys(S)

Residue	GSNOR WT	GSNOR K101A	GSNOR K101Q	GSNOR K101Acetylated
C97	6.41	4.87	6.75	9.20
C100	10.21	7.35	5.82	5.84
C103	6.06	12.53	8.39	8.59
C111	5.44	8.13	10.60	9.81

Table 3.4.1-2 Predicted cysteine thiol pKa

Residue	GSNOR WT	GSNOR K101A	GSNOR K101Q	GSNOR K101Acetylated
C97	6.33	12.78	8.48	12.21
C100	8.80	6.60	4.96	8.62
C103	6.43	8.02	7.93	6.42
C111	6.26	4.00	9.58	8.23

3.4.2 Kinetic parameters of wild-type and mutant GSNOR

To assess the role of the conserved lysine residue at position 101, site directed mutagenesis was performed using human GSNOR (NM_000671.3) as the template. Successful mutation from lysine (K) to either alanine (A) or glutamine (Q) was confirmed by sequencing. Lysine to alanine substitution removes a positively charged side chain, which could affect the protein microenvironment for the cluster of cysteine residues (C97, C100, C103 and C111) involved in structural zinc binding. Out of the naturally occurring amino acids, the structure of glutamine best resembles that of acetylated lysine. Therefore, lysine to glutamine substitution will offer some insight regarding the effect of K101 acetylation.

When kinetic parameters of wild-type and mutant GSNOR were assessed, it was determined that wild-type GSNOR exhibits an apparent K_m of 30.2 ± 0.89 μM towards GSNO and a k_{cat} of 2467 ± 57.9 min^{-1} **(Figure 3.4.2-1)**. Both of these values are comparable to previously reported K_m of 28 μM and k_{cat} of 2640 min^{-1} [54]. Catalytic efficiency of GSNOR was calculated as k_{cat} / K_m. For the wild-type enzyme, catalytic efficiency was determined to be 1360000 ± 9900 $s^{-1}M^{-1}$ **(Table 3.4.2)**.

GSNOR K101A exhibits an apparent K_m of 27.6 ± 1.65 μM towards GSNO and a k_{cat} / K_m of 1330000 ± 69400 $s^{-1}M^{-1}$ **(Figure 3.4.2-1, Table 3.4.2)**. Both of these parameters are not significantly different from the wild-type enzyme, indicating that K101 is not involved in substrate binding and does not directly participate in catalysis. On the other hand, K101Q mutant shows an apparent K_m of 29.2 ± 3.18 μM towards GSNO and a k_{cat} / K_m of 1090000 ± 81600 $s^{-1}M^{-1}$ **(Figure 3.4.2-1, Table 3.4.2)**. The experimental K_m for K101Q is also comparable to wild-type, but catalytic efficiency of

this mutant decreased by approximately 20%. Since glutamine was chosen to mimic the structure of acetylated lysine, the observed decrease in catalytic efficiency suggests acetylation could be involved in the post-translational regulation of GSNOR activity.

Enzyme activity as a function of cofactor (NADH) concentration was evaluated for wild-type and mutant GSNOR **(Figure 3.4.2-2)**. Apparent K_m towards NADH was determined to be 34.2 ± 2.72 μM for wild-type GSNOR, 41.3 ± 1.31 μM for K101A, and 35.2 ± 0.81 μM for K101Q. Based on these K_m values, it appears the K101A mutant displays slightly reduced affinity for NADH. This could be due to some alterations in protein structure as a result of the mutation.

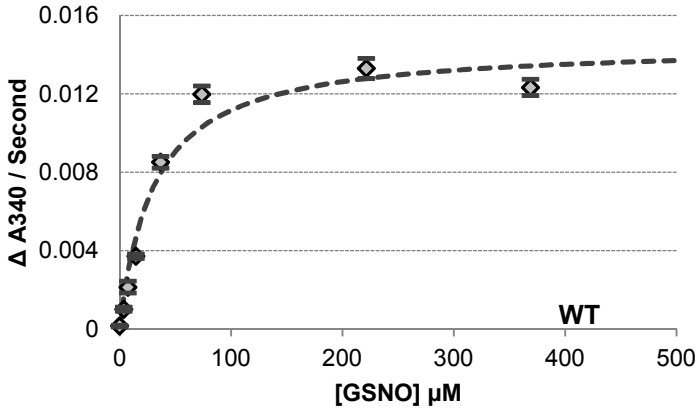

K_m^{GSNO} = 30.2 ± 0.89 µM

k_{cat} = 2468 ± 57.9 min^{-1}

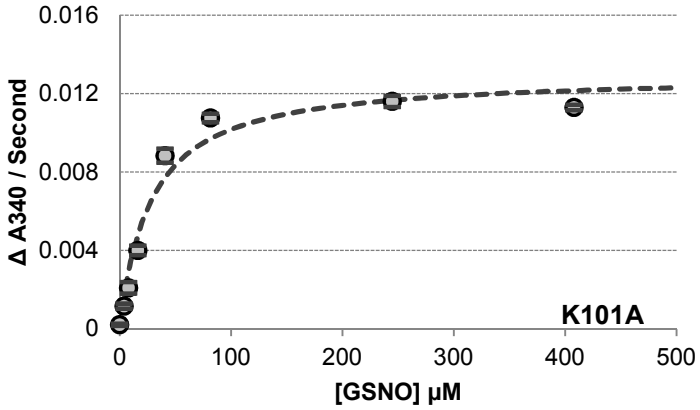

K_m^{GSNO} = 27.6 ± 1.65 µM

k_{cat} = 2205 ± 18.2 min^{-1}

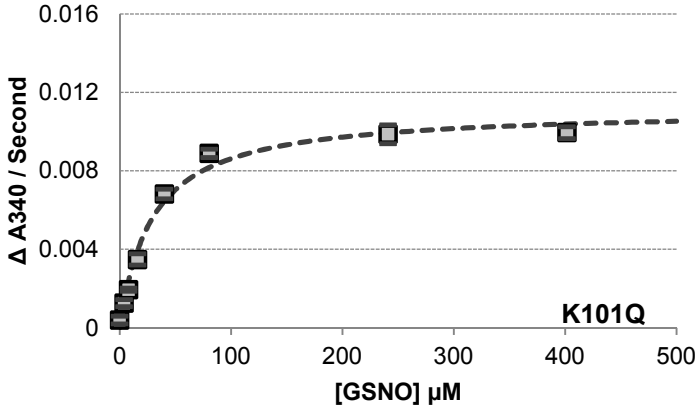

K_m^{GSNO} = 29.2 ± 3.18 µM

k_{cat} = 1893 ± 62.1 min^{-1}

Figure 3.4.2-1 Michaelis-Menten kinetics of wild-type and mutant GSNOR

Initial reaction rates of wild-type GSNOR **(WT)**, GSNOR K101A **(K101A)** and GSNOR K101Q **(K101Q)** were determined by monitoring absorbance decrease at 340 nm. Various GSNO concentrations (ranging from 0 μM to approximately 400 μM) were used. Each reaction contains 80 μM NADH and is initiated by the addition of 2 μg of enzyme. PBS (pH 7.4) was used as the reaction buffer. Error bars represent standard deviation (n=3).

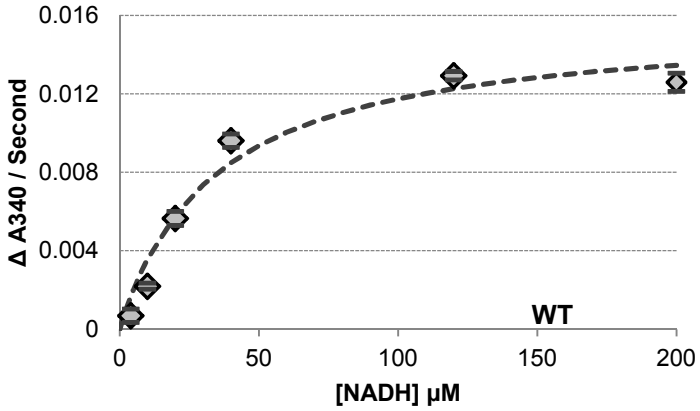

K_m^{NADH} = 34.2 ± 2.72 µM

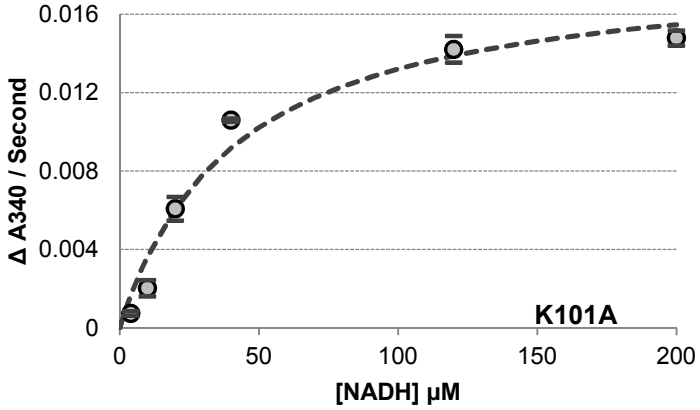

K_m^{NADH} = 41.3 ± 1.3 µM

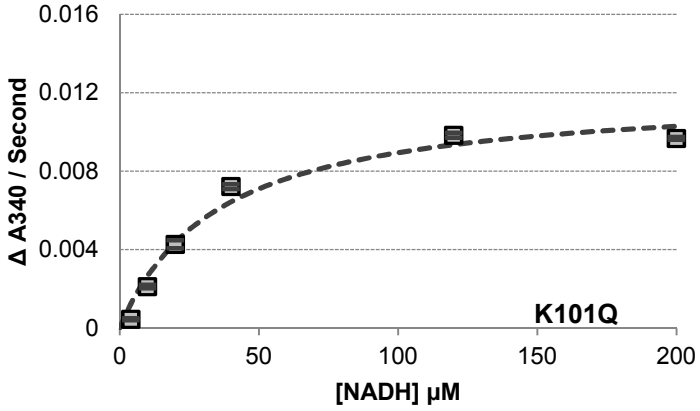

K_m^{NADH} = 35.2 ± 0.81 µM

Figure 3.4.2-2 GSNOR activity as a function of cofactor concentration

Initial reaction rates of wild-type GSNOR **(WT)**, GSNOR K101A **(K101A)** and GSNOR K101Q **(K101Q)** were determined by monitoring absorbance decrease at 340 nm. Each reaction contains 200 μM GSNO and various concentrations of NADH (ranging from 0 to 200 μM). Reaction is initiated by the addition of 2 μg of enzyme. Error bars represent standard deviation (n=3).

Table 3.4.2 Kinetic parameters of wild-type and mutant GSNOR

	Wild-type GSNOR	
		% of WT
K_m^{GSNO} (μM)	30.2 ± 0.89	100 ± 3.0
K_m^{NADH} (μM)	34.2 ± 2.72	100 ± 7.9
k_{cat} (min^{-1})	2468 ± 57.9	100 ± 2.3
k_{cat} / K_m (x 10^3 s^{-1} M^{-1})	1360 ± 9.9	100 ± 0.7
	GSNOR K101A	
		% of WT
K_m^{GSNO} (μM)	27.6 ± 1.65	92 ± 5.5
K_m^{NADH} (μM)	41.3 ± 1.3	121 ± 3.8*
k_{cat} (min^{-1})	2205 ± 18.2	89 ± 0.7*
k_{cat} / K_m (x 10^3 s^{-1} M^{-1})	1330 ± 69.4	98 ± 5.1
	GSNOR K101Q	
		% of WT
K_m^{GSNO} (μM)	29.2 ± 3.18	97 ± 10.5
K_m^{NADH} (μM)	35.2 ± 0.81	103 ± 2.4
k_{cat} (min^{-1})	1893 ± 62.1	77 ± 2.5*
k_{cat} / K_m (x 10^3 s^{-1} M^{-1})	1090 ± 81.6	80 ± 6.0*

Values given as mean ± SD

*statistically significant ($p < 0.05$)

3.4.3 Chemical acetylation of GSNOR

Lysine acetylation was discovered more than 50 years ago on N-terminal tails of nuclear histone proteins [215, 216]. Since then, a large number of non-histone proteins have been shown to be regulated by transient N^{ε}-acetylation on select lysine residues [214, 217]. Previous findings in our lab suggest acetylation of the CxxC motif flanking lysine in PDI affects its enzyme activity. From the previous section, we observed a decrease in GSNOR catalytic efficiency when its CxxC flanking lysine was mutated to glutamine, suggesting lysine modification may be involved in the regulation of GSNOR activity. In this section, *in vitro* acetylation was performed on wild-type GSNOR and GSNOR K101A using acetic anhydride. It is important to point out that this chemical acetylation method is not specific as acetic anhydride could also modify amino acid residues other than lysine, such as serine and threonine. As a result, caution must be exercised when interpreting experimental findings. The rationale behind this set of experiment is if acetylation of K101 affects GSNOR activity, then this effect should not be observed in the K101A mutant.

First, immunoblots were produced to verify lysine residues were acetylated. For both wild-type GSNOR and K101A, treatment with 20 mM acetic anhydride results in strong signals when probed with anti-acetyl-lysine antibody **(Figure 3.4.3-1 A)**. Chemical acetylation appears to be correlated with decreases in enzyme activity for both wild-type (~50% reduction) and alanine mutant (~45% reduction). Due to its reactivity, using acetic anhydride to study lysine acetylation has some limitations. For example, residues other than lysine may also become modified; and we cannot control which lysine residue gets acetylated. Despite these drawbacks, the observed reduction in GSNOR

activity following acetic anhydride treatment provides promising preliminary data for acetylation mediated down regulation of GSNOR activity. Methanol control (GSNOR treated with 2% methanol, without acetic anhydride) is included for comparison since acetic anhydride stock solution is prepared using methanol. Surprisingly, K101A exhibits ~25% reduction in activity when treated with methanol while wild-type GSNOR is unaffected **(Figure 3.4.3-1 B)**. The underlying cause for this differential response is currently unknown. From computational predictions, we know that K101 mutation is associated with alterations in cysteine thiol pKa and protein structure in the vicinity of the structural zinc binding site. However, causal relationship between these predicted changes and enzyme's susceptibility towards methanol-induced effects has yet to be established. As a solvent, methanol does not have the same hydrogen bonding capacity as water. This may perturb protein-solvent hydrogen bond network, thus affecting dynamic properties of GSNOR. Differential response to methanol suggests even though kinetic parameters were not dramatically different between wild-type GSNOR and K101A, some other property of the enzyme must have been altered in the K to A mutant in order to elicit this response.

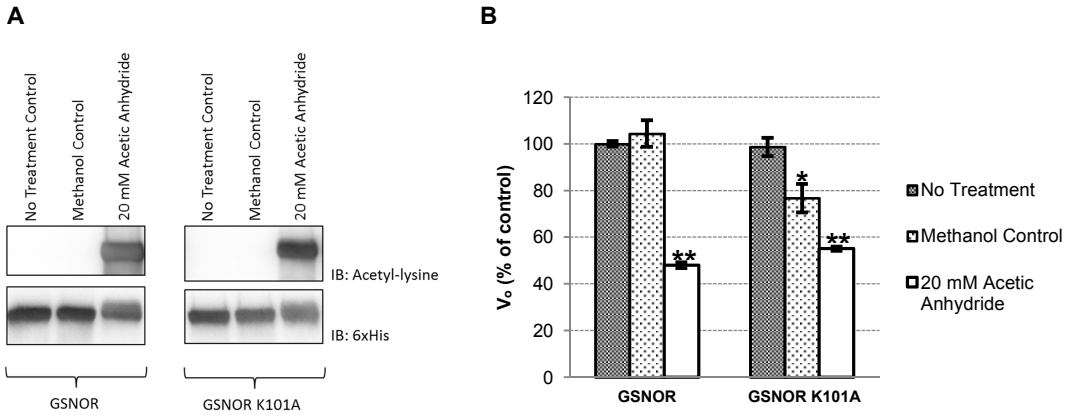

Figure 3.4.3-1 Effect of chemical acetylation on GSNOR activity

Chemical acetylation of wild-type GSNOR and GSNOR K101A was performed using acetic anhydride. **(A)** Samples were run on SDS-PAGE gels and transferred to PVDF. Membranes were probed with anti-acetyl-lysine and anti-His antibodies. **(B)** Enzyme activity was measured as rate of absorbance decrease at 340 nm. Each reaction contains 80 μM NADH and 200 μM GSNO. Initial reaction rates are graphed as percentage of the no treatment control group. Error bars represent standard deviation (n=4). *statistically different from no treatment control. **statistically different from no treatment control and methanol control.

3.4.4 In vitro S-nitrosation studies

Earlier this year, Guerra *et al.* predicted potential *S*-nitrosation sites within GSNOR using the software GPS-SNO and demonstrated *S*-nitrosation decreases enzyme activity *in vitro* [218]. The group further suggested GSNOR can be *S*-nitrosated by its own substrate GSNO and the transient down-regulation of activity permits robust nitric oxide signaling [218]. Inhibition of enzyme activity by its own substrate seems paradoxical. This signaling model proposed by Guerra *et al.*, coupled with computationally predicted cysteine thiol pKa changes following K101 mutation/modification, prompted us to investigate whether GSNOR activity can be regulated by *S*-nitrosation; and whether K101 mutation renders any of the zinc-coordinating cysteines more susceptible to oxidation.

For this purpose, both wild-type GSNOR and K101A mutant were treated with 0.5 mM GSNO for 30 minutes before activities were assayed. Contrary to results published by Guerra and colleagues, GSNO pre-treatment did not have any observable effect on enzyme activity **(Figure 3.4.4-1)**; suggesting either GSNOR is not modified by its substrate GSNO, or modification has no effect on enzyme activity. To complement this finding, biotin-switch or mass spectrometry should be performed to assess the *S*-nitrosation status of GSNOR following treatment. Different *S*-nitrosating agents can also be explored since protein *S*-nitrosation occurs via multiple mechanisms.

Similarly, treating GSNOR K101A with 0.5 mM GSNO did not effect enzyme activity; demonstrating mutation of K101 did not make C97, C100, C103 or C111 more susceptible to *S*-nitrosation despite predicted changes in pKa values. In this case, it is highly likely that these 4 cysteine residues are not modified since modification would

affect their ability to coordinate zinc, which would translate into significant attenuation of enzyme activity. This finding is not unexpected as structural cysteine-zinc complexes are usually chemically inert [219, 220].

GSNOR is a cysteine-rich protein. Human GSNOR contains a total of 15 cysteine residues, 6 of which are involved in zinc binding. At the moment, not much is known regarding the chemical reactivity of these residues and whether reversible *S*-nitrosation is one of the mechanisms regulating GSNOR activity. Contrary to recently published findings, our results show GSNO pre-treatment does not have any effect on GSNOR activity. Additional research in this area is needed to address this discrepancy.

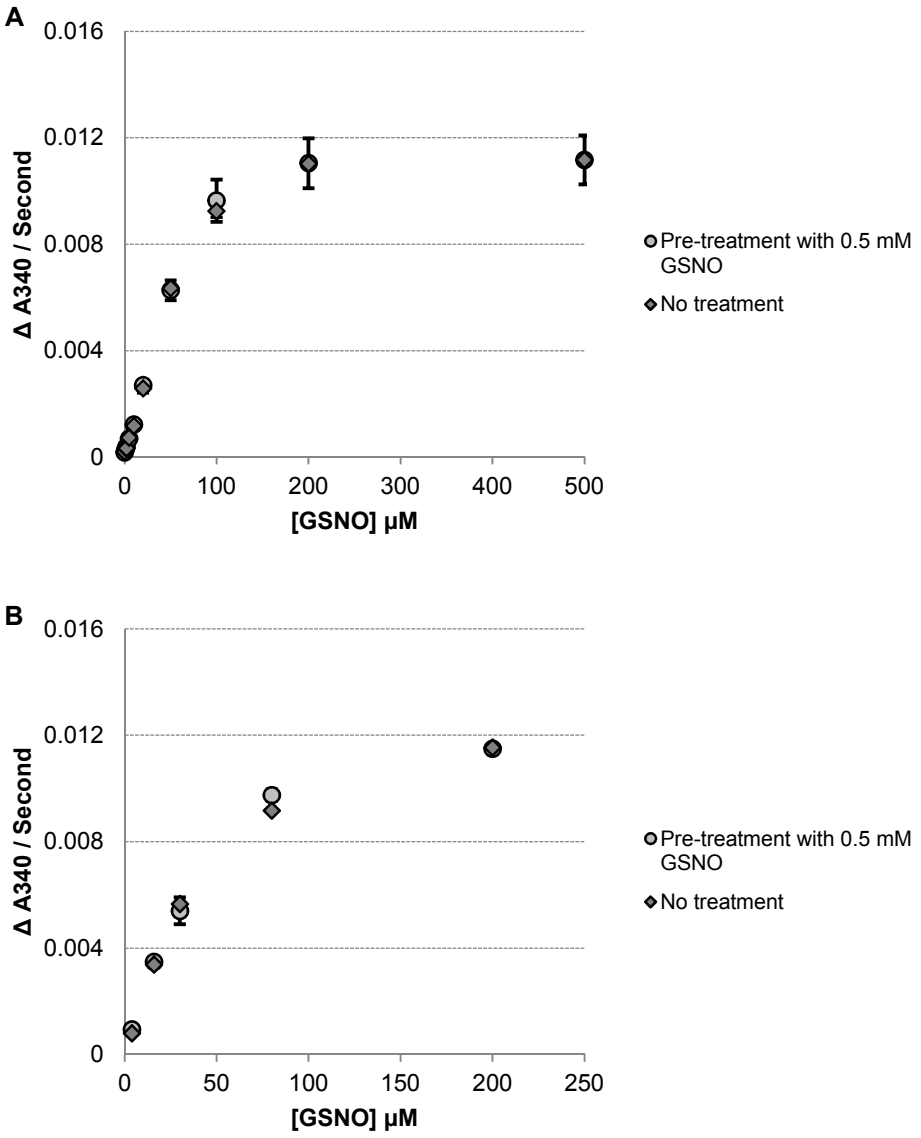

Figure 3.4.4-1 GSNO pre-treatment does not affect GSNOR activity

(A) Wild-type GSNOR and **(B)** GSNOR K101A are treated with 0.5 mM GSNO for 30 minutes. Unreacted GSNO is removed using Zeba desalting columns. Enzyme activities at various GSNO concentrations are assayed by monitoring the decrease in absorbance at 340 nm. Each reaction contains 200 µM NADH and is initiated by the addition of 2 µg of either wild-type or mutant GSNOR. Error bars represent standard deviation (n=3).

3.4.5 Potential allosteric GSNO binding site and implications for the regulation of GSNOR activity

When looking at GSNOR activity as a function of GSNO concentration, the shape of the Michaelis-Menten curve caught our attention. It appears to deviate from the classical hyperbola and exhibits increased response to substrate at low concentrations. This let us to speculate perhaps GSNOR could be rapidly activated by some factor. In addition, semi-logarithmic transformation produced an asymmetrical S-curve **(Figure 3.4.5-1 A)**, which is characteristic of enzymes that do not conform to simple kinetics [221]. Hill plot was also constructed to determine cooperativity **(Figure 3.4.5-1 B)**. The Hill coefficient of GSNOR (calculated as slope of the best fit line) was greater than 1, which indicates the existence of some form of positive cooperation. Upon further investigation, computational docking results suggest GSNOR may have an allosteric binding site for GSNO near the structural zinc domain **(Figure 3.4.5-3 A)**. MD simulations show consistent interaction between GSNO and this putative allosteric region, which brings forth the possibility that GSNO binding to this site could affect the activity of GSNOR. Based on this model, Asn184 and Gly320 appear to interact with GSNO directly; while Lys187 and Lys322 interacts indirectly through the solvent network of hydrogen bonds **(Figure 3.4.5-3 B)**. Docking scores, which is used to predict binding affinity, also support the existence of an allosteric binding site for GSNO. Specifically, GSNO binding to the known active site exhibits a score of -8.60; while GSNO binding to the putative allosteric site has a score of -10.4 (low scores indicate stable systems and are associated with favorable interactions.)

Our hypothesis of allosteric regulation was tested using the fluorogenic substrate OAbz-GSNO. GSNOR-mediated reduction of OAbz-GSNO was examined in the absence, as well as in the presence, of GSNO. Results indicate including GSNO in the reaction leads to enhanced OAbz-GSNO reduction, as evidenced by higher rates of fluorescence increase **(Figure 3.4.5-2)**. On the other hand, OAbz-GSNO fluorescence is not affected by GSNO alone. Based on these observations, we propose GSNO binding to the allosteric site enhances GSNOR activity.

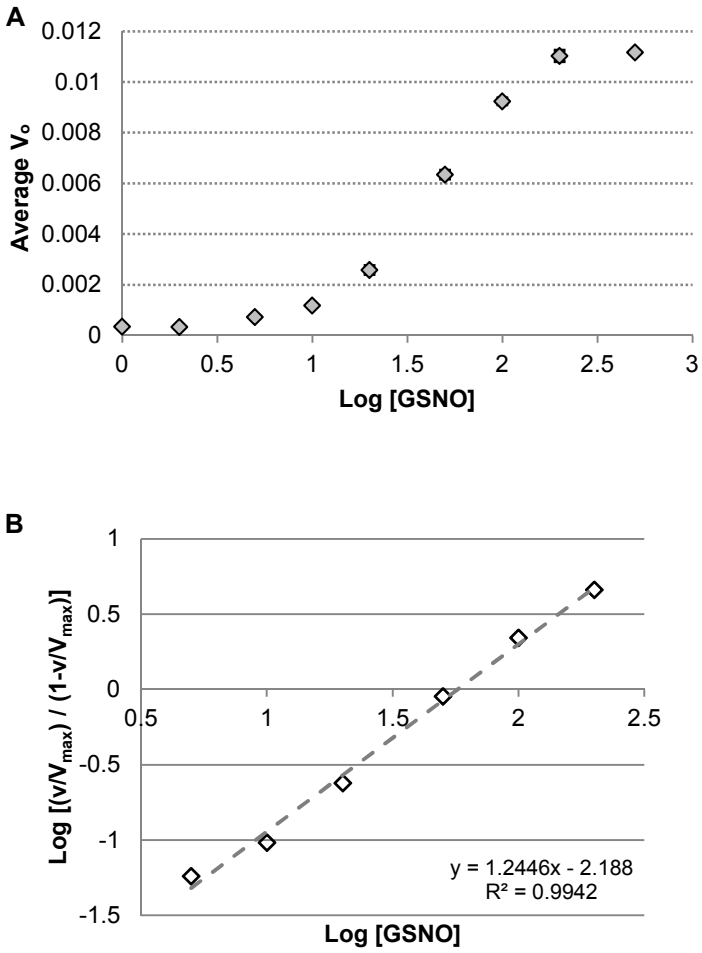

Figure 3.4.5-1 Logarithmic plots of GSNOR kinetics

Initial reaction rates of wild-type GSNOR are determined by monitoring absorbance decrease at 340 nm. Each reaction contains 80 μM NADH and is initiated by the addition of 2 μg enzyme. **(A)** Semi-logarithmic plot. **(B)** Hill plot.

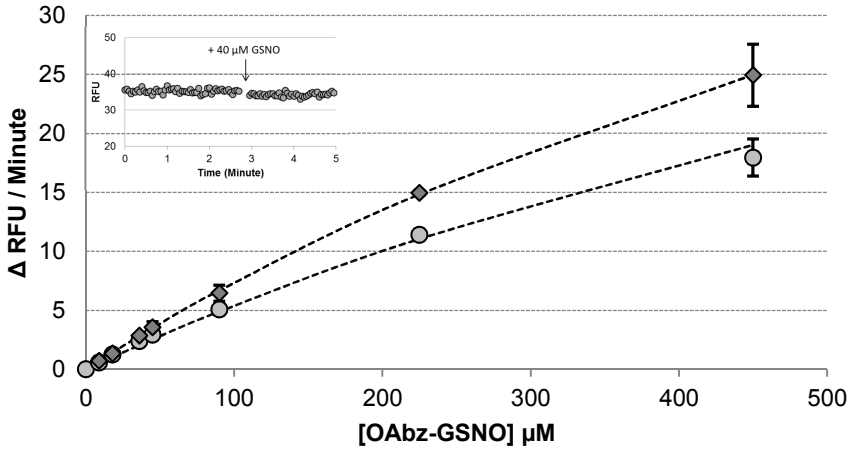

Figure 3.4.5-2 GSNO enhances GSNOR-mediated reduction of OAbz-GSNO

GSNOR activity is measured by monitoring fluorescence increase (excitation at 312 nm, emission at 415 nm) due to OAbz-GSNO reduction in the absence of GSNO (circles) and in the presence of 40 µM GSNO (diamonds). Each reaction contains 120 µM NADH and various concentrations of OAb-GSNO. PBS is used as the reaction buffer. Reaction is initiated by the addition of 2 µg of wild-type GSNOR. Error bars represent standard deviation (n=3).

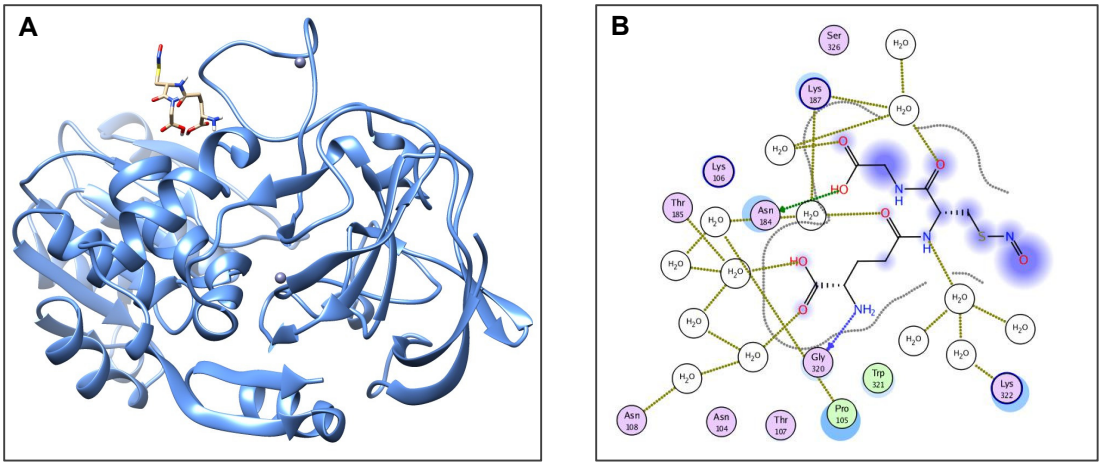

Figure 3.4.5-3 Putative allosteric GSNO binding site

High resolution (1.9 Å) X-ray crystal structure of GSNOR from *Homo sapiens* (PDB ID: 3QJ5) was used as the base structure for GSNO docking. **(A)** Putative allosteric GSNO binding site is near the structural zinc domain. **(B)** Predicted interactions between GSNO and GSNOR based on the average structure from MD simulations.

3.5 Conclusion

This chapter focuses on kinetic evaluation of GSNOR activity to identify potential mechanisms of regulation. First, the role of CxxC flanking K101 was assessed by site-directed mutagenesis. Results show mutation of K101 to glutamine leads to approximately 20% reduction in catalytic efficiency. Since the structure of glutamine is similar to the structure of acetylated lysine, K101 acetylation may represent a post-translational modification involved in the down-regulation of GSNOR activity. Chemical acetylation using acetic anhydride also results in decreased enzyme activity. This project will be carried forward. *In vitro* acetylation using recombinant acetyltransferase and mass spectrometry will be performed to provide unambiguous evidence regarding the site of lysine acetylation and its effect on GSNOR activity.

Contrary to previously proposed model that *S*-nitrosation mediated by GSNO attenuates GSNOR activity, treatment with 0.5 mM GSNO did not have any effect on enzyme activity for both the wild-type and K101A mutant. Instead, our findings suggest a different mode of regulation, in which GSNOR activity is enhanced when GSNO binds to an allosteric site. This proposed mechanism would allow GSNOR to exhibit greater activity when substrate is abundant, effectively restoring cellular homeostasis.

CHAPTER 4

Functional Aspects of Neutral Sphingomyelinase II

4.1 Introduction

Sphingolipids are major constituents of the plasma membrane in eukaryotic cells. This class of lipids typically consists of a sphingosine backbone, a long chain fatty acid, and a variable polar head group. Originally considered to serve only structural roles, these lipids are now recognized as important participants in a wide range of signal transduction pathways [222, 223]. In particular, sphingomyelin-based pathways have received considerable attention in recent years. Structurally, sphingomyelin (SM) has a polar phosphorylcholine head group and the composition of the long chain fatty acid varies from tissue to tissue and can be either saturated or mono-unsaturated with 14 to 24 carbons [224, 225]. Results based on cell fractionation studies and degradation experiments suggest that more than half of the cellular SM mass is confined to the plasma membrane [226]. The exact percentage may vary from one cell type to another, though it has been reported that cells with extensive plasma membrane recycling have a larger fraction of SM in intracellular compartments [227].

SM's role in signaling is multifaceted. Its hydrolysis generates bioactive ceramide, a lipid second messenger molecule capable of modulating cellular events such as cell cycle arrest, differentiation, inflammation and apoptosis [132-134]. SM hydrolysis is specifically catalyzed by the family of enzymes known as sphingomyelinase (EC 3.1.4.12). This enzyme family is further divided into three groups (acid, neutral and alkaline) based on their distinct catalytic pH optimum. Of the different forms of sphingomyelinases identified and studied to date, the magnesium-dependent neutral sphingomyelinase II (NSMase II) has emerged as the predominant sphingomyelinase implicated in a diverse set of cellular functions and disease pathologies [180, 228].

During recent years, a large number of studies have identified NSMase II as a mediator of cellular stress response, mainly through the production of ceramide. Exposures to oxidative stress [160, 163], pro-inflammatory cytokines [169], and anti-cancer compounds [187, 229] can up-regulate NSMase II expression and activity, which increases cellular ceramide levels to signal apoptosis or senescence.

In addition to ceramide generation, NSMase II catalyzed SM degradation may also affect the formation of lipid rafts within the plasma membrane. Lipid rafts are ordered microdomains enriched in SM and cholesterol. These microdomains are detergent resistant and have been proposed to serve as platforms for the attachment of different proteins involved in signaling [230]. Specific proteins can be selectively included or excluded from these laterally organized microdomains, thus facilitating various signaling events [231, 232]. A consistent ratio between SM and cholesterol needs to be maintained in the plasma membrane to support lipid raft formation, and there is evidence indicating plasma membrane SM and cholesterol levels are coordinately regulated [233]. For example, reduction of SM level by the addition of purified bacterial sphingomyelinase to cultured cells decreases membrane's ability to solubilize cholesterol, which leads to increased cholesterol esterification and transport to intracellular sites, as well as down-regulation of cholesterol *de novo* synthesis [234-236]. Although NSMase II was not directly implicated in these studies, it is reasonable to hypothesize that stress induced NSMase II activation could also affect plasma membrane cholesterol content and lipid raft formation.

Cortisol is the principle glucocorticoid hormone in humans. It is produced by the adrenal cortex and released into circulation according to a distinct circadian pattern [237].

Disruptions to this daily rhythm have been observed in patients with breast and ovarian cancer [238]. In this chapter, cortisol exposure was used as a stressor and its effect on NSMase II expression and activity were assessed. The ability of NSMase II to modulate plasma membrane cholesterol content was also explored.

The regulation of NSMase II activity is not well understood and contradictory findings have been reported. For instance, while Liu and Hannun observed physiological concentrations of GSH can effectively inhibit NSMase II activity [188]; Dotson *et al.* reported increases in activity in response to reducing agents, such as GSH and 2-mercaptoethanol [239]. Despite these seemingly contradictory findings, cellular redox environment clearly has an effect on NSMase II activity. In addition, human NSMase II contains a total of 23 cysteine residues, for which the redox sensitivity has not been fully assessed. Since our lab is interested in the post-translational modification *S*-nitrosation, the last part of this project will focus on *in vitro* NSMase II activity in response to GSNO treatment.

4.2 Material

Ampicillin (A0166), cortisol (H0888), DNase I (DN25), imidazole (I0125), isopropyl β-D-1-thiogalactopyranoside (I6758), lysozyme (L7651), magnesium chloride (M2570), phenylmethylsulfonyl fluoride (7626), and Triton X-100 (T9284) were purchased from Sigma-Aldrich. Sodium chloride (S2830) was purchased from ACP Chemicals. Kanamycin (BP906) and Tris-HCl (BP153) were purchased from Fisher Scientific. Dithiothreitol (100597) was purchased from MP Biomedicals. Fluoromount G (0100-01) was purchased from Southern Biotech.

4.3 Methods

4.3.1 Cell culture

Triple negative breast cancer cells (HTB 126) were purchased from ATCC and maintained in DMEM high-glucose medium (HyClone SH30022.01) supplemented with 10% fetal bovine serum (GIBCO 12483), 100 μg/mL streptomycin and 100 U/mL penicillin. Human embryonic kidney cells (HEK 293) were also obtained from ATCC and cultured in DMEM nutrient mixture F-12 Ham (Sigma D6421) supplemented with 10% fetal bovine serum, 100 μg/mL streptomycin and 100 U/mL penicillin. All cells were maintained in a humidified incubator at 37°C with 5% CO_2. For regular maintenance, cells were sub-cultured when confluency reached approximately 85%.

4.3.2 Cortisol treatment

Cortisol stock solution (100 mM) was prepared in dimethyl sulfoxide (DMSO). Cultured HTB 126 cells were treated with cortisol at a final concentration of 80 μM for 24 hours before analysis. Cells mock-treated with DMSO were used as controls.

4.3.3 NSMase II over-expression

HEK 293 cells were grown in 6-well plates or on 4-chamber slides. Transient transfection was performed using pCMV-SPORT6 NSMase II expression plasmid (Open Biosystems 6399438) with Lipofectamine LTX reagent (Invitrogen A12621) according to manufacturer's recommendations. Transfection was carried out for 36 hours prior to subsequent analysis. Success of transfection was assessed using immunoblots, as well as indirect immunofluorescence.

4.3.4 Immunofluorescence

Following cortisol treatment or transfection, cells were fixed with 2% paraformaldehyde for 1 hour at room temperature. After paraformaldehyde was removed, cells were washed three times using PBS and blocked with 5% BSA for 1 hour. Then, blocking buffer was removed and cells were incubated with rabbit anti-NSMase II antibody (1:100; Santa Cruz Biotechnology sc-67305) for 2 hours. After washing with PBS three times, cells were further incubated with goat anti-rabbit Alexa 488 (1:500; Invitrogen A-11008) for 1 hour. To visualize the nuclei, cells were stained with either Hoechst 33342 for 5 minutes, or propidium iodide for 15 minutes. Finally, cells were washed 3 times with PBS and mounted using Fluoromount G. Images were taken on a Leica microscope using 40X oil objective.

4.3.5 PFO-D4-GFP_GST expression and purification

The construct PFO-D4-GFP_GST was kindly provided by Dr. Irina Pikuleva from Case Western Reserve University. This construct was transformed into BL21(DE3) *E.coli* (New England BioLabs C2527) using standard heat shock method. Ampicillin at a concentration of 100 μg/mL was used for selection. When the bacterial culture has

reached an optical density of approximately 0.6, PFO-D4-GFP_GST expression was induced by the addition of IPTG to a final concentration of 1 mM. The induced culture was grown for an additional 5 hours at 37°C before cells were harvested by centrifugation (4000 *g*, 30 minutes, 4°C). Following centrifugation, the bacterial cell pellet was resuspended in lysis buffer (50 mM Tris-HCl pH 8, 150 mM NaCl, 1 mM PMSF, 1% Triton X100, 1 mg/mL DNase I and 10 mg/mL lysozyme). Crude lysate was further lysed by pulse sonication (20 seconds on, 20 seconds off, 10 cycles). Another round of centrifugation (11300 *g*, 30 minutes, 4°C) was performed and the clarified lysate was applied to a glutathione sepharose 4B column pre-equilibrated with wash buffer (50 mM Tris-HCl pH 8, 150 mM NaCl). After the lysate has passed through the column, 5 column volumes of wash buffer was used to remove non-bound sample components followed by elution using wash buffer supplemented with 10 mM GSH. Finally, eluted PFO-D4-GFP_GST was concentrated and buffer exchanged into PBS pH 7.4 using Amicon centrifugal filter (Millipore UFC903008) before storage at -80°C.

4.3.6 PFO-D4-GFP staining

HEK 293 cells were grown on 4-chamber slides. Following transfection, cells were fixed with 2% paraformaldehyde for 1 hour at room temperature. Fixed cells were then washed 3 times using PBS and stained with PFO-D4-GFP_GST (1 mM) for 30 minutes. To visualize the nuclei, Hoechst 33342 stain was added for 5 minutes. Finally, cells were washed 3 times with PBS, mounted using Fluoromount G and imaged on a Leica microscope with 40X oil objective.

4.3.7 SMPD3 sub-cloning

Human full length SMPD3, which encodes NSMase II, was sub-cloned into bacterial expression vector pET28b using Cold Fusion Cloning Kit (MJS BioLynx Inc. SYMC010A1). The cloning strategy involves direct ligation of PCR amplified gene of interest to the linearized destination vector. Primers used for PCR were designed according to manufacturer's guidelines and contain bases complimentary to the gene of interest, as well as bases complementary to the linearized destination vector. The following primers were used for SMPD3 sub-cloning:

Forward 5' – GTG CCG CGC GGC AGC CAT ATG GTT TTG TAC ACG ACC CCC – 3'

Reverse 5' – GTG GTG GTG GTG GTG CTC GAG TGC CTC CTC CTC CCC CGA AGA C– 3'

Prior to ligation, destination vector pET28b was linearized by digestion with restriction enzymes NdeI and XhoI; and both PCR amplified SMPD3 and linearized pET28b were gel purified (Qiagen 20021). Ligation reaction was performed following manufacturer's protocol and the ligated plasmid DNA was transformed directly into chemically competent DH5 *E.coli* (New England BioLabs C2987). Colonies were screened using diagnostic restriction enzyme digest and partial sequencing (Robart's Research Institute).

4.3.8 NSMase II expression and purification

pET28b_SMPD3 was transformed into BL21(DE3) *E.coli* (New England BioLabs C2527). This plasmid encodes full length human NSMase II with two terminal 6X-Histidine tags to facilitate purification. A single colony from the transformation plate was inoculated into 25 mL of 2X YT medium containing 50 μg/mL kanamycin and the culture was grown overnight at 37°C with shaking. This overnight culture was then used to inoculate 1L of 2X YT medium containing 50 μg/mL kanamycin and the culture was

again grown at 37°C until optical density reached approximately 0.6. Protein expression was induced by the addition of IPTG to a final concentration of 0.4 mM. The induced culture was grown for an additional 24 hours at room temperature before cells were harvested by centrifugation (4000 *g*, 30 minutes, 4°C). Following centrifugation, the bacterial cell pellet was resuspended in lysis buffer (50 mM Tris-HCl pH 7.5, 300 mM NaCl, 5 mM $MgCl_2$, 0.2% Triton X100, 1 mM DTT, 1 mM PMSF, 50 μg/mL DNase I and 100 μg/mL lysozyme). The crude lysate was incubated on ice for 30 minutes and further lysed by pulse sonication (20 seconds on, 20 seconds off, 30 cycles). Another round of centrifugation (11300 *g*, 30 minutes, 4°C) was performed and the clarified lysate was applied to nickel affinity (Sigma P6611) column pre-equilibrated with lysis buffer. Nickel affinity purification was performed strictly following manufacturer's protocol published by Sigma Aldrich with some modifications in buffer composition. The wash buffer contains 50 mM Tris-HCl pH 7.5, 300 mM NaCl, 5 mM $MgCl_2$, 0.2% Triton X100, and 15 mM imidazole while the elution buffer contains 50 mM Tris-HCl pH 7.5, 300 mM NaCl, 5 mM $MgCl_2$, 0.2% Triton X100, and 300 mM imidazole. Eluted protein was buffer exchanged into storage solution (50 mM Tris-HCl pH 7.5, 5 mM $MgCl_2$ and 0.2% Triton X100) using Amicon centrifugal filter (Millipore UFC903008) before storage at -80°C.

4.3.9 NSMase Activity assay

NSMase activity was assessed using Amplex Red Sphingomyelinase Assay kit (Invitrogen A12220) in accordance with manufacturer's published protocol. In this fluorescence-based assay, NSMase activity is monitored indirectly using Amplex Red reagent, which is a fluorogenic probe for H_2O_2. Briefly, NSMase catalyzed SM

hydrolysis produces ceramide and phosphorylcholine. Then, phosphorylcholine is acted upon by alkaline phosphatase and choline oxidase to produce H_2O_2, which reacts with Amplex Red in the presence of horseradish peroxidase to generate a highly fluorescent end product.

4.3.10 Mass spectrometry

Purified NSMase II (1 mg/mL) was treated with 0.5 mM GSNO for 30 minutes in the dark. Enzyme mock-treated with PBS was used as the control. Following GSNO treatment, free –SH groups in NSMase II were labeled using 20 mM iodoacetamide (2 hours, room temperature, in the dark). Excess iodoacetamide was removed by passing the samples through desalting columns (Fisher Scientific 89882). Then, 10 mM sinapinic acid was used to reduce *S*-nitrosated thiols (1 hour, room temperature), followed by 20 mM *N*-ethylmaleimide treatment to label previously *S*-nitrosated thiols (50°C, 30 minutes). After labeling, excess *N*-ethylmaleimide was removed and samples were buffered exchanged into 50 mM ammonium bicarbonate (pH8.0) using desalting columns. Finally, protein samples were digested with trypsin (Promega V511A) overnight at 37°C (1:20 trypsin to protein ratio). C18 Zip Tips (Millipore ZTC18S096) were used to clean up the tryptic peptides before MS analysis.

4.4 Results and Discussion

4.4.1 Effect of cortisol treatment on NSMase II expression and activity

NSMase II catalyzed ceramide generation is involved in cellular stress response. Stressors such as hydrogen peroxide can selectively up-regulate the expression or activity of NSMase II; concomitant increase in ceramide levels then mediates the appropriate stress response (*e.g.*, cell cycle arrest, apoptosis) [228]. In this section, cortisol exposure was used as the stressor and its effect on endogenous NSMase II expression and activity was investigated. Triple negative breast cancer cells (HTB 126) were exposed to 80 μM cortisol for 24 hours. Following treatment, cell viability was assessed using Trypan Blue. Results show cortisol exposure does not negatively affect viability. Both control and treated cells exhibit similar viability at approximately 95% **(Figure 4.4.1-1 A)**. NSMaseII expression level and activity were determined using immunofluorescence and Amplex Red enzyme-coupled assay, respectively. In both cases, no significant difference was observed between DMSO-treated control cells and cortisol-treated cells **(Figure 4.4.1-1 B-D)**. However, cortisol-treated cells are larger in size than their control counterparts **(Figure 4.4.1-1 B)**. Although the underlying mechanism has not yet been determined, it is possible that cortisol could play a role in promoting cell growth or inhibiting cell division.

To explore the reason for lack of NSMase II activation in response to cortisol, the following factor should be considered:

1. HTB126 is a triple negative breast cancer cell line. Its basal level of NSMase II expression and activity needs to be carefully evaluated. For this project, Amplex Red assay kit was used to estimate NSMase II activity. This method is indirect and measures

enzyme coupled hydrogen peroxide generation. Although this assay works well with purified NSMase II *in vitro*, it may not be suitable for complex cellular lysate samples since enzymes/molecules within the lysate could affect hydrogen peroxide levels. Measurement of cellular ceramide levels will complement our NSMase II activity results.

2. Acute stress and chronic stress may elicit different responses. Varying the length of cortisol exposure will offer insight in this area.

3. In literature, NSMase II was almost always over-expressed before cells were exposed to stimuli/stressor; whereas we looked at endogenous NSMase II. Different experiment methods will affect results obtained.

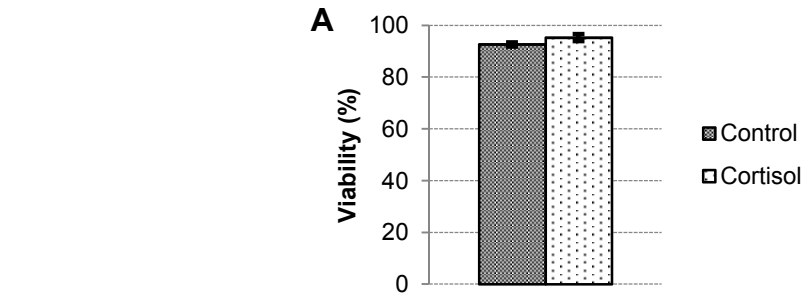
A
100
80
60
40
20
0
Viability (%)
Control
Cortisol

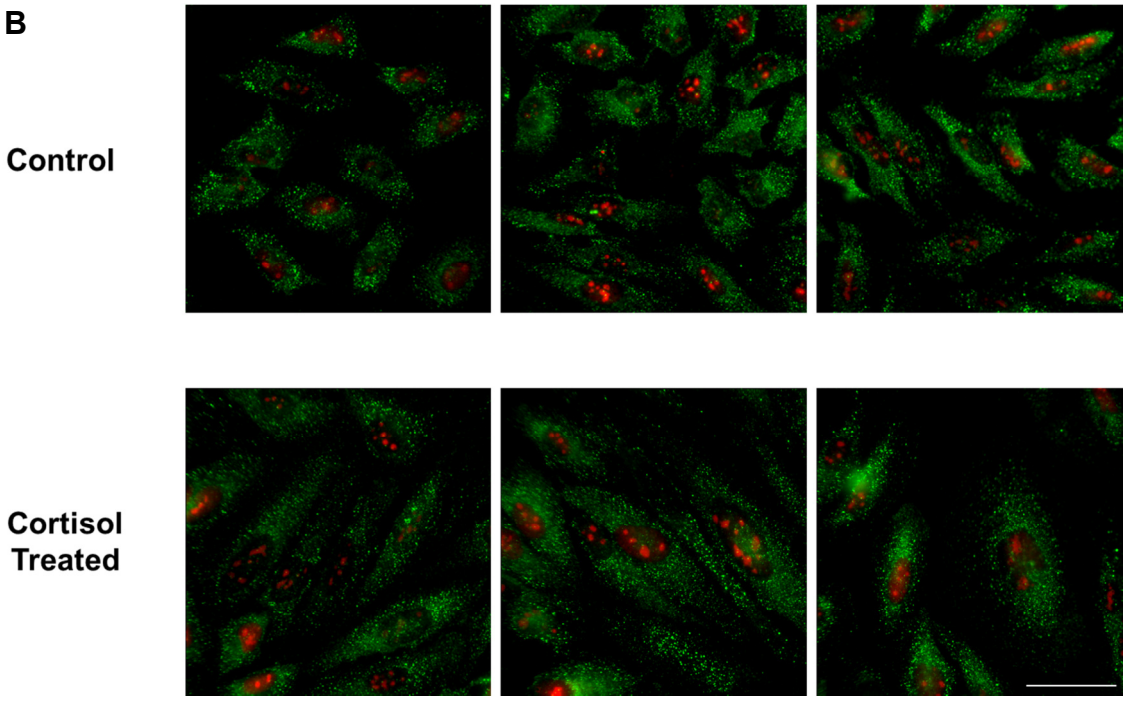
B
Control
Cortisol
Treated

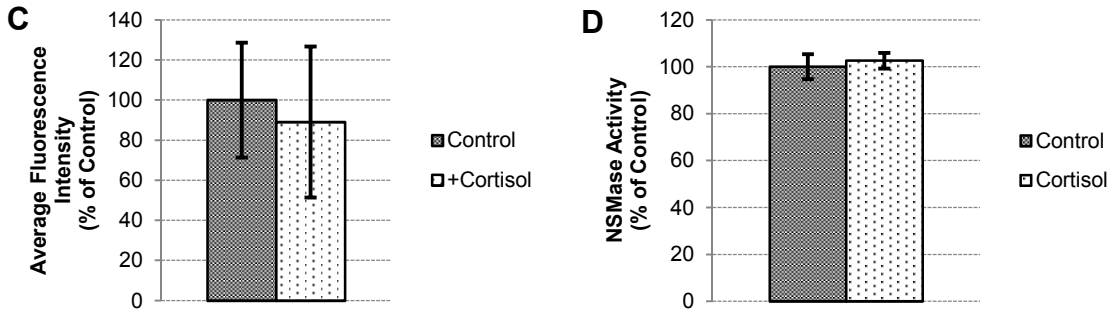
C
140
120
100
80
60
40
20
0
Average Fluorescence Intensity (% of Control)
Control
+Cortisol
D
120
100
80
60
40
20
0
NSMase Activity (% of Control)
Control
Cortisol

Figure 4.4.1-1 Effect of cortisol treatment on NSMase II expression and activity

HTB 126 cells were treated with 80 μM cortisol for 24 hours. **(A)** Viability was assessed using trypan blue exclusion assay. Percent viable is shown as mean ± SD (n=4). **(B)** After cortisol treatment, cells were fixed using 2% paraformaldehyde, stained with anti-NSMase II antibody, followed by Alexa 488 conjugated secondary antibody. Nuclei were visualized using propidium iodide. 3 representative images were shown from 3 independent experiments. Scale bar = 25 μm. **(C)** Fluorescence from ~50 cells were quantified using *ImageJ* as integrated density. Cumulative results were shown as % of control. Error bars represent SD. **(D)** NSMase activity from cell lysate was estimated using the Amplex Red activity assay kit. Results are shown as % of control. Error bars represent SD.

4.4.2 NSMase II over-expression is associated with decreases in plasma membrane cholesterol content

Within the plasma membrane, SM preferentially associates with cholesterol to form ordered microdomains [240] and evidence exist for the coordinated regulation of SM and cholesterol levels [233]. To determine whether plasma membrane cholesterol levels can be indirectly regulated by NSMase II activity, transient transfection was performed to over-express untagged NSMase II in HEK 293 cells. Transfection success was confirmed using immunoblotting **(Figure 4.4.2-1 A)**. Activity assay was performed and more than 2-fold increase in activity was observed following transfection **(Figure 4.4.2-1 B)**, demonstrating that over-expressed NSMase II is active. PFO-D4-GFP_GST was used to label plasma membrane cholesterol and imaging results indicated an inverse relationship between NSMase II expression/activity and plasma membrane cholesterol content **(Figure 4.4.2-2)**. This demonstrates modulation of NSMase II activity is accompanied by alterations in plasma membrane cholesterol level; which is suggestive that in addition to ceramide generation, NSMase II may also elicit physiological responses by affecting lipid raft formation.

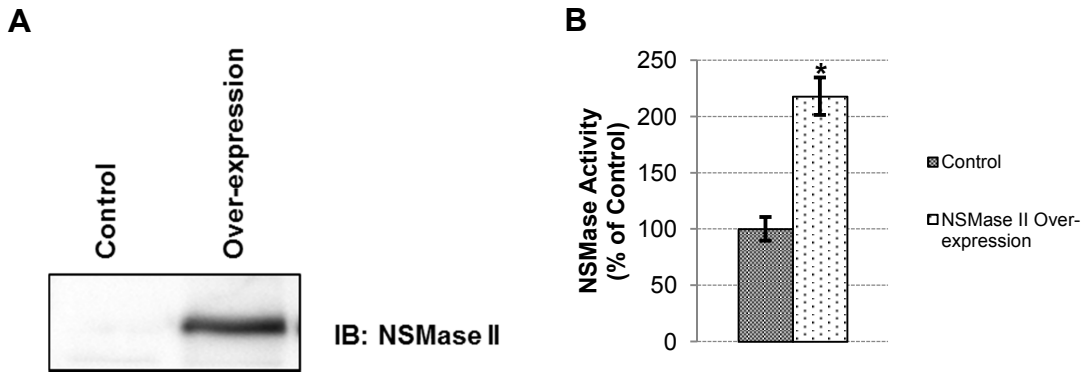

Figure 4.4.2-1 Over-expression of NSMase II is correlated with increased activity

HEK 293 cells were transiently transfected to over-express NSMase II. **(A)** 36 hours after transfection, cells were harvested and lysed using non-denaturing lysis buffer. Protein concentrations were determined for each sample and equal amounts were run on SDS-PAGE. Following separation, proteins were transferred to PVDF membrane and blotted for NSMase II. **(B)** NSMase activity from cell lysate was estimated using Amplex Red NSMase activity assay kit. Results are shown as % of control. Error bars represent SD. *Statistically different from control ($p < 0.05$).

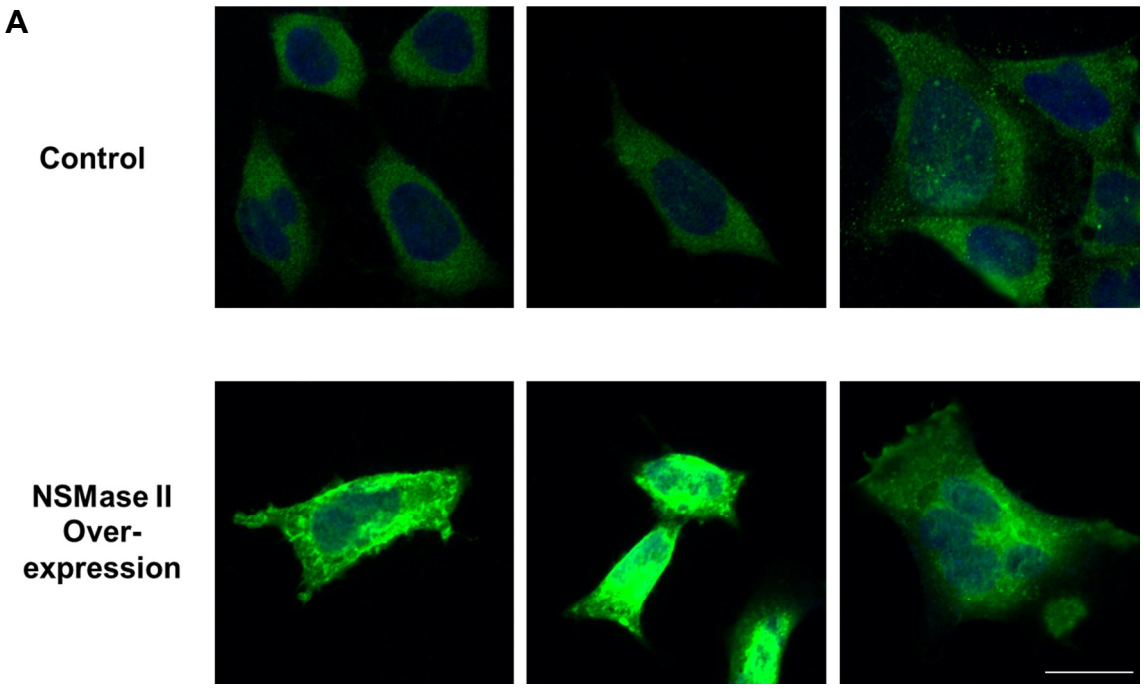
A
Control
NSMase II Over-expression

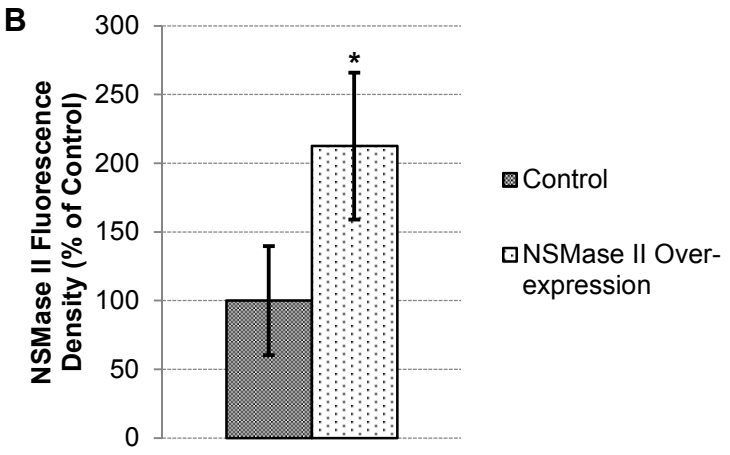
B
NSMase II Fluorescence Density (% of Control)
300
250
200
150
100
50
0
*
Control
NSMase II Over-expression

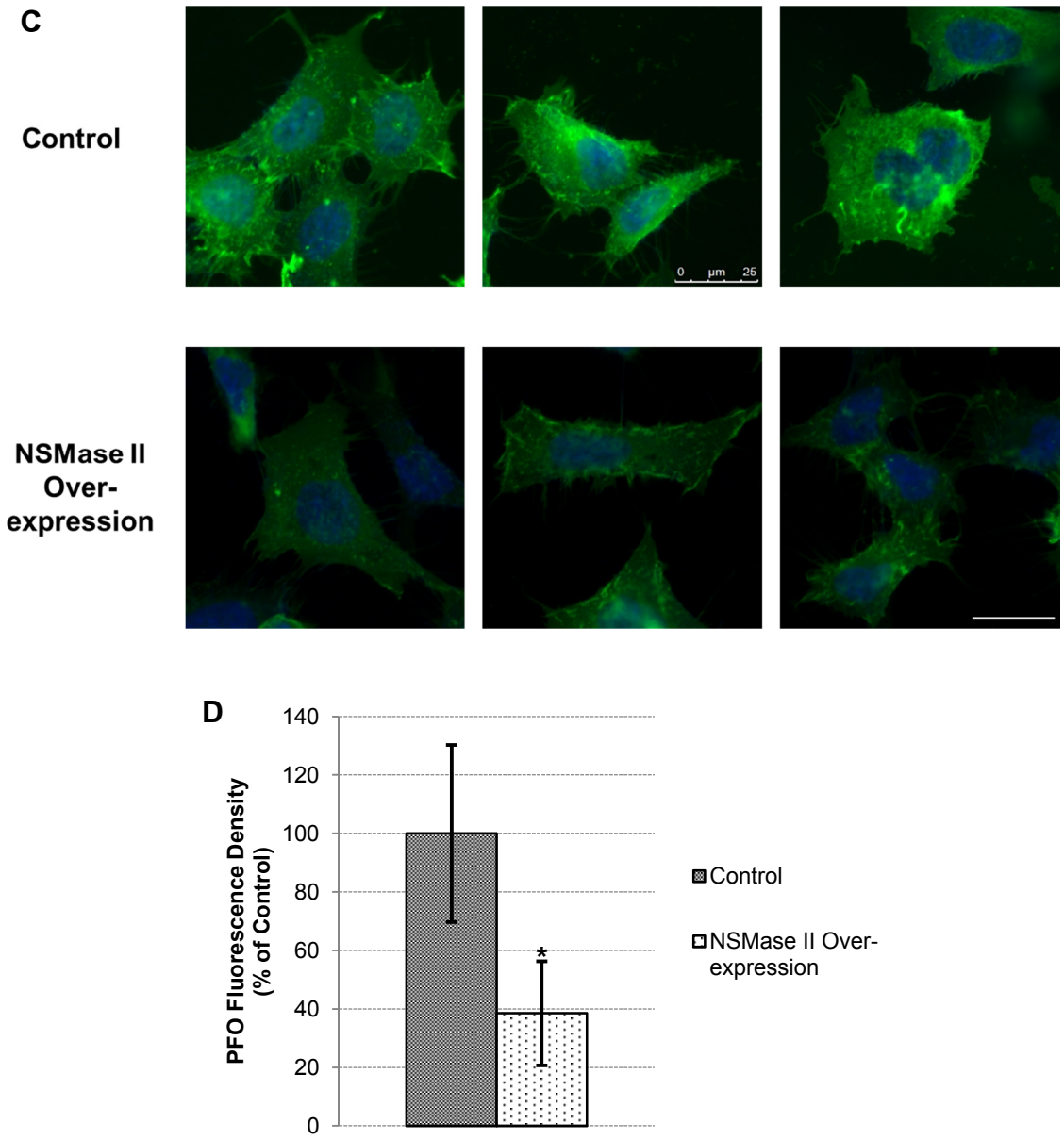

Figure 4.4.2-2 NSMase II over-expression is correlated with decreased plasma membrane cholesterol level

HEK 293 cells were plated on 4 chamber slides and transiently transfected to over-express NSMase II. **(A)** 36 hours after transfection, cells were fixed using 2% paraformaldehyde, stained with anti-NSMase II antibody, followed by Alexa 488 conjugated secondary antibody. Nuclei were visualized using Hoechst 33342 stain. 3 representative images were shown from 3 independent experiments. Scale bar = 25 µm.

(B) Fluorescence from ~50 cells were quantified using *ImageJ* as integrated density. Cumulative results were shown as % of control. Error bars represent SD. **(C)** Cells were fixed using 2% paraformaldehyde and labeled with the plasma membrane cholesterol probe PFO-D4-GFP_GST. Nuclei were visualized using Hoechst 33342 stain. 3 representative images were shown from 3 independent experiments. Scale bar = 25 μm. **(B)** Fluorescence from ~50 cells were quantified using *ImageJ* as integrated density. Cumulative results were shown as % of control. Error bars represent SD. *Statistically different from control ($p < 0.05$).

4.4.3 S-nitrosation mediated down-regulation of NSMase II activity

Exposure to cigarette smoke and hydrogen peroxide has been shown to lead to NSMase II activation, which augments ceramide mediated apoptosis in bronchial epithelial cells [160]. Interestingly, when we treated HTB 126 cells with hydrogen peroxide, NSMase II activity decreased by approximately 40% and cell viability was not negatively affected **(Figure 4.4.3-1)**. This led us to speculate whether NSMase II activity is selectively down-regulated in cancer cells in order to evade ceramide induced apoptosis. Since human NSMase II is a redox-sensitive enzyme with a total of 23 cysteine residues, *S*-nitrosation became the candidate modification under investigation. Currently, reactivity of these cysteine residues, as well as their susceptibility towards modification, are not fully understood. We purified recombinant NSMase II from bacteria and our enzyme preparation is catalytically functional **(Figure 4.4.3-2 A)**. Incubation with GSNO decreases NSMase II activity in a concentration dependent manner **(Figure 4.4.3-2 B)**, suggesting potential regulation of enzyme activity through protein *S*-nitrosation.

Numerous attempts were made to identify candidate *S*-nitrosation sites using mass spectrometry. This has proven to be challenging due to low sequence coverage and low signal intensity. Very few peptides were detected and none of them contain cysteine residues **(Table 4.4.3)**. This might be due to inherent properties of membrane proteins and peptide enrichment is likely needed in order to achieve better sequence coverage.

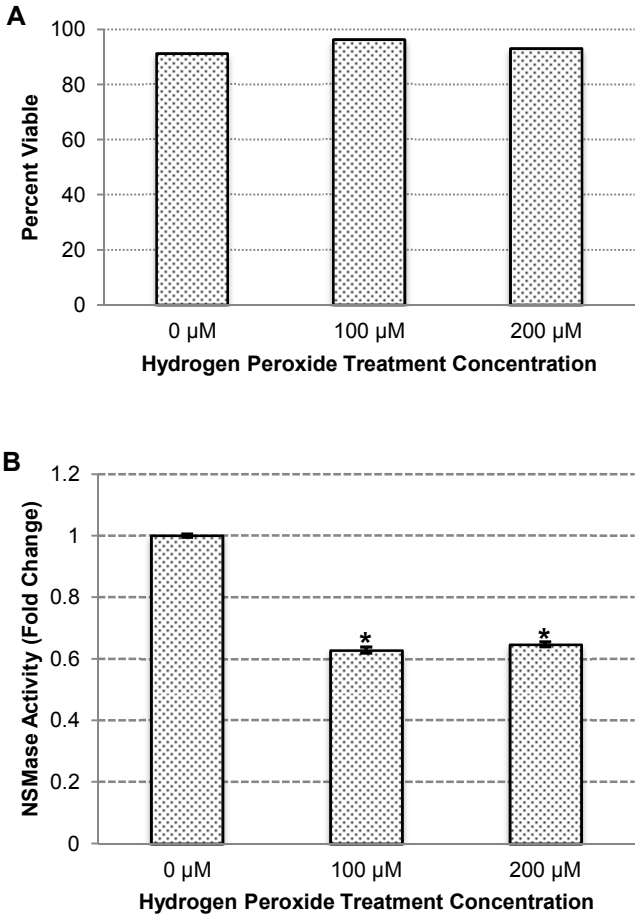

Figure 4.4.3-1 Effect of hydrogen peroxide treatment on HTB 126 cells

HTB 126 cells were treated with hydrogen peroxide in complete cell culture medium for 30 minuts. **(A)** Viability was assessed using Trypan Blue. **(B)** Following treatment, culture medium was removed and cells were washed 3 times with DPBS. Lysates were prepared by homogenization and total protein concentration was determined using Bradford reagent. NSMase II activity from cellular lysates (protein concentrations were equalized) was assayed using Amplex Red assay kit. Error bars represent SD (n=3). *statistically different from control.

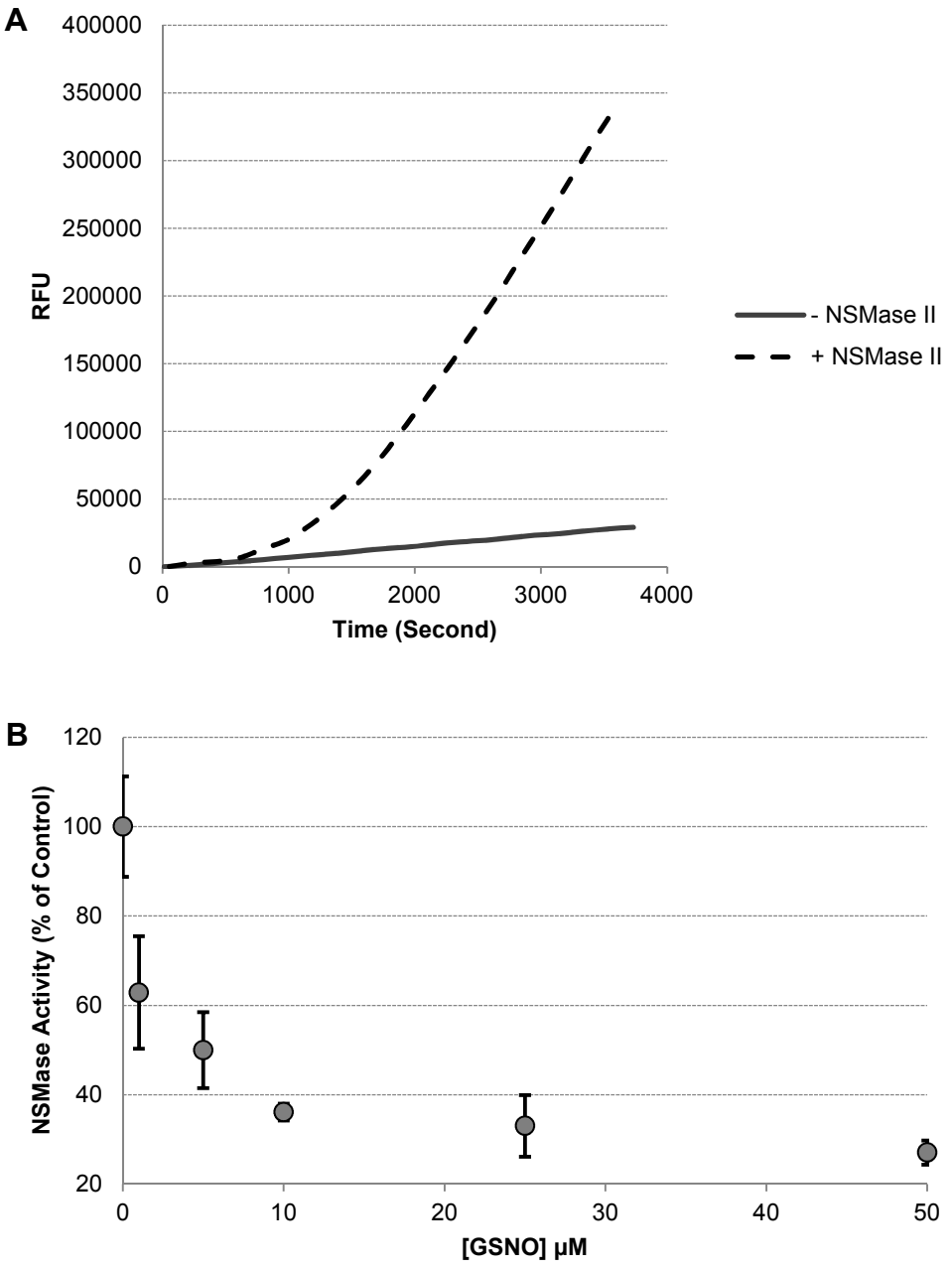

Figure 4.4.3-2 *In vitro* GSNO treatment attenuates NSMase II activity

Recombinant NSMase II was purified from *E.coli*. **(A)** NSMase II activity from purified enzyme preparation was assayed using Amplex Red assay kit. **(B)** Purified NSMase II was treated with various concentrations of GSNO for 30 minutes. Enzyme activity was then assessed using Amplex Red assay kit. Error bars represent SD.

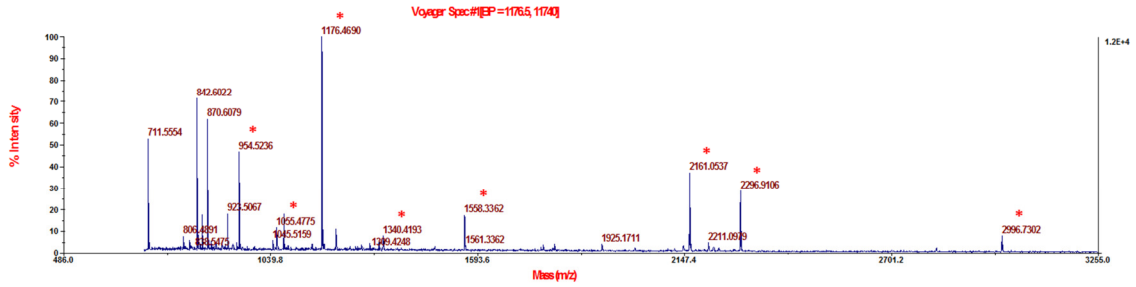

Figure 4.4.3-3 MALDI-MS spectrum of NSMase II tryptic digest

Purified NSMase II is treated with 0.5 mM GSNO and differentially labeled with iodoacetamide and *N*-ethylmaleimide. Sample is digested with trypsin and analyzed using Applied Biosystems Voyager DE-Pro Mass Spectrometer. Spectra peaks were manually compared to theoretical digest masses predicted by UCSF Protein Prospector.

Table 4.4.3 NSMase II peptides identified by MALDI-MS

Theoretical Mass (m/z)	Observed Mass (m/z)	Peptide Sequence
954.5156 954.5479	954.5255	(R)RPYIYSR(L) (R)NGAARPQIK(I)
1055.5408	1055.4794	(R)EYLAFPTSK(S)
1074.5538	1074.4829	(K)VLESEEGRR(E)
1176.6120	1176.4709	(R)VNNLFNTQAR(A)
1214.6124	1214.4341	(K)VQVGSTPQDQR(I)
1340.7096	1340.4207	(R)LAASFIPTTYEK(R)
1558.7761	1558.3383	(K)LEQQHSLFTHYR(D)
2161.0268	2160.0500	(R)IGGEEGGRPPEADDPVPGGQAR(N)
2297.0137	2296.9139	(R)GQTPNHNQQDGDSGSLGSPSASR(E)
2997.4800	2996.7330	(K)IYIDSPTNTSISAASFSSLVSPQGGDGVAR(A)

4.5 Conclusion

Cortisol exposure at a concentration of 80 μM led to increases in cell size. However, NSMase II expression and activity were not affected. When looking at the relationship between NSMase II and plasma membrane cholesterol, it was observed that increased NSMase II activity is correlated with decreased cholesterol. This suggests NSMase II activity may contribute to the regulation of lipid raft signaling events. In addition, we presented evidence that *S*-nitrosation is potentially involved in the down-regulation of NSMase II activity. Further studies will need to be performed to identify specific residues involved.

CHAPTER 5

General Conclusion

Protein *S*-nitrosation is the covalent attachment of NO derived nitroso group to reactive cysteine thiols. This reversible post-translational modification affects many aspects of protein function, such as activity, localization and stability. In the cellular environment, *S*-nitrosated proteins often exist in equilibrium with GSNO via transnitrosation. As a result, enzymes with GSNO metabolizing activity can indirectly drive protein denitrosation. Multiple enzyme systems have been shown to metabolize GSNO. Of these enzymes, GSNOR is the most efficient at removing the NO equivalents stored in GSNO. In addition, aberrant GSNOR activity is implicated in a large number of human diseases. GSNOR inhibition represents a relatively recent therapeutic approach and the evaluation of small molecule inhibitors is an active area of research. Conventionally, GSNOR activity is assayed by looking at absorbance decreases at 340 nm, which corresponds to NADH and GSNO consumption. While this method is easy to use, its application is limited to purified enzyme *in vitro*. In chapter 2, we reported the synthesis and characterization of OAbz-GSNO, a fluorogenic substrate for GSNOR. The fluorescence of OAbz-GSNO is enhanced upon reduction of its –SNO moiety; and the rate of fluorescence increase is correlated with GSNOR activity. This substrate is membrane permeable and can be used to monitor endogenous GSNOR activity in live cells. Overall, OAbz-GSNO is the first compound to be reported which can be used to measure GSNOR activity, both *in vitro* and in live cells. This substrate represents an additional tool researchers could use to assess the activity of GSNOR.

It is well-established that GSNOR plays an important role in maintaining SNO homeostasis. However, regulation of its activity remains poorly understood. Chapter 3 focuses on the identification of potential post-translational mechanisms involved in the regulation of GSNOR activity. Site-directed mutagenesis and chemical acetylation experiments provided evidence that acetylation of Lys101, which is adjacent to the zinc

finger motif, may negatively regulate GSNOR activity. Through kinetic and computational studies, we also identified a putative allosteric GSNO binding site. Results suggest GSNO binding to this allosteric site may enhance GSNOR activity. Our model of substrate activation allows GSNOR to exhibit enhanced activity when GSNO is present, effectively returning the system to homeostasis.

NSMase II catalyzes the hydrolysis of sphingomyelin to generate bioactive ceramide, a second messenger molecule capable of mediating a variety of cellular events. Activation of NSMase II is an important mechanism of cellular stress response. In chapter 4, we exposed cultured breast cancer cells to cortisol and observed that this treatment did not have any effect on NSMase II expression/activity. Interestingly, cortisol-treated cells grew to be much larger in size than their control counterparts. The underlying mechanism has yet to be determined. NSMase II over-expression was correlated with decreased plasma membrane cholesterol levels. Since cholesterol is an important component in the formation of lipid rafts, this finding carries the implication that induction of NSMase II not only generates ceramide, but could also affect additional signaling pathways mediated through lipid rafts. *In vitro* treatment with GSNO attenuates NSMase II activity, suggesting that protein *S*-nitrosation may be one of the modifications involved in the regulation of NSMase II activity.

REFERENCES

[1] Furchgott, R. F.; Zawadski, J. Acetylcholine Relaxes Arterial Smooth-Muscle by Releasing a Relaxing Substance from Endothelial-Cells. *Fed Proc* **39:**581-581; 1980.

[2] Ignarro, L. J.; Buga, G. M.; Wood, K. S.; Byrns, R. E.; Chaudhuri, G. Endothelium-Derived Relaxing Factor Produced and Released from Artery and Vein Is Nitric-Oxide. *P Natl Acad Sci USA* **84:**9265-9269; 1987.

[3] Palmer, R. M. J.; Ferrige, A. G.; Moncada, S. Nitric-Oxide Release Accounts for the Biological-Activity of Endothelium-Derived Relaxing Factor. *Nature* **327:**524-526; 1987.

[4] Furchgott, R. F.; Khan, M. T.; Jothianandan, D. Comparison of Endothelium-Dependent Relaxation and Nitric Oxide-Induced Relaxation in Rabbit Aorta. *Fed Proc* **46:**385-385; 1987.

[5] Moncada, S.; Radomski, M. W.; Palmer, R. M. J. Endothelium-Derived Relaxing Factor - Identification as Nitric-Oxide and Role in the Control of Vascular Tone and Platelet-Function. *Biochem Pharmacol* **37:**2495-2501; 1988.

[6] Amezcua, J. L.; Palmer, R. M. J.; Desouza, B. M.; Moncada, S. Nitric-Oxide Synthesized from L-Arginine Regulates Vascular Tone in the Coronary Circulation of the Rabbit. *Brit J Pharmacol* **97:**1119-1124; 1989.

[7] Loscalzo, J.; Welch, G. Nitric-Oxide and Its Role in the Cardiovascular-System. *Prog Cardiovasc Dis* **38:**87-104; 1995.

[8] Rees, D. D.; Palmer, R. M. J.; Moncada, S. Role of Endothelium-Derived Nitric-Oxide in the Regulation of Blood-Pressure. *P Natl Acad Sci USA* **86:**3375-3378; 1989.

[9] Stamler, J. S.; Loh, E.; Roddy, M. A.; Currie, K.; Creager, M. Nitric Oxide Regulates Systemic Arterial Blood Pressure and Pulmonary Vascular Tone in Normal Subjects. *Biology of Nitric Oxide, Pt 3* **8:**447-448; 1994.

[10] Murohara, T.; Asahara, T.; Silver, M.; Bauters, C.; Masuda, H.; Kalka, C.; Kearney, M.; Chen, D. H.; Chen, D. F.; Symes, J. F.; Fishman, M. C.; Huang, P. L.; Isner, J. M. Nitric oxide synthase modulates angiogenesis in response to tissue ischemia. *J Clin Invest* **101:**2567-2578; 1998.

[11] Schuman, E. M.; Madison, D. V. A Requirement for the Intercellular Messenger Nitric-Oxide in Long-Term Potentiation. *Science* **254:**1503-1506; 1991.

[12] Bon, C.; Bohme, G. A.; Doble, A.; Stutzmann, J. M.; Blanchard, J. C. A Role for Nitric-Oxide in Long-Term Potentiation. *Eur J Neurosci* **4:**420-424; 1992.

[13] Wink, D. A.; Hines, H. B.; Cheng, R. Y. S.; Switzer, C. H.; Flores-Santana, W.; Vitek, M. P.; Ridnour, L. A.; Colton, C. A. Nitric oxide and redox mechanisms in the immune response. *J Leukocyte Biol* **89:**873-891; 2011.

[14] Nathan, C. F.; Hibbs, J. B. Role of Nitric-Oxide Synthesis in Macrophage Antimicrobial Activity. *Current Opinion in Immunology* **3:**65-70; 1991.

[15] Witte, M. B.; Barbul, A. Role of nitric oxide in wound repair. *Am J Surg* **183:**406-412; 2002.

[16] Palmer, R. M. J.; Ashton, D. S.; Moncada, S. Vascular Endothelial-Cells Synthesize Nitric-Oxide from L-Arginine. *Nature* **333:**664-666; 1988.

[17] Stuehr, D. J.; Kwon, N. S.; Nathan, C. F.; Griffith, O. W.; Feldman, P. L.; Wiseman, J. N omega-hydroxy-L-arginine is an intermediate in the biosynthesis of nitric oxide from L-arginine. *J Biol Chem* **266:**6259-6263; 1991.

[18] Knowles, R. G.; Moncada, S. Nitric-Oxide Synthases in Mammals. *Biochem J* **298:**249-258; 1994.

[19] Forstermann, U.; Closs, E. I.; Pollock, J. S.; Nakane, M.; Schwarz, P.; Gath, I.; Kleinert, H. Nitric-Oxide Synthase Isozymes - Characterization, Purification, Molecular-Cloning, and Functions. *Hypertension* **23:**1121-1131; 1994.

[20] Forstermann, U.; Sessa, W. C. Nitric oxide synthases: regulation and function. *Eur Heart J* **33:**829-+; 2012.

[21] Bohme, G. A.; Bon, C.; Lemaire, M.; Reibaud, M.; Piot, O.; Stutzmann, J. M.; Doble, A.; Blanchard, J. C. Altered Synaptic Plasticity and Memory Formation in Nitric-Oxide Synthase Inhibitor-Treated Rats. *P Natl Acad Sci USA* **90:**9191-9194; 1993.

[22] Zhou, L.; Zhu, D. Y. Neuronal nitric oxide synthase: Structure, subcellular localization, regulation, and clinical implications. *Nitric Oxide-Biol Ch* **20:**223-230; 2009.

[23] Togashi, H.; Sakuma, I.; Yoshioka, M.; Kobayashi, T.; Yasuda, H.; Kitabatake, A.; Saito, H.; Gross, S. S.; Levi, R. A Central-Nervous-System Action of Nitric-Oxide in Blood-Pressure Regulation. *J Pharmacol Exp Ther* **262:**343-347; 1992.

[24] Esplugues, J. V. NO as a signalling molecule in the nervous system. *Brit J Pharmacol* **135:**1079-1095; 2002.

[25] Fleming, I.; Busse, R. Molecular mechanisms involved in the regulation of the endothelial nitric oxide synthase. *Am J Physiol-Reg I* **284:**R1-R12; 2003.

[26] Azuma, H.; Ishikawa, M.; Sekizaki, S. Endothelium-Dependent Inhibition of Platelet-Aggregation. *Brit J Pharmacol* **88:**411-415; 1986.

[27] Li, H. G.; Forstermann, U. Nitric oxide in the pathogenesis of vascular disease. *Journal of Pathology* **190:**244-254; 2000.

[28] Cary, S. P. L.; Winger, J. A.; Derbyshire, E. R.; Marletta, M. A. Nitric oxide signaling: no longer simply on or off. *Trends Biochem Sci* **31:**231-239; 2006.

[29] Martinez-Ruiz, A.; Cadenas, S.; Lamas, S. Nitric oxide signaling: Classical, less classical, and nonclassical mechanisms. *Free Radical Bio Med* **51:**17-29; 2011.

[30] Brown, G. C.; Cooper, C. E. Nanomolar Concentrations of Nitric-Oxide Reversibly Inhibit Synaptosomal Respiration by Competing with Oxygen at Cytochrome-Oxidase. *Febs Lett* **356:**295-298; 1994.

[31] Erusalimsky, J. D.; Moncada, S. Nitric oxide and mitochondrial signaling from physiology to pathophysiology. *Arterioscl Throm Vas* **27:**2524-2531; 2007.

[32] Heinrich, T. A.; da Silva, R. S.; Miranda, K. M.; Switzer, C. H.; Wink, D. A.; Fukuto, J. M. Biological nitric oxide signalling: chemistry and terminology. *Brit J Pharmacol* **169:**1417-1429; 2013.

[33] Forman, H. J.; Fukuto, J. M.; Torres, M. Redox signaling: thiol chemistry defines which reactive oxygen and nitrogen species can act as second messengers. *Am J Physiol-Cell Ph* **287:**C246-C256; 2004.

[34] Foster, M. W.; Hess, D. T.; Stamler, J. S. Protein S-nitrosylation in health and disease: a current perspective. *Trends Mol Med* **15:**391-404; 2009.

[35] Derakhshan, B.; Hao, G.; Gross, S. S. Balancing reactivity against selectivity: The evolution of protein S-nitrosylation as an effector of cell signaling by nitric oxide. *Cardiovasc Res* **75:**210-219; 2007.

[36] Stamler, J. S.; Toone, E. J.; Lipton, S. A.; Sucher, N. J. (S)NO signals: Translocation, regulation, and a consensus motif. *Neuron* **18:**691-696; 1997.

[37] Doulias, P. T.; Greene, J. L.; Greco, T. M.; Tenopoulou, M.; Seeholzer, S. H.; Dunbrack, R. L.; Ischiropoulos, H. Structural profiling of endogenous S-nitrosocysteine residues reveals unique features that accommodate diverse mechanisms for protein S-nitrosylation. *P Natl Acad Sci USA* **107:**16958-16963; 2010.

[38] Marino, S. M.; Gladyshev, V. N. Structural Analysis of Cysteine S-Nitrosylation: A Modified Acid-Based Motif and the Emerging Role of Trans-Nitrosylation. *J Mol Biol* **395:**844-859; 2010.

[39] Anand, P.; Stamler, J. S. Enzymatic mechanisms regulating protein S-nitrosylation: implications in health and disease. *J Mol Med (Berl)* **90:**233-244; 2012.

[40] Guikema, B.; Lu, Q.; Jourd'heuil, D. Chemical considerations and biological selectivity of protein nitrosation: Implications for NO-mediated signal transduction. *Antioxid Redox Sign* **7:**593-606; 2005.

[41] Broniowska, K. A.; Hogg, N. The Chemical Biology of S-Nitrosothiols. *Antioxid Redox Sign* **17:**969-980; 2012.

[42] Lancaster, J. R. Nitroxidative, nitrosative, and nitrative stress: Kinetic predictions of reactive nitrogen species chemistry under biological conditions. *Chem Res Toxicol* **19:**1160-1174; 2006.

[43] Lim, C. H.; Dedon, P. C.; Deen, W. A. Kinetic Analysis of Intracellular Concentrations of Reactive Nitrogen Species. *Chem Res Toxicol* **21:**2134-2147; 2008.

[44] Ibiza, S.; Perez-Rodriguez, A.; Ortega, A.; Martinez-Ruiz, A.; Barreiro, O.; Garcia-Dominguez, C. A.; Victor, V. M.; Esplugues, J. V.; Rojas, J. M.; Sanchez-Madrid, F.; Serrador, J. M. Endothelial nitric oxide synthase regulates N-Ras activation on the Golgi complex of antigen-stimulated T cells. *P Natl Acad Sci USA* **105:**10507-10512; 2008.

[45] Iwakiri, Y.; Satoh, A.; Chatterjee, S.; Toomre, D. K.; Chalouni, C. M.; Fulton, D.; Groszmann, R. J.; Shah, V. H.; Sessa, W. C. Nitric oxide synthase generates nitric oxide locally to regulate compartmentalized protein S-nitrosylation and protein trafficking. *P Natl Acad Sci USA* **103:**19777-19782; 2006.

[46] Liu, X. P.; Miller, M. J. S.; Joshi, M. S.; Thomas, D. D.; Lancaster, J. R. Accelerated reaction of nitric oxide with O-2 within the hydrophobic interior of biological membranes. *P Natl Acad Sci USA* **95:**2175-2179; 1998.

[47] Gow, A. J.; Buerk, D. G.; Ischiropoulos, H. A novel reaction mechanism for the formation of S-nitrosothiol in vivo. *J Biol Chem* **272:**2841-2845; 1997.

[48] Schmidt, H. H. H. W.; Hofmann, H.; Schindler, U.; Shutenko, Z. S.; Cunningham, D. D.; Feelisch, M. No center dot NO from NO synthase. *P Natl Acad Sci USA* **93:**14492-14497; 1996.

[49] Basu, S.; Keszler, A.; Azarova, N. A.; Nwanze, N.; Perlegas, A.; Shiva, S.; Broniowska, K. A.; Hogg, N.; Kim-Shapiro, D. B. A novel role for cytochrome c: Efficient catalysis of S-nitrosothiol formation. *Free Radic Biol Med* **48:**255-263; 2010.

[50] Broniowska, K. A.; Keszler, A.; Basu, S.; Kim-Shapiro, D. B.; Hogg, N. Cytochrome c-mediated formation of S-nitrosothiol in cells. *Biochem J* **442:**191-197; 2012.

[51] Boese, M.; Mordvintcev, P. I.; Vanin, A. F.; Busse, R.; Mulsch, A. S-Nitrosation of Serum-Albumin by Dinitrosyl-Iron Complex. *J Biol Chem* **270:**29244-29249; 1995.

[52] Bosworth, C. A.; Toledo, J. C.; Zmijewski, J. W.; Li, Q.; Lancaster, J. R. Dinitrosyliron complexes and the mechanism(s) of cellular protein nitrosothiol formation from nitric oxide. *P Natl Acad Sci USA* **106:**4671-4676; 2009.

[53] Benhar, M.; Forrester, M. T.; Stamler, J. S. Protein denitrosylation: enzymatic mechanisms and cellular functions. *Nat Rev Mol Cell Bio* **10:**721-732; 2009.

[54] Jensen, D. E.; Belka, G. K.; Du Bois, G. C. S-Nitrosoglutathione is a substrate for rat alcohol dehydrogenase class III isoenzyme. *Biochem J* **331 (Pt 2):**659-668; 1998.

[55] Jourd'heuil, D.; Laroux, F. S.; Miles, A. M.; Wink, D. A.; Grisham, M. B. Effect of superoxide dismutase on the stability of S-nitrosothiols. *Arch Biochem Biophys* **361:**323-330; 1999.

[56] Hou, Y. C.; Guo, Z. M.; Li, J.; Wang, P. G. Seleno compounds and glutathione peroxidase catalyzed decomposition of S-nitrosothiols. *Biochem Bioph Res Co* **228:**88-93; 1996.

[57] Nikitovic, D.; Holmgren, A. S-nitrosoglutathione is cleaved by the thioredoxin system with liberation of glutathione and redox regulating nitric oxide. *J Biol Chem* **271:**19180-19185; 1996.

[58] Bateman, R. L.; Rauh, D.; Tavshanjian, B.; Shokat, K. M. Human carbonyl reductase 1 is an S-nitrosoglutathione reductase. *J Biol Chem* **283:**35756-35762; 2008.

[59] Broniowska, K. A.; Diers, A. R.; Hogg, N. S-Nitrosoglutathione. *Bba-Gen Subjects* **1830:**3173-3181; 2013.

[60] Persson, B.; Hedlund, J.; Jornvall, H. The MDR superfamily. *Cell Mol Life Sci* **65:**3879-3894; 2008.

[61] Hoog, J. O.; Ostberg, L. J. Mammalian alcohol dehydrogenases--a comparative investigation at gene and protein levels. *Chem Biol Interact* **191:**2-7; 2011.

[62] Pares, X.; Vallee, B. L. New Human-Liver Alcohol-Dehydrogenase Forms with Unique Kinetic Characteristics. *Biochem Bioph Res Co* **98:**122-130; 1981.

[63] Wagner, F. W.; Pares, X.; Holmquist, B.; Vallee, B. L. Physical and enzymatic properties of a class III isozyme of human liver alcohol dehydrogenase: chi-ADH. *Biochemistry-Us* **23:**2193-2199; 1984.

[64] Julia, P.; Boleda, M. D.; Farres, J.; Pares, X. Mammalian alcohol dehydrogenase: characteristics of class III isoenzymes. *Alcohol Alcohol Suppl* **1:**169-173; 1987.

[65] Koivusalo, M.; Baumann, M.; Uotila, L. Evidence for the identity of glutathione-dependent formaldehyde dehydrogenase and class III alcohol dehydrogenase. *Febs Lett* **257:**105-109; 1989.

[66] Uotila, L.; Koivusalo, M. Formaldehyde Dehydrogenase from Human Liver - Purification, Properties, and Evidence for Formation of Glutathione Thiol Esters by Enzyme. *J Biol Chem* **249:**7653-7663; 1974.

[67] Jones, D. P.; Thor, H.; Andersson, B.; Orrenius, S. Detoxification Reactions in Isolated Hepatocytes - Role of Glutathione Peroxidase, Catalase, and Formaldehyde Dehydrogenase in Reactions Relating to N-Demethylation by Cytochrome-P-450 System. *J Biol Chem* **253:**6031-6037; 1978.

[68] Hur, M. W.; Edenberg, H. J. Cloning and Characterization of the Adh5 Gene Encoding Human Alcohol Dehydrogenase-5, Formaldehyde Dehydrogenase. *Gene* **121:**305-311; 1992.

[69] Kwon, H. S.; Kim, M. S.; Edenberg, H. J.; Hur, M. W. Sp3 and Sp4 can repress transcription by competing with Sp1 for the core cis-elements on the human ADH5/FDH minimal promoter. *J Biol Chem* **274:**20-28; 1999.

[70] Zaman, K.; Palmer, L. A.; Doctor, A.; Hunt, J. F.; Gaston, B. Concentration-dependent effects of endogenous S-nitrosoglutathione on gene regulation by specificity proteins Sp3 and Sp1. *Biochem J* **380:**67-74; 2004.

[71] Kwon, H. S.; Lee, D. K.; Lee, J. J.; Edenberg, H. J.; Ahn, Y. H.; Hur, M. W. Posttranscriptional regulation of human ADH5/FDH and Myf6 gene expression by upstream AUG codons. *Arch Biochem Biophys* **386:**163-171; 2001.

[72] Yang, Z. N.; Bosron, W. F.; Hurley, T. D. Structure of human chi chi alcohol dehydrogenase: A glutathione-dependent formaldehyde dehydrogenase. *J Mol Biol* **265:**330-343; 1997.

[73] Engeland, K.; Hoog, J. O.; Holmquist, B.; Estonius, M.; Jornvall, H.; Vallee, B. L. Mutation of Arg-115 of Human Class-Iii Alcohol-Dehydrogenase - a Binding-Site Required for Formaldehyde Dehydrogenase-Activity and Fatty-Acid Activation. *P Natl Acad Sci USA* **90:**2491-2494; 1993.

[74] Sanghani, P. C.; Boston, W. F.; Hurley, T. D. Human glutathione-dependent formaldehyde dehydrogenase. Structural changes associated with ternary complex formation. *Biochemistry-Us* **41:**15189-15194; 2002.

[75] Sanghani, P. C.; Davis, W. I.; Zhai, L. M.; Robinson, H. Structure-function relationships in human glutathione-dependent formaldehyde dehydrogenase. role of Glu-67 and Arg-368 in the catalytic mechanism. *Biochemistry-Us* **45:**4819-4830; 2006.

[76] Sanghani, P. C.; Robinson, H.; Bennett-Lovsey, R.; Hurley, T. D.; Bosron, W. F. Structure-function relationships in human Class III alcohol dehydrogenase (formaldehyde dehydrogenase). *Chem-Biol Interact* **143:**195-200; 2003.

[77] Sanghani, P. C.; Robinson, H.; Bosron, W. F.; Hurley, T. D. Human glutathione-dependent formaldehyde dehydrogenase. Structures of Apo, Binary, and inhibitory ternary complexes. *Biochemistry-Us* **41:**10778-10786; 2002.

[78] Auld, D. S.; Bergman, T. The role of zinc for alcohol dehydrogenase structure and function. *Cell Mol Life Sci* **65:**3961-3970; 2008.

[79] Jelokova, J.; Karlsson, C.; Estonius, M.; Jornvall, H.; Hoog, J. O. Features of Structural Zinc in Mammalian Alcohol-Dehydrogenase - Site-Directed Mutagenesis of the Zinc Ligands. *Eur J Biochem* **225:**1015-1019; 1994.

[80] Danielsson, O.; Jornvall, H. Enzymogenesis - Classical Liver Alcohol-Dehydrogenase Origin from the Glutathione-Dependent Formaldehyde Dehydrogenase Line. *P Natl Acad Sci USA* **89:**9247-9251; 1992.

[81] Gutheil, W. G.; Holmquist, B.; Vallee, B. L. Purification, Characterization, and Partial Sequence of the Glutathione-Dependent Formaldehyde Dehydrogenase from Escherichia-Coli - a Class-Iii Alcohol-Dehydrogenase. *Biochemistry-Us* **31:**475-481; 1992.

[82] Luque, T.; Atrian, S.; Danielsson, O.; Jornvall, H.; Gonzalezduarte, R. Structure of the Drosophila-Melanogaster Glutathione-Dependent Formaldehyde Dehydrogenase Octanol Dehydrogenase Gene (Class-Iii Alcohol-Dehydrogenase) - Evolutionary Pathway of the Alcohol-Dehydrogenase Genes. *Eur J Biochem* **225:**985-993; 1994.

[83] Barber, R. D.; Rott, M. A.; Donohue, T. J. Characterization of a glutathione-dependent formaldehyde dehydrogenase from Rhodobacter sphaeroides. *J Bacteriol* **178:**1386-1393; 1996.

[84] Adinolfi, A.; Adinolfi, M.; Hopkinson, D. A. Immunological and Biochemical-Characterization of the Human Alcohol-Dehydrogenase Chi-Adh Isozyme. *Annals of Human Genetics* **48:**1-10; 1984.

[85] Estonius, M.; Svensson, S.; Hoog, J. O. Alcohol dehydrogenase in human tissues: Localisation of transcripts coding for five classes of the enzyme. *Febs Lett* **397:**338-342; 1996.

[86] Lee, S. L.; Wang, M. F.; Lee, A. I.; Yin, S. J. The metabolic role of human ADH3 functioning as ethanol dehydrogenase. *Febs Lett* **544:**143-147; 2003.

[87] Sanghani, P. C.; Stone, C. L.; Ray, B. D.; Pindel, E. V.; Hurley, T. D.; Bosron, W. F. Kinetic mechanism of human glutathione-dependent formaldehyde dehydrogenase. *Biochemistry-Us* **39:**10720-10729; 2000.

[88] Hedberg, J. J.; Hoog, J. O.; Nilsson, J. A.; Xi, Z.; Elfwing, A.; Grafstrom, R. C. Expression of alcohol dehydrogenase 3 in tissue and cultured cells from human oral mucosa. *Am J Pathol* **157:**1745-1755; 2000.

[89] Teng, S.; Beard, K.; Pourahmad, J.; Moridani, M.; Easson, E.; Poon, R.; O'Brien, P. J. The formaldehyde metabolic detoxification enzyme systems and molecular cytotoxic mechanism in isolated rat hepatocytes. *Chem-Biol Interact* **130:**285-296; 2001.

[90] Thompson, C. M.; Ceder, R.; Grafstrom, R. C. Formaldehyde dehydrogenase: Beyond phase I metabolism. *Toxicol Lett* **193:**1-3; 2010.

[91] Staab, C. A.; Hellgren, M.; Hoog, J. O. Dual functions of alcohol dehydrogenase 3: implications with focus on formaldehyde dehydrogenase and S-nitrosoglutathione reductase activities. *Cell Mol Life Sci* **65:**3950-3960; 2008.

[92] Godoy, L.; Gonzalez-Duarte, R.; Albalat, R. S-nitrosogluthathione reductase activity of amphioxus ADH3: insights into the nitric oxide metabolism. *Int J Biol Sci* **2:**117-124; 2006.

[93] Kubienova, L.; Ticha, T.; Jahnova, J.; Luhova, L.; Petrivalsky, M. S-Nitrosoglutathione Reductase: The Key Enzyme Regulator of S-nitrosylation. *Chem Listy* **107:**202-208; 2013.

[94] Thrasher, J. D.; Kilburn, K. H. Embryo toxicity and teratogenicity of formaldehyde. *Arch Environ Health* **56:**300-311; 2001.

[95] Kolomyitseva, E. N.; Semin, Y. A.; Poverennyi, A. M. Effects of the Reaction-Products of Formaldehyde with Various Amines on Nucleic-Acids and Their Components. *Mol Biol+* **12:**946-952; 1978.

[96] Conaway, C. C.; Whysner, J.; Verna, L. K.; Williams, G. M. Formaldehyde mechanistic data and risk assessment: Endogenous protection from DNA adduct formation. *Pharmacol Therapeut* **71:**29-55; 1996.

[97] Xu, Z. Q.; Yang, F. X.; Yi, Z. W. Mechanism Research of Toxic and Harmful Environmental Factors on Renal Damage in Children. *Prog Safety Sci Tech* **8:**2472-2481; 2010.

[98] James, W.; Jia, C. R.; Kedia, S. Uneven Magnitude of Disparities in Cancer Risks from Air Toxics. *Int J Env Res Pub He* **9:**4365-4385; 2012.

[99] Pontel, L. B.; Rosado, I. V.; Burgos-Barragan, G.; Garaycoechea, J. I.; Yu, R.; Arends, M. J.; Chandrasekaran, G.; Broecker, V.; Wei, W.; Liu, L. M.; Swenberg, J. A.; Crossan, G. P.; Patel, K. J. Endogenous Formaldehyde Is a Hematopoietic Stem Cell Genotoxin and Metabolic Carcinogen. *Mol Cell* **60:**177-188; 2015.

[100] Lai, Y. Q.; Yu, R.; Hartwell, H. J.; Moeller, B. C.; Bodnar, W. M.; Swenberg, J. A. Measurement of Endogenous versus Exogenous Formaldehyde-Induced DNA-Protein Crosslinks in Animal Tissues by Stable Isotope Labeling and Ultrasensitive Mass Spectrometry. *Cancer Res* **76:**2652-2661; 2016.

[101] Uotila, L.; Koivusalo, M. Purification and Properties of S-Formylglutathione Hydrolase from Human Liver. *J Biol Chem* **249:**7664-7672; 1974.

[102] Board, P. G.; Coggan, M. Genetic-Heterogeneity of S-Formylglutathione Hydrolase. *Annals of Human Genetics* **50:**35-39; 1986.

[103] Iborra, F. J.; Renaupiqueras, J.; Portoles, M.; Boleda, M. D.; Guerri, C.; Pares, X. Immunocytochemical and Biochemical Demonstration of Formaldehyde Dehydrogenase (Class-Iii Alcohol-Dehydrogenase) in the Nucleus. *J Histochem Cytochem* **40:**1865-1878; 1992.

[104] Sophos, N. A.; Vasiliou, V. Aldehyde dehydrogenase gene superfamily: the 2002 update. *Chem-Biol Interact* **143:**5-22; 2003.

[105] Cinti, D. L.; Keyes, S. R.; Lemelin, M. A.; Denk, H.; Schenkman, J. B. Biochemical Properties of Rat-Liver Mitochondrial Aldehyde Dehydrogenase with Respect to Oxidation of Formaldehyde. *J Biol Chem* **251:**1571-1577; 1976.

[106] Mukerjee, N.; Pietruszko, R. Human Mitochondrial Aldehyde Dehydrogenase Substrate-Specificity - Comparison of Esterase with Dehydrogenase Reaction. *Arch Biochem Biophys* **299:**23-29; 1992.

[107] Liu, L. M.; Hausladen, A.; Zeng, M.; Que, L.; Heitman, J.; Stamler, J. S. A metabolic enzyme for S-nitrosothiol conserved from bacteria to humans. *Nature* **410:**490-494; 2001.

[108] Williamson, D. H.; Lund, P.; Krebs, H. A. Redox State of Free Nicotinamide-Adenine Dinucleotide in Cytoplasm and Mitochondria of Rat Liver. *Biochem J* **103:**514-+; 1967.

[109] Cronholm, T. Effect of Ethanol on the Redox State of the Coenzyme Bound to Alcohol-Dehydrogenase Studied in Isolated Hepatocytes. *Biochem J* **248:**567-572; 1987.

[110] Staab, C. A.; Alander, J.; Brandt, M.; Lengqvist, J.; Morgenstern, R.; Grafstrom, R. C.; Hoog, J. O. Reduction of S-nitrosoglutathione by alcohol dehydrogenase 3 is

facilitated by substrate alcohols via direct cofactor recycling and leads to GSH-controlled formation of glutathione transferase inhibitors. *Biochem J* **413:**493-504; 2008.

[111] Hedberg, J. J.; Griffiths, W. J.; Nilsson, S. J. F.; Hoog, J. O. Reduction of S-nitrosoglutathione by human alcohol dehydrogenase 3 is an irreversible reaction as analysed by electrospray mass spectrometry. *Eur J Biochem* **270:**1249-1256; 2003.

[112] Liu, L.; Yan, Y.; Zeng, M.; Zhang, J.; Hanes, M. A.; Ahearn, G.; McMahon, T. J.; Dickfeld, T.; Marshall, H. E.; Que, L. G.; Stamler, J. S. Essential roles of S-nitrosothiols in vascular homeostasis and endotoxic shock. *Cell* **116:**617-628; 2004.

[113] Hatzistergos, K. E.; Paulino, E. C.; Dulce, R. A.; Takeuchi, L. M.; Bellio, M. A.; Kulandavelu, S.; Cao, Y. N.; Balkan, W.; Kanashiro-Takeuchi, R. M.; Hare, J. M. S-Nitrosoglutathione Reductase Deficiency Enhances the Proliferative Expansion of Adult Heart Progenitors and Myocytes Post Myocardial Infarction. *J Am Heart Assoc* **4**; 2015.

[114] Gaston, B.; Reilly, J.; Drazen, J. M.; Fackler, J.; Ramdev, P.; Arnelle, D.; Mullins, M. E.; Sugarbaker, D. J.; Chee, C.; Singel, D. J.; Loscalzo, J.; Stamler, J. S. Endogenous Nitrogen-Oxides and Bronchodilator S-Nitrosothiols in Human Airways. *P Natl Acad Sci USA* **90:**10957-10961; 1993.

[115] Cohn, L.; Elias, J. A.; Chupp, G. L. ASTHMA: Mechanisms of disease persistence and progression. *Annu Rev Immunol* **22:**789-815; 2004.

[116] Que, L. G.; Liu, L. M.; Yan, Y.; Whitehead, G. S.; Gavett, S. H.; Schwartz, D. A.; Stamler, J. S. Protection from experimental asthma by an endogenous bronchodilator. *Science* **308:**1618-1621; 2005.

[117] Ferrini, M. E.; Simons, B. J.; Bassett, D. J. P.; Bradley, M. O.; Roberts, K.; Jaffar, Z. S-Nitrosoglutathione Reductase Inhibition Regulates Allergen-Induced Lung Inflammation and Airway Hyperreactivity. *Plos One* **8**; 2013.

[118] Blonder, J. P.; Mutka, S. C.; Sun, X. C.; Qiu, J.; Green, L. H.; Mehra, N. K.; Boyanapalli, R.; Suniga, M.; Look, K.; Delany, C.; Richards, J. P.; Looker, D.; Scoggin, C.; Rosenthal, G. J. Pharmacologic inhibition of S-nitrosoglutathione reductase protects against experimental asthma in BALB/c mice through attenuation of both bronchoconstriction and inflammation. *Bmc Pulm Med* **14**; 2014.

[119] Riordan, J. R. Cystic fibrosis as a disease of misprocessing of the cystic fibrosis transmembrane conductance regulator glycoprotein. *American Journal of Human Genetics* **64:**1499-1504; 1999.

[120] Zaman, K.; McPherson, M.; Vaughan, J.; Hunt, J.; Mendes, F.; Gaston, B.; Palmer, L. A. S-nitrosoglutathione increases cystic fibrosis transmembrane regulator maturation. *Biochem Bioph Res Co* **284:**65-70; 2001.

[121] Andersson, C.; Gaston, B.; Roomans, G. M. S-nitrosoglutathione induces functional Delta F508-CFTR in airway epithelial cells. *Biochem Bioph Res Co* **297:**552-557; 2002.

[122] Zaman, K.; Carraro, S.; Doherty, J.; Henderson, E. M.; Lendermon, E.; Liu, L.; Verghese, G.; Zigler, M.; Ross, M.; Park, E.; Palmer, L. A.; Doctor, A.; Stamler, J. S.; Gaston, B. S-nitrosylating agents: a novel class of compounds that increase cystic fibrosis transmembrane conductance regulator expression and maturation in epithelial cells. *Mol Pharmacol* **70:**1435-1442; 2006.

[123] Zaman, K.; Sawczak, V.; Zaidi, A.; Butler, M.; Bennett, D.; Getsy, P.; Zeinomar, M.; Greenberg, Z.; Forbes, M.; Rehman, S.; Jyothikumar, V.; DeRonde, K.; Sattar, A.; Smith, L.; Corey, D.; Straub, A.; Sun, F.; Palmer, L.; Periasamy, A.; Randell, S.; Kelley, T. J.; Lewis, S. J.; Gaston, B. Augmentation of CFTR maturation by S-nitrosoglutathione reductase. *Am J Physiol-Lung C* **310:**L263-L270; 2016.

[124] Sanghani, P. C.; Davis, W. I.; Fears, S. L.; Green, S. L.; Zhai, L. M.; Tang, Y. P.; Martin, E.; Bryan, N. S.; Sanghani, S. P. Kinetic and Cellular Characterization of Novel Inhibitors of S-Nitrosoglutathione Reductase. *J Biol Chem* **284:**24354-24362; 2009.

[125] Sun, X. C.; Wasley, J. W. F.; Qiu, J.; Blonder, J. P.; Stout, A. M.; Green, L. S.; Strong, S. A.; Colagiovanni, D. B.; Richards, J. P.; Mutka, S. C.; Chun, L.; Rosenthal, G. J. Discovery of S-Nitrosoglutathione Reductase Inhibitors: Potential Agents for the Treatment of Asthma and Other Inflammatory Diseases. *Acs Med Chem Lett* **2:**402-406; 2011.

[126] Green, L. S.; Chun, L. E.; Patton, A. K.; Sun, X. C.; Rosenthal, G. J.; Richards, J. P. Mechanism of Inhibition for N6022, a First-in-Class Drug Targeting S-Nitrosoglutathione Reductase. *Biochemistry-Us* **51:**2157-2168; 2012.

[127] Jiang, H.; Polhemus, D. J.; Islam, K. N.; Torregrossa, A. C.; Li, Z.; Potts, A.; Lefer, D. J.; Bryan, N. S. Nebivolol Acts as a S-Nitrosoglutathione Reductase Inhibitor: A New Mechanism of Action. *J Cardiovasc Pharmacol Ther*; 2016.

[128] Wei, W.; Li, B.; Hanes, M. A.; Kakar, S.; Chen, X.; Liu, L. M. S-Nitrosylation from GSNOR Deficiency Impairs DNA Repair and Promotes Hepatocarcinogenesis. *Sci Transl Med* **2**; 2010.

[129] Ozawa, K.; Tsumoto, H.; Wei, W.; Tang, C. H.; Komatsubara, A. T.; Kawafune, H.; Shimizu, K.; Liu, L.; Tsujimoto, G. Proteomic analysis of the role of S-nitrosoglutathione reductase in lipopolysaccharide-challenged mice. *Proteomics* **12:**2024-2035; 2012.

[130] Leung, J.; Wei, W.; Liu, L. M. S-nitrosoglutathione reductase deficiency increases mutagenesis from alkylation in mouse liver. *Carcinogenesis* **34:**984-989; 2013.

[131] Marozkina, N. V.; Wei, C.; Yemen, S.; Wallrabe, H.; Nagji, A. S.; Liu, L.; Morozkina, T.; Jones, D. R.; Gaston, B. S-Nitrosoglutathione Reductase in Human Lung Cancer. *Am J Resp Cell Mol* **46:**63-70; 2012.

[132] Hannun, Y. A. The sphingomyelin cycle and the second messenger function of ceramide. *J Biol Chem* **269:**3125-3128; 1994.

[133] Hannun, Y. A.; Obeid, L. M. Principles of bioactive lipid signalling: lessons from sphingolipids. *Nature reviews. Molecular cell biology* **9:**139-150; 2008.

[134] Hill, P. A.; Tumber, A. Ceramide-induced cell death/survival in murine osteoblasts. *The Journal of endocrinology* **206:**225-233; 2010.

[135] Otterbach, B.; Stoffel, W. Acid sphingomyelinase-deficient mice mimic the neurovisceral form of human lysosomal storage disease (Niemann-Pick disease). *Cell* **81:**1053-1061; 1995.

[136] Schneider, P. B.; Kennedy, E. P. Sphingomyelinase in normal human spleens and in spleens from subjects with Niemann-Pick disease. *J Lipid Res* **8:**202-209; 1967.

[137] Kirschnek, S.; Paris, F.; Weller, M.; Grassme, H.; Ferlinz, K.; Riehle, A.; Fuks, Z.; Kolesnick, R.; Gulbins, E. CD95-mediated apoptosis in vivo involves acid sphingomyelinase. *J Biol Chem* **275:**27316-27323; 2000.

[138] Komatsu, M.; Takahashi, T.; Abe, T.; Takahashi, I.; Ida, H.; Takada, G. Evidence for the association of ultraviolet-C and H(2)O(2)-induced apoptosis with acid sphingomyelinase activation. *Biochim Biophys Acta* **1533:**47-54; 2001.

[139] Li, X.; Gulbins, E.; Zhang, Y. Oxidative stress triggers Ca-dependent lysosome trafficking and activation of acid sphingomyelinase. *Cell Physiol Biochem* **30:**815-826; 2012.

[140] Santana, P.; Pena, L. A.; Haimovitz-Friedman, A.; Martin, S.; Green, D.; McLoughlin, M.; Cordon-Cardo, C.; Schuchman, E. H.; Fuks, Z.; Kolesnick, R. Acid sphingomyelinase-deficient human lymphoblasts and mice are defective in radiation-induced apoptosis. *Cell* **86:**189-199; 1996.

[141] Smith, E. L.; Schuchman, E. H. The unexpected role of acid sphingomyelinase in cell death and the pathophysiology of common diseases. *Faseb J* **22:**3419-3431; 2008.

[142] Zeidan, Y. H.; Hannun, Y. A. The acid sphingomyelinase/ceramide pathway: biomedical significance and mechanisms of regulation. *Current molecular medicine* **10:**454-466; 2010.

[143] Duan, R. D. Alkaline sphingomyelinase: an old enzyme with novel implications. *Biochim Biophys Acta* **1761:**281-291; 2006.

[144] Duan, R. D.; Nyberg, L.; Nilsson, A. Alkaline sphingomyelinase activity in rat gastrointestinal tract: distribution and characteristics. *Biochim Biophys Acta* **1259:**49-55; 1995.

[145] Zhang, Y.; Cheng, Y.; Hansen, G. H.; Niels-Christiansen, L. L.; Koentgen, F.; Ohlsson, L.; Nilsson, A.; Duan, R. D. Crucial role of alkaline sphingomyelinase in sphingomyelin digestion: a study on enzyme knockout mice. *J Lipid Res* **52:**771-781; 2011.

[146] Tomiuk, S.; Hofmann, K.; Nix, M.; Zumbansen, M.; Stoffel, W. Cloned mammalian neutral sphingomyelinase: functions in sphingolipid signaling? *Proc Natl Acad Sci U S A* **95:**3638-3643; 1998.

[147] Sawai, H.; Domae, N.; Nagan, N.; Hannun, Y. A. Function of the cloned putative neutral sphingomyelinase as lyso-platelet activating factor-phospholipase C. *J Biol Chem* **274:**38131-38139; 1999.

[148] Zumbansen, M.; Stoffel, W. Neutral sphingomyelinase 1 deficiency in the mouse causes no lipid storage disease. *Mol Cell Biol* **22:**3633-3638; 2002.

[149] Hofmann, K.; Tomiuk, S.; Wolff, G.; Stoffel, W. Cloning and characterization of the mammalian brain-specific, Mg2+-dependent neutral sphingomyelinase. *Proc Natl Acad Sci U S A* **97:**5895-5900; 2000.

[150] Marchesini, N.; Luberto, C.; Hannun, Y. A. Biochemical properties of mammalian neutral sphingomyelinase 2 and its role in sphingolipid metabolism. *J Biol Chem* **278:**13775-13783; 2003.

[151] Krut, O.; Wiegmann, K.; Kashkar, H.; Yazdanpanah, B.; Kronke, M. Novel tumor necrosis factor-responsive mammalian neutral sphingomyelinase-3 is a C-tail-anchored protein. *J Biol Chem* **281:**13784-13793; 2006.

[152] Corcoran, C. A.; He, Q.; Ponnusamy, S.; Ogretmen, B.; Huang, Y.; Sheikh, M. S. Neutral sphingomyelinase-3 is a DNA damage and nongenotoxic stress-regulated gene that is deregulated in human malignancies. *Molecular Cancer Research* **6:**795-807; 2008.

[153] Tani, M.; Hannun, Y. A. Analysis of membrane topology of neutral sphingomyelinase 2. *Febs Lett* **581:**1323-1328; 2007.

[154] Wu, B. X.; Clarke, C. J.; Matmati, N.; Montefusco, D.; Bartke, N.; Hannun, Y. A. Identification of Novel Anionic Phospholipid Binding Domains in Neutral Sphingomyelinase 2 with Selective Binding Preference. *J Biol Chem* **286:**22362-22371; 2011.

[155] Tani, M.; Hannun, Y. A. Neutral sphingomyelinase 2 is palmitoylated on multiple cysteine residues. Role of palmitoylation in subcellular localization. *J Biol Chem* **282:**10047-10056; 2007.

[156] Marchesini, N.; Osta, W.; Bielawski, J.; Luberto, C.; Obeid, L. M.; Hannun, Y. A. Role for mammalian neutral sphingomyelinase 2 in confluence-induced growth arrest of MCF7 cells. *J Biol Chem* **279:**25101-25111; 2004.

[157] Milhas, D.; Clarke, C. J.; Idkowiak-Baldys, J.; Canals, D.; Hannun, Y. A. Anterograde and retrograde transport of neutral sphingomyelinase-2 between the Golgi and the plasma membrane. *Bba-Mol Cell Biol L* **1801:**1361-1374; 2010.

[158] Clarke, C. J.; Truong, T. G.; Hannun, Y. A. Role for neutral sphingomyelinase-2 in tumor necrosis factor alpha-stimulated expression of vascular cell adhesion molecule-1 (VCAM) and intercellular adhesion molecule-1 (ICAM) in lung epithelial cells: p38 MAPK is an upstream regulator of nSMase2. *J Biol Chem* **282:**1384-1396; 2007.

[159] Levy, M.; Castillo, S. S.; Goldkorn, T. nSMase2 activation and trafficking are modulated by oxidative stress to induce apoptosis. *Biochem Biophys Res Commun* **344:**900-905; 2006.

[160] Levy, M.; Khan, E.; Careaga, M.; Goldkorn, T. Neutral sphingomyelinase 2 is activated by cigarette smoke to augment ceramide-induced apoptosis in lung cell death. *Am J Physiol Lung Cell Mol Physiol* **297:**L125-133; 2009.

[161] Filosto, S.; Castillo, S.; Danielson, A.; Franzi, L.; Khan, E.; Kenyon, N.; Last, J.; Pinkerton, K.; Tuder, R.; Goldkorn, T. Neutral sphingomyelinase 2: a novel target in cigarette smoke-induced apoptosis and lung injury. *Am J Respir Cell Mol Biol* **44:**350-360; 2011.

[162] Poirier, C.; Berdyshev, E. V.; Dimitropoulou, C.; Bogatcheva, N. V.; Biddinger, P. W.; Verin, A. D. Neutral sphingomyelinase 2 deficiency is associated with lung anomalies similar to emphysema. *Mamm Genome* **23:**758-763; 2012.

[163] Clement, A. B.; Gamerdinger, M.; Tamboli, I. Y.; Lutjohann, D.; Walter, J.; Greeve, I.; Gimpl, G.; Behl, C. Adaptation of neuronal cells to chronic oxidative stress is associated with altered cholesterol and sphingolipid homeostasis and lysosomal function. *J Neurochem* **111:**669-682; 2009.

[164] Chaube, R.; Kallakunta, V. M.; Espey, M. G.; McLarty, R.; Faccenda, A.; Ananvoranich, S.; Mutus, B. Endoplasmic reticulum stress-mediated inhibition of NSMase2 elevates plasma membrane cholesterol and attenuates NO production in endothelial cells. *Bba-Mol Cell Biol L* **1821:**313-323; 2012.

[165] De Palma, C.; Meacci, E.; Perrotta, C.; Bruni, P.; Clementi, E. Endothelial nitric oxide synthase activation by tumor necrosis factor alpha through neutral

sphingomyelinase 2, sphingosine kinase 1, and sphingosine 1 phosphate receptors: a novel pathway relevant to the pathophysiology of endothelium. *Arterioscler Thromb Vasc Biol* **26:**99-105; 2006.

[166] Won, J. S.; Im, Y. B.; Khan, M.; Singh, A. K.; Singh, I. The role of neutral sphingomyelinase produced ceramide in lipopolysaccharide-mediated expression of inducible nitric oxide synthase. *J Neurochem* **88:**583-593; 2004.

[167] Kucuksayan, E.; Konuk, E. K.; Demir, N.; Mutus, B.; Aslan, M. Neutral sphingomyelinase inhibition decreases ER stress-mediated apoptosis and inducible nitric oxide synthase in retinal pigment epithelial cells. *Free Radic Biol Med* **72:**113-123; 2014.

[168] Tellier, E.; Negre-Salvayre, A.; Bocquet, B.; Itohara, S.; Hannun, Y. A.; Salvayre, R.; Auge, N. Role for furin in tumor necrosis factor alpha-induced activation of the matrix metalloproteinase/sphingolipid mitogenic pathway. *Mol Cell Biol* **27:**2997-3007; 2007.

[169] Clarke, C. J.; Cloessner, E. A.; Roddy, P. L.; Hannun, Y. A. Neutral sphingomyelinase 2 (nSMase2) is the primary neutral sphingomyelinase isoform activated by tumour necrosis factor-alpha in MCF-7 cells. *Biochem J* **435:**381-390; 2011.

[170] Clarke, C. J.; Guthrie, J. M.; Hannun, Y. A. Regulation of neutral sphingomyelinase-2 (nSMase2) by tumor necrosis factor-alpha involves protein kinase C-delta in lung epithelial cells. *Mol Pharmacol* **74:**1022-1032; 2008.

[171] Barth, B. M.; Gustafson, S. J.; Kuhn, T. B. Neutral sphingomyelinase activation precedes NADPH oxidase-dependent damage in neurons exposed to the proinflammatory cytokine tumor necrosis factor-alpha. *J Neurosci Res* **90:**229-242; 2012.

[172] Adam, D.; Wiegmann, K.; Adam-Klages, S.; Ruff, A.; Kronke, M. A novel cytoplasmic domain of the p55 tumor necrosis factor receptor initiates the neutral sphingomyelinase pathway. *J Biol Chem* **271:**14617-14622; 1996.

[173] Adam-Klages, S.; Schwandner, R.; Adam, D.; Kreder, D.; Bernardo, K.; Kronke, M. Distinct adapter proteins mediate acid versus neutral sphingomyelinase activation through the p55 receptor for tumor necrosis factor. *J Leukoc Biol* **63:**678-682; 1998.

[174] Adam-Klages, S.; Adam, D.; Wiegmann, K.; Struve, S.; Kolanus, W.; Schneider-Mergener, J.; Kronke, M. FAN, a novel WD-repeat protein, couples the p55 TNF-receptor to neutral sphingomyelinase. *Cell* **86:**937-947; 1996.

[175] Tcherkasowa, A. E.; Adam-Klages, S.; Kruse, M. L.; Wiegmann, K.; Mathieu, S.; Kolanus, W.; Kronke, M.; Adam, D. Interaction with factor associated with neutral sphingomyelinase activation, a WD motif-containing protein, identifies receptor for activated C-kinase 1 as a novel component of the signaling pathways of the p55 TNF receptor. *J Immunol* **169:**5161-5170; 2002.

[176] Philipp, S.; Puchert, M.; Adam-Klages, S.; Tchikov, V.; Winoto-Morbach, S.; Mathieu, S.; Deerberg, A.; Kolker, L.; Marchesini, N.; Kabelitz, D.; Hannun, Y. A.; Schutze, S.; Adam, D. The Polycomb group protein EED couples TNF receptor 1 to neutral sphingomyelinase. *Proc Natl Acad Sci U S A* **107:**1112-1117; 2010.

[177] Nalivaeva, N. N.; Rybakina, E. G.; Pivanovich, I.; Kozinets, I. A.; Shanin, S. N.; Bartfai, T. Activation of neutral sphingomyelinase by IL-1beta requires the type 1 interleukin 1 receptor. *Cytokine* **12:**229-232; 2000.

[178] Rybakina, E. G.; Nalivaeva, N. N.; Pivanovich, Y. U.; Shanin, S. N.; Kozinets, A.; Korneva, E. A. The role of neutral sphingomyelinase in interleukin-1beta signal transduction in mouse cerebral cortex cells. *Neurosci Behav Physiol* **31:**439-444; 2001.

[179] Kim, M. Y.; Linardic, C.; Obeid, L.; Hannun, Y. Identification of Sphingomyelin Turnover as an Effector Mechanism for the Action of Tumor-Necrosis-Factor-Alpha and Gamma-Interferon - Specific Role in Cell-Differentiation. *J Biol Chem* **266:**484-489; 1991.

[180] Shamseddine, A. A.; Airola, M. V.; Hannun, Y. A. Roles and regulation of neutral sphingomyelinase-2 in cellular and pathological processes. *Adv Biol Regul* **57:**24-41; 2015.

[181] Kim, W. J.; Okimoto, R. A.; Purton, L. E.; Goodwin, M.; Haserlat, S. M.; Dayyani, F.; Sweetser, D. A.; McClatchey, A. I.; Bernard, O. A.; Look, A. T.; Bell, D. W.; Scadden, D. T.; Haber, D. A. Mutations in the neutral sphingomyelinase gene SMPD3 implicate the ceramide pathway in human leukemias. *Blood* **111:**4716-4722; 2008.

[182] Revill, K.; Wang, T.; Lachenmayer, A.; Kojima, K.; Harrington, A.; Li, J. Y.; Hoshida, Y.; Llovet, J. M.; Powers, S. Genome-Wide Methylation Analysis and Epigenetic Unmasking Identify Tumor Suppressor Genes in Hepatocellular Carcinoma. *Gastroenterology* **145:**1424-+; 2013.

[183] Bhati, R.; Patterson, C.; Livasy, C. A.; Fan, C.; Ketelsen, D.; Hu, Z. Y.; Reynolds, E.; Tanner, C.; Moore, D. T.; Gabrielli, F.; Perou, C. M.; Klauber-DeMore, N. Molecular characterization of human breast tumor vascular cells. *Am J Pathol* **172:**1381-1390; 2008.

[184] Kosaka, N.; Iguchi, H.; Hagiwara, K.; Yoshioka, Y.; Takeshita, F.; Ochiya, T. Neutral Sphingomyelinase 2 (nSMase2)-dependent Exosomal Transfer of Angiogenic MicroRNAs Regulate Cancer Cell Metastasis. *J Biol Chem* **288:**10849-10859; 2013.

[185] Ito, H.; Murakami, M.; Furuhata, A.; Gao, S. Q.; Yoshida, K.; Sobue, S.; Hagiwara, K.; Takagi, A.; Kojima, T.; Suzuki, M.; Banno, Y.; Tanaka, K.; Tamiya-Koizumi, K.; Kyogashima, M.; Nozawa, Y.; Murate, T. Transcriptional regulation of neutral sphingomyelinase 2 gene expression of a human breast cancer cell line, MCF-7,

induced by the anti-cancer drug, daunorubicin. *Bba-Gene Regul Mech* **1789:**681-690; 2009.

[186] Goswami, R.; Ahmed, M.; Kilkus, J.; Han, T.; Dawson, S. A.; Dawson, G. Differential regulation of ceramide in lipid-rich microdomains (rafts): Antagonistic role of palmitoyl: Protein thioesterase and neutral sphingomyelinase 2. *J Neurosci Res* **81:**208-217; 2005.

[187] Park, B.; Lee, Y. M.; Kim, J. S.; Her, Y.; Kang, J. H.; Oh, S. H.; Kim, H. M. Neutral sphingomyelinase 2 modulates cytotoxic effects of protopanaxadiol on different human cancer cells. *BMC Complement Altern Med* **13:**194; 2013.

[188] Liu, B.; Hannun, Y. A. Inhibition of the neutral magnesium-dependent sphingomyelinase by glutathione. *J Biol Chem* **272:**16281-16287; 1997.

[189] Okamoto, Y.; Obeid, L. M.; Hannun, Y. A. Bcl-xL interrupts oxidative activation of neutral sphingomyelinase. *Febs Lett* **530:**104-108; 2002.

[190] Clarke, C. J.; Mediwala, K.; Jenkins, R. W.; Sutton, C. A.; Tholanikunnel, B. G.; Hannun, Y. A. Neutral Sphingomyelinase-2 Mediates Growth Arrest by Retinoic Acid through Modulation of Ribosomal S6 Kinase. *J Biol Chem* **286:**21565-21576; 2011.

[191] Ito, H.; Tanaka, K.; Hagiwara, K.; Kobayashi, M.; Hoshikawa, A.; Mizutani, N.; Takagi, A.; Kojima, T.; Sobue, S.; Ichihara, M.; Suzuki, M.; Tamiya-Koizumi, K.; Nakamura, M.; Banno, Y.; Nozawa, Y.; Murate, T. Transcriptional regulation of neutral sphingomyelinase 2 in all-trans retinoic acid-treated human breast cancer cell line, MCF-7. *J Biochem-Tokyo* **151:**599-610; 2012.

[192] Filosto, S.; Fry, W.; Knowlton, A. A.; Goldkorn, T. Neutral Sphingomyelinase 2 (nSMase2) Is a Phosphoprotein Regulated by Calcineurin (PP2B). *J Biol Chem* **285:**10213-10222; 2010.

[193] Filosto, S.; Ashfaq, M.; Chung, S.; Fry, W.; Goldkorn, T. Neutral Sphingomyelinase 2 Activity and Protein Stability Are Modulated by Phosphorylation of Five Conserved Serines. *J Biol Chem* **287:**514-522; 2012.

[194] Broillet, M. C. S-Nitrosylation of proteins. *Cell Mol Life Sci* **55:**1036-1042; 1999.

[195] Nakamura, T.; Prikhodko, O. A.; Pirie, E.; Nagar, S.; Akhtar, M. W.; Oh, C. K.; McKercher, S. R.; Ambasudhan, R.; Okamoto, S.; Lipton, S. A. Aberrant protein S-nitrosylation contributes to the pathophysiology of neurodegenerative diseases. *Neurobiol Dis* **84:**99-108; 2015.

[196] Benhar, M. Emerging Roles of Protein S-Nitrosylation in Macrophages and Cancer Cells. *Curr Med Chem* **23:**2602-2617; 2016.

[197] Lima, B.; Lam, G. K.; Xie, L.; Diesen, D. L.; Villamizar, N.; Nienaber, J.; Messina, E.; Bowles, D.; Kontos, C. D.; Hare, J. M.; Stamler, J. S.; Rockman, H. A. Endogenous S-nitrosothiols protect against myocardial injury. *Proc Natl Acad Sci U S A* **106:**6297-6302; 2009.

[198] Wu, H.; Romieu, I.; Sienra-Monge, J. J.; del Rio-Navarro, B. E.; Anderson, D. M.; Jenchura, C. A.; Li, H. L.; Ramirez-Aguilar, M.; Lara-Sanchez, I. D.; London, S. J. Genetic variation in S-nitrosoglutathione reductase (GSNOR) and childhood asthma. *J Allergy Clin Immun* **120:**322-328; 2007.

[199] Moore, P. E.; Ryckman, K. K.; Williams, S. M.; Patel, N.; Summar, M. L.; Sheller, J. R. Genetic Variants of GSNOR and ADRB2 Influence Response to Albuterol in African-American Children With Severe Asthma. *Pediatr Pulm* **44:**649-654; 2009.

[200] Gomes, S. A.; Rangel, E. B.; Premer, C.; Dulce, R. A.; Cao, Y.; Florea, V.; Balkan, W.; Rodrigues, C. O.; Schally, A. V.; Hare, J. M. S-nitrosoglutathione reductase (GSNOR) enhances vasculogenesis by mesenchymal stem cells. *Proc Natl Acad Sci U S A* **110:**2834-2839; 2013.

[201] Raffay, T. M.; Martin, R. J.; Reynolds, J. D. Can Nitric Oxide-Based Therapy Prevent Bronchopulmonary Dysplasia? *Clin Perinatol* **39:**613-+; 2012.

[202] Raffay, T. M.; Dylag, A. M.; Di Fiore, J. M.; Smith, L. A.; Einisman, H. J.; Li, Y.; Lakner, M. M.; Khalil, A. M.; MacFarlane, P. M.; Martin, R. J.; Gaston, B. S-Nitrosoglutathione Attenuates Airway Hyperresponsiveness in Murine Bronchopulmonary Dysplasia. *Mol Pharmacol* **90:**418-426; 2016.

[203] Colagiovanni, D. B.; Drolet, D. W.; Langlois-Forget, E.; Piche, M. P.; Looker, D.; Rosenthal, G. J. A nonclinical safety and pharmacokinetic evaluation of N6022: A first-in-class S-nitrosoglutathione reductase inhibitor for the treatment of asthma. *Regul Toxicol Pharm* **62:**115-124; 2012.

[204] Chen, Q. M.; Sievers, R. E.; Varga, M.; Kharait, S.; Haddad, D. J.; Patton, A. K.; Delany, C. S.; Mutka, S. C.; Blonder, J. P.; Dube, G. P.; Rosenthal, G. J.; Springer, M. L. Pharmacological inhibition of S-nitrosoglutathione reductase improves endothelial vasodilatory function in rats in vivo. *J Appl Physiol* **114:**752-760; 2013.

[205] Ramachandran, N.; Jacob, S.; Zielinski, B.; Curatola, G.; Mazzanti, L.; Mutus, B. N-dansyl-S-nitrosohomocysteine a fluorescent probe for intracellular thiols and S-nitrosothiols. *Biochim Biophys Acta* **1430:**149-154; 1999.

[206] Chen, X.; Wen, Z.; Xian, M.; Wang, K.; Ramachandran, N.; Tang, X.; Schlegel, H. B.; Mutus, B.; Wang, P. G. Fluorophore-labeled S-nitrosothiols. *J Org Chem* **66:**6064-6073; 2001.

[207] Root, P.; Mutus, B. O-Aminobenzoyl-S-nitrosohomocysteine, a fluorogenic probe for cell-surface thiol determinations via a microtiter plate assay. *Anal Biochem* **320:**299-302; 2003.

[208] David E. Golan, A. H. T. J., Ehrin J. Armstrong, April W. Armstrong *Principles of Pharmacology: The Pathophysiologic Basis of Drug Therapy.* Wolters Kluwer.

[209] Chivers, P. T.; Prehoda, K. E.; Raines, R. T. The CXXC motif: A rheostat in the active site. *Biochemistry-Us* **36:**4061-4066; 1997.

[210] Chivers, P. T.; Laboissiere, M. C. A.; Raines, R. T. The CXXC motif: Imperatives for the formation of native disulfide bonds in the cell. *Embo Journal* **15:**2659-2667; 1996.

[211] Walker, K. W.; Gilbert, H. F. Scanning and escape during protein-disulfide isomerase-assisted protein folding. *J Biol Chem* **272:**8845-8848; 1997.

[212] Pan, J. L.; Bardwell, J. C. A. The origami of thioredoxin-like folds. *Protein Sci* **15:**2217-2227; 2006.

[213] Kimura, T.; Nishida, A.; Ohara, N.; Yamagishi, D.; Horibe, T.; Kikuchi, M. Functional analysis of the CXXC motif using phage antibodies that cross-react with protein disulphide-isomerase family proteins. *Biochem J* **382:**169-176; 2004.

[214] Pehar, M.; Lehnus, M.; Karst, A.; Puglielli, L. Proteomic Assessment Shows That Many Endoplasmic Reticulum (ER)-resident Proteins Are Targeted by N-epsilon-Lysine Acetylation in the Lumen of the Organelle and Predicts Broad Biological Impact. *J Biol Chem* **287:**22436-22440; 2012.

[215] Phillips, D. M. The presence of acetyl groups of histones. *Biochem J* **87:**258-263; 1963.

[216] Allfrey, V. G.; Faulkner, R.; Mirsky, A. E. Acetylation and Methylation of Histones and Their Possible Role in the Regulation of Rna Synthesis. *Proc Natl Acad Sci U S A* **51:**786-794; 1964.

[217] Xiong, Y.; Guan, K. L. Mechanistic insights into the regulation of metabolic enzymes by acetylation. *J Cell Biol* **198:**155-164; 2012.

[218] Guerra, D.; Ballard, K.; Truebridge, I.; Vierling, E. S-Nitrosation of Conserved Cysteines Modulates Activity and Stability of S-Nitrosoglutathione Reductase (GSNOR). *Biochemistry-Us* **55:**2452-2464; 2016.

[219] Pace, N. J.; Weerapana, E. Zinc-binding cysteines: diverse functions and structural motifs. *Biomolecules* **4:**419-434; 2014.

[220] Lee, Y. M.; Lim, C. Physical basis of structural and catalytic Zn-binding sites in proteins. *J Mol Biol* **379:**545-553; 2008.

[221] Ascenzi, P.; Amiconi, G. Logarithmic Plots in Enzymology - Representation of the Michaelis-Menten Equation. *Biochem Educ* **15:**83-84; 1987.

[222] Igarashi, Y. Functional roles of sphingosine, sphingosine 1-phosphate, and methylsphingosines: in regard to membrane sphingolipid signaling pathways. *J Biochem* **122:**1080-1087; 1997.

[223] Morales, A.; Lee, H.; Goni, F. M.; Kolesnick, R.; Fernandez-Checa, J. C. Sphingolipids and cell death. *Apoptosis* **12:**923-939; 2007.

[224] Kishimoto, Y.; Agranoff, B. W.; Radin, N. S.; Burton, R. M. Comparison of the fatty acids of lipids of subcellular brain fractions. *J Neurochem* **16:**397-404; 1969.

[225] O'Brien, J. S.; Blankenhorn, D. H. Fatty Acid Composition of Sphingomyelin and Lecithin in Normal Human Serum. *Proc Soc Exp Biol Med* **119:**862-866; 1965.

[226] Koval, M.; Pagano, R. E. Intracellular transport and metabolism of sphingomyelin. *Biochim Biophys Acta* **1082:**113-125; 1991.

[227] Allan, D.; Kallen, K. J. Transport of lipids to the plasma membrane in animal cells. *Prog Lipid Res* **32:**195-219; 1993.

[228] Wu, B. X.; Clarke, C. J.; Hannun, Y. A. Mammalian Neutral Sphingomyelinases: Regulation and Roles in Cell Signaling Responses. *Neuromol Med* **12:**320-330; 2010.

[229] Ramachandran, C. K.; Murray, D. K.; Nelson, D. H. Dexamethasone increases neutral sphingomyelinase activity and sphingosine levels in 3T3-L1 fibroblasts. *Biochem Biophys Res Commun* **167:**607-613; 1990.

[230] Simons, K.; Ikonen, E. Functional rafts in cell membranes. *Nature* **387:**569-572; 1997.

[231] Brown, D. A.; London, E. Functions of lipid rafts in biological membranes. *Annu Rev Cell Dev Bi* **14:**111-136; 1998.

[232] Simons, K.; Toomre, D. Lipid rafts and signal transduction. *Nat Rev Mol Cell Bio* **1:**31-39; 2000.

[233] Ridgway, N. D. Interactions between metabolism and intracellular distribution of cholesterol and sphingomyelin. *Biochim Biophys Acta* **1484:**129-141; 2000.

[234] Slotte, J. P.; Harmala, A. S.; Jansson, C.; Porn, M. I. Rapid turn-over of plasma membrane sphingomyelin and cholesterol in baby hamster kidney cells after exposure to sphingomyelinase. *Biochim Biophys Acta* **1030:**251-257; 1990.

[235] Slotte, J. P.; Bierman, E. L. Depletion of plasma-membrane sphingomyelin rapidly alters the distribution of cholesterol between plasma membranes and intracellular cholesterol pools in cultured fibroblasts. *Biochem J* **250:**653-658; 1988.

[236] Gupta, A. K.; Rudney, H. Plasma membrane sphingomyelin and the regulation of HMG-CoA reductase activity and cholesterol biosynthesis in cell cultures. *J Lipid Res* **32:**125-136; 1991.

[237] Buckingham, J. C. Glucocorticoids: exemplars of multi-tasking. *Br J Pharmacol* **147 Suppl 1:**S258-268; 2006.

[238] Touitou, Y.; Bogdan, A.; Levi, F.; Benavides, M.; Auzeby, A. Disruption of the circadian patterns of serum cortisol in breast and ovarian cancer patients: relationships with tumour marker antigens. *Br J Cancer* **74:**1248-1252; 1996.

[239] Dotson, P. P.; Karakashian, A. A.; Nikolova-Karakashian, M. N. Neutral sphingomyelinase-2 is a redox sensitive enzyme: role of catalytic cysteine residues in regulation of enzymatic activity through changes in oligomeric state. *Biochem J* **465:**371-382; 2015.

[240] Barenholz, Y. Sphingomyelin and cholesterol: from membrane biophysics and rafts to potential medical applications. *Subcell Biochem* **37:**167-215; 2004.

APPENDICES

Appendix A – NMR Characterization

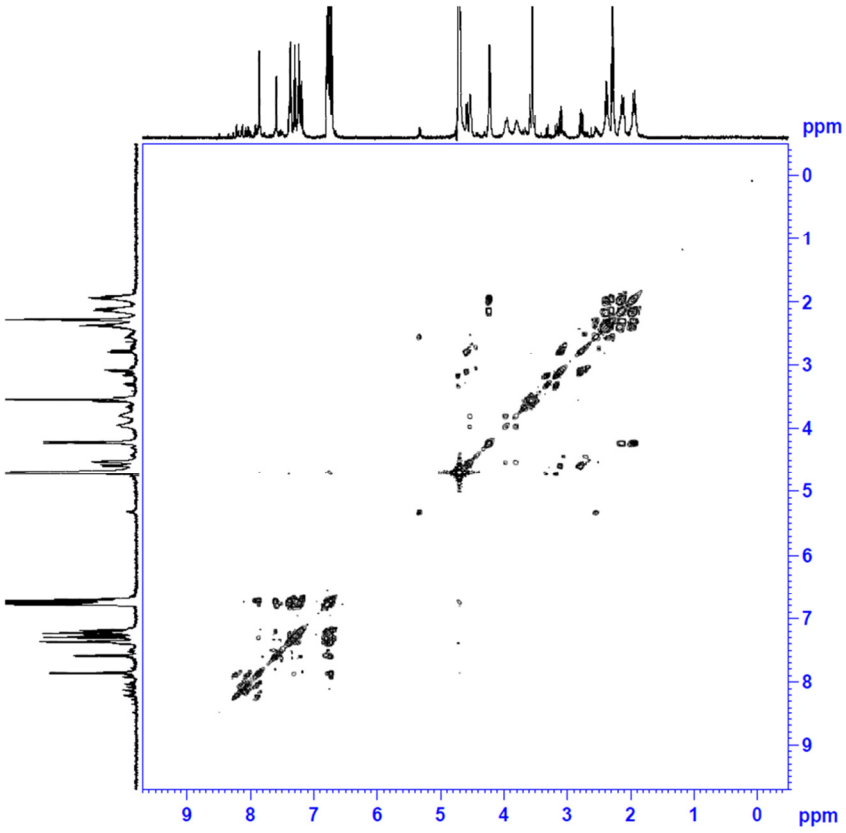

Figure A.1 Correlation spectroscopy (COSY) of OAbz-GSNO

Pooled OAbz-GSNO was lyophilized and re-dissolved in minimum volume D_2O. Spectrum was collected on a Bruker 500 MHz Avance III spectrometer using a BBFO probe. This COSY spectrum was used to assign ^1H NMR peaks for OAbz-GSNO.

Appendix B – Recombinant Protein Sequence

MGSSHHHHHH SSGLVPRGSH MANEVIKCKA AVAWEAGKPL SIEEIEVAPP
KAHEVRIKII ATAVCHTDAY TLSGADPEGC FPVILGHEGA GIVESVGEGV
TKLKAGDTVI PLYIPQCGEC KFCLNPKTNL CQKIRVTQGK GLMPDGTSRF
TCKGKTILHY MGTSTFSEYT VVADISVAKI DPLAPLDKVC LLGCGISTGY
GAAVNTAKLE PGSVCAVFGL GGVGLAVIMG CKVAGASRII GVDINKDKFA
RAKEFGATEC INPQDFSKPI QEVLIEMTDG GVDYSFECIG NVKVMRAALE
ACHKGWGVSV VVGVAASGEE IATRPFQLVT GRTWKGTAFG GWKSVESVPK
LVSEYMSKKI KVDEFVTHNL SFDEINKAFE LMHSGKSIRT VVKILEHHHH
HH*

Figure B.1 Recombinant GSNOR protein sequence

MGSSHHHHHH SSGLVPRGSH MVLYTTPFPN SCLSALHCVS WALIFPCYWL
VDRLAASFIP TTYEKRQRAD DPCCLQLLCT ALFTPIYLAL LVASLPFAFL
GFLFWSPLQS ARRPYIYSRL EDKGLAGGAA LLSEWKGTGP GKSFCFATAN
VCLLPDSLAR VNNLFNTQAR AKEIGQRIRN GAARPQIKIY IDSPTNTSIS
AASFSSLVSP QGGDGVARAV PGSIKRTASV EYKGDGGRHP GDEAANGPAS
GDPVDSSSPE DACIVRIGGE EGGRPPEADD PVPGGQARNG AGGGPRGQTP
NHNQQDGDSG SLGSPSASRE SLVKGRAGPD TSASGEPGAN SKLLYKASVV
KKAAARRRRH PDEAFDHEVS AFFPANLDFL CLQEVFDKRA ATKLKEQLHG
YFEYILYDVG VYGCQGCCSF KCLNSGLLFA SRYPIMDVAY HCYPNKCNDD
ALASKGALFL KVQVGSTPQD QRIVGYIACT HLHAPQEDSA IRCGQLDLLQ
DWLADFRKST SSSSAANPEE LVAFDVVCGD FNFDNCSSDD KLEQQHSLFT
HYRDPCRLGP GEEKPWAIGT LLDTNGLYDE DVCTPDNLQK VLESEEGRRE
YLAFPTSKSS GQKGRKELLK GNGRRIDYML HAEEGLCPDW KAEVEEFSFI
TQLSGLTDHL PVAMRLMVSS GEEEAHHHHH H*

Figure B.2 Recombinant NSMase II protein sequence

Appendix C – Protein Purification Gels

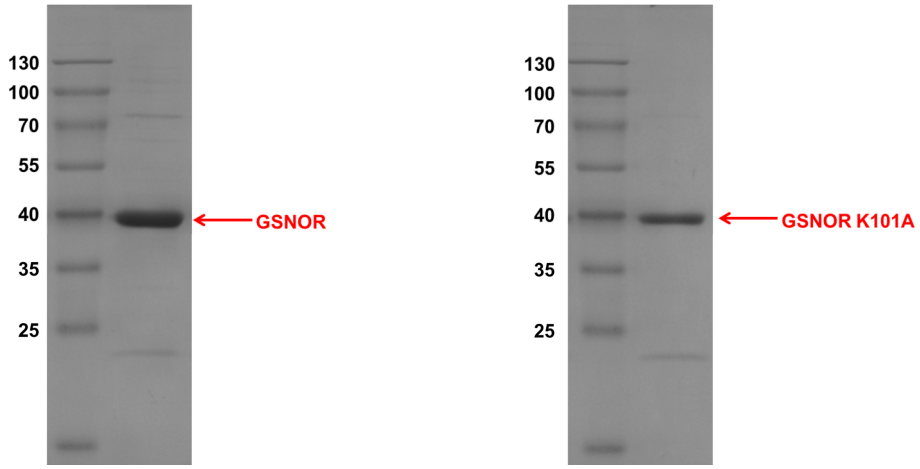

Figure C.1 GSNOR and GSNOR K101A protein purification gels

Following Nickel affinity chromatography and buffer exchange, purified proteins were analyzed on 10% SDS-PAGE gels under reducing conditions. Protein bands were visualized using Coomassie Brilliant Blue.

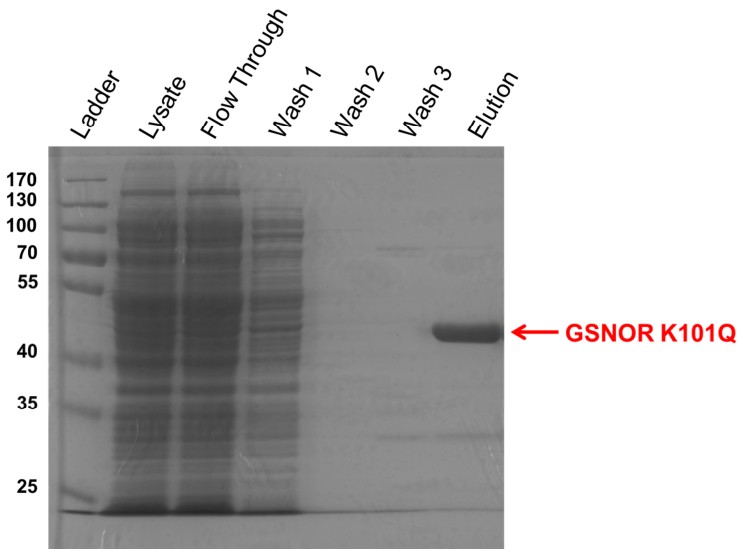

Figure C.2 GSNOR K101Q protein purification gel

Following Nickel affinity chromatography and buffer exchange, purified GSNOR K101Q was analyzed on 10% SDS-PAGE gel under reducing conditions. Protein bands were visualized using Coomassie Brilliant Blue.

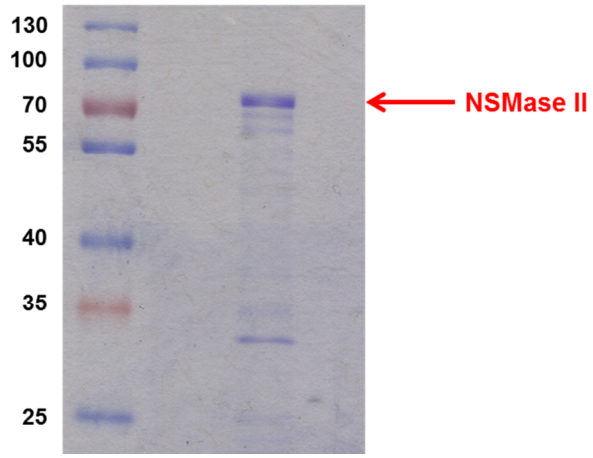

Figure C.3 NSMase II protein purification gel

Following Nickel affinity chromatography and buffer exchange, purified NSMase II was analyzed on 10% SDS-PAGE gel under reducing conditions. Protein bands were visualized using Coomassie Brilliant Blue.

VITA AUCTORIS

NAME:	Bei Lei Sun
PLACE OF BIRTH:	Henan, P. R. China
EDUCATION:	University of Windsor, B.Sc.
	Windsor, Ontario, Canada, 2010